SONOLYTIC, SONOCATALYTIC AND PHOTOCATALYTIC DESTRUCTION OF PHARMACEUTICALS AND PERSONAL CARE PRODUCTS IN WATER

by

Başak Savun Hekimoğlu

B.S. in Environmental Engineering, Trakya University, 2008

M.S. in Environmental Technology, Boğaziçi University, 2011

Submitted to the Institute of Environmental Sciences in partial fulfillment of

the requirements for the degree of

Doctor of Philosophy

in

Environmental Sciences

Boğaziçi University

2019

To my biggest treasure, Irmak Hekimoğlu

ACKNOWLEDGEMENTS

First and foremost, I want to thank my thesis supervisor Prof. Dr. Nilsun H. İnce. She has been a pillar of strength, a role model and an inspiration. She has been there providing her endless support and guidance at all times and she has given me all the freedom to pursue my research. I thank her wholeheartedly, for the example she provided both as a great scientist and person.

I would like to express my appreciation to the members of my committee Prof. Dr. İdil Arslan Alaton, Prof. Dr. Ayşen Erdinçler, Prof. Dr. Rana Kıdak and Assoc. Prof. Başak Güven for spending their valuable time to evaluate this thesis and for their valuable and supportive comments.

The financial support provided by Boğaziçi University Research Fund to the projects 18Y00D1 and 18Y00P7 is greatly acknowledged.

I wish to express my thanks to Assoc. Prof. Ulaş Tezel for his permission and support to the LC/MS/MS analysis of the byproducts. I am also thankful to Dr. Bilge Gedik Uluocak for her assistance in nanoparticle image analysis. I would like to acknowledge Merve Sıvacı for her help with the Microtox analysis. I would also like to thank Prof. Victoria Aviyente and Evrim Arslan for their valuable collaboration in the computational modeling and assessment of oxidation byproducts.

A very special thanks goes to my lovely friends İlkay Civelek, Elif İçağasıoğlu, Hazal Çetin, Cemre Birben, Ayşe Mergenci, Seda Farımaz Tuncel, Mübeccel Aydın, for all their support throughout my study and bringing so much joy to my life.

I want to express my gratitude and deepest appreciation to Irmak Hekimoğlu for being such an amazing daughter, helping in every way she can and making it possible for me to finish what I started. I used to think that it’s my job as a mother to teach her about the world. But the truth is, she taught me more about life, unconditional love, selflessness and tolerance. Most importantly, she reminded me that so many things can be fixed with a hug. I would also like to say thank you to my husband Dr. Mustafa Hekimoğlu for sharing this entire amazing journey with me, standing by me all through with patience and for being a constant source of support.

Words cannot express how grateful I am to my parents Selma and Mustafa Bülent Savun, who raised me with a love of science, for all of the sacrifices that they've made on my behalf. I can never pay back the support given by my dear uncle Levent Derya Savun. I am also thankful to my dear aunts Duygu Karakurt and Sibel Karakurt for always believing in me. I can't ever imagine my life without them. Last but definitely not least, I would like to express my appreciation to Assoc. Prof. Nahide Gülşah Deniz who has always been a big sister, a guide and an inspiration to me.

Finally, my grandmother Nebahat Karakurt, who is gone for over fifteen years now, continues to hold the most special part of my heart. There are some who bring a light so great to the world that even after they have gone, the light remains. Grandma, thank you for sharing your light.

ABSTRACT

SONOLYTIC, SONOCATALYTIC AND PHOTOCATALYTIC DESTRUCTION OF PHARMACEUTICALS AND PERSONAL CARE PRODUCTS IN WATER

Pharmaceuticals and personal care products are used for health and cosmetic reasons and discharged readily to sewage treatment facilities to be transported to freshwater systems due to their low biodegradability. Ultrasound is an excellent tool for the destruction of such refractory chemicals, but the method is energy-intensive and ineffective for carbon-mineralization. Hence, combination of ultrasound with solid particles, or other processes (e.g. adsorption, homogeneous/heterogeneous AOP's) is expected to improve the efficiency. The present study encompasses a thorough investigation of single ultrasound and combinations with adsorption, catalysis and photolysis for the destruction of PPCPs in water. The probe chemicals were salicylic acid, methylparaben and caffeine, while the catalysts were zero-valent iron (ZVI), sepiolite, TiO_2, nanoparticles of sepiolite-SDS, and sepiolite-TiO_2. The study also includes the use of an experimental design method for the analysis and evaluation of the operating parameters/factors, characterization of sonolytic and sonocatalytic systems, and determination of the individual and interaction effects of the operating parameters on the process efficiency. A summary of findings is as follows: i) ultrasound-assisted advanced Fenton reaction is much more effective than unassisted Fenton, via preventing H_2O_2 addition, which inhibits the mineralization process; ii) sepiolite is a good adsorbent and catalyst particularly when the surface is modified by sonication or when it is converted to a nanocomposite with sodium-dodecyl-sulfate (SDS); iii) Photocatalytic and sonocatalytic activity of TiO_2 is significantly enhanced by modification of the catalyst surface to produce sepiolite/TiO_2 nanoparticles.

ÖZET

SU ORTAMINDAKİ TIBBİ İLAÇ VE KİŞİSEL BAKIM ÜRÜNLERİNİN ULTRASES, KATALİTİK ULTRASES VE FOTOKATALİTİK OLARAK PARÇALANMASI

Tıbbi ilaçlar ve kişisel bakım ürünleri sağlık ve kozmetik amaçlı kullanılmakta olup, düşük biyolojik bozunabilirlikleri sebebiyle atık su arıtma tesislerinden tatlı su sistemlerine kolayca deşarj edilmektedirler. Ultrasonik dalgalar giderilmesi zor kimyasalların arıtılması için mükemmel bir araçtır ancak bu method aşırı enerji tüketir ve yeterli TOK giderimi sağlayamaz. Bu nedenle, ultrasonik dalgaların suya katı parçacıklar ekleme veya diğer prosesler (adsorpsiyon, homojen/heterojen ileri oksidasyon prosesleri) ile birleştirerek etkinliğinin arttırılması beklenmektedir. Bu tez çalışmasının içeriği su ortamındaki tıbbi ilaç ve kişisel bakım ürünlerinin sonoliz, adsorpsiyon, sonokataliz ve fotokataliz işlemleriyle giderilmesinin araştırılması ile ilgilidir. Deneysel çalışmalarda prob madde olarak salisilik asit, metilparaben ve kafein, katalizör olarak ise sıfır-değerlikli demir, lületaşı (sepiyolit), TiO_2, ve laboratuarda sentezlenen sepiyolit-SDS ve sepiyolit-TiO_2 nano-kompozitleri kullanılmıştır. Bu çalışmada ayrıca işletme parametre ve etkenlerinin analizi, sistem karakterizasyonu ve optimizasyonu, işletme parametrelerinin sistem verimine yaptıkları bireysel ve etkileşim etkileri deneysel bir tasarım protokolü kullanılarak değerlendirilmiştir. Bulguların özeti şunlardır: i) ultrason destekli ileri Fenton reaksiyonu, mineralizasyon işlemini engelleyen H_2O_2 ilavesinin önlenmesi sayesinde çok daha etkilidir; ii) sepiyolit, özellikle yüzeyi sonikasyon ile modifiye edildiğinde veya sodyum-dodesil-sülfat (SDS) ile bir nano-bileşiğe dönüştürüldüğünde iyi bir adsorban ve katalizördür; iii) TiO_2'nin fotokatalitik ve sonokatalitik aktivitesi, katalizör yüzeyinin sepiyolit/TiO_2 nanopartikülleri üretmek üzere modifikasyonu ile önemli ölçüde arttırılır.

TABLE OF CONTENTS

LIST OF FIGURES

LIST OF TABLES

LIST OF SYMBOLS/ABBREVIATIONS

Symbol	Explanation	Unit
•OH	Hydroxyl Radical	
AIC	Akaike Information Criterion	
AOP	Advanced Oxidation Process	
BBD	Box-Behnken Design	
C_0	Initial Concentration	mg L^{-1}
CAF	Caffeine	
CCD	Central Composite Design	
Cp	Heat capacity of water	J g^{-1} $^{o}C^{-1}$
DOC	Dissolved Organic Carbon	mg L^{-1}
DOE	Design of Experiments	
e^-/h^+	Electron/Hole Pair	
EC50	Half Maximal Effective Concentration	mg L^{-1}
ECOSAR	Ecological Structure Activity Relationships	
EDC	Endocrine Disrupting Compounds	
f	Frequency	kHz
FFD	Full Factorial Design	
H_2O_2	Hydrogen Peroxide	
k	Degradation Rate Coefficient	min^{-1}
LHD	Latin Hypercube Design	
MAPE	Mean Absolute Percentage Errors	
MP	Methylparaben	
MW	Molecular Weight	g mol^{-1}
NPOC	Non-Purgeable Organic Carbon	
OFAT	One-factor-at-a-time	
P	Power	W
P_d	Power Dissipated in The System	W
PPCPs	Pharmaceuticals and Personal Care Products	
R1	Reactor 1	
R2	Reactor 2	
R2	Reactor 3	
ROS	Reactive Oxygen Species	

Symbol	Explanation	Unit
RSM	Response Surface Methodology	
S	Concentration of Sepiolite	mg L^{-1}
SA	Salicylic Acid	
SDS	Sodium Dodecyl Sulfate	
SEM	Scanning Electron Microscope	
Sep/TiO_2	Sepiolite-TiO_2 nanocomposite	
STP	Sewage Treatment Plant	
TiO_2	Titanium Dioxide	
TOC	Total Organic Carbon	mg L^{-1}
US	Ultrasonic Irradiation	
UV	Ultraviolet Irradiation	
UV-Vis	Ultraviolet and Visible	
WWTP	Wastewater Treatment Plants	
ZVI	Zero Valent Iron	
SL	Sonoluminescence	
MBSL	Multi-Bubble Sonoluminescence	
SBSL	Single-Bubble Sonoluminescence	

1. INTRODUCTION

The excessive use of PPCP's and their discharge to sewage treatment plants (STP's) has lately raised significant environmental concern, due to their presence in freshwater systems via inefficient treatment in biochemical processes and ultimate discharge to freshwater systems with the plant effluents (Pietrogrande and Basaglia 2007; Hummel et al. 2006; Zuccato et al. 2008; Kasprzyk-Hordern et al. 2008). The environmental concern is due to their recognition with acute or chronic adverse effects on aquatic organisms and potential risk to humans if the reclaimed water is returned to water supply systems (Nakada et al. 2007). The most common PPCP's that are frequently detected STP effluents and fresh water environments are salicylic acid, methylparaben and caffeine.

Salicylic acid (SA), also known as 2-hydroxybenzoic acid is a widely used PPCP in pharmaceutical and cosmetic formulations. It is easily produced by hydrolytic deacetylation of acetylsalicylic acid, and is commonly used as an ingredient in acne treatment formulations, shampoos, facial cleansers and moisturizers. As such, it is readily discharged to sewage treatment facilities via excretion and wash waters, and due to its bio-persistence it is transmitted to natural water systems. Owing to its moderate toxicity to aquatic organisms, SA must be eliminated either in the STP effluent before it is discharged, or in water treatment operations (Savun-Hekimoğlu and Ince 2017).

Methylparaben (MP) is a common bactericide and antimicrobial agent used in the formulation of various PPCPs such as tooth pastes, bath gels, beauty creams and deodorants. The compound and its metabolites are recognized with estrogenic activity, so that it is linked with the occurrence of breast cancer (Lin et al., 2009). The chemical structure of MP is unique with an aromatic ring linked to a hydroxyl group and a methyl chain, both in para-position conferring the highly chemical stability of the compound. Consequently, MP is neither decomposed in biochemical treatment systems, nor in physical-chemical operations (e.g. coagulation, precipitation) of WTP's, such that it is often detected in surface water, groundwater and drinking water systems, as well as in breast milk (Soni et al., 2002; Eriksson et al., 2008; Schlumpf et al., 2010; Yu et al., 2012; Albero et al., 2012; Chen et al., 2012).

Caffeine with its psychoactive properties is not only a common ingredient of beverages, but also of some analgesic pharmaceuticals and personal care products (PPCPs) (Marques et al., 2013). As such, it is readily and uncontrollably discharged into sewage treatment facilities, where due to its high solubility (21.7 g L^{-1}) and low biodegradability, it bypasses the treatment operation. The presence of

caffeine in the effluents of sewage treatment plants is verified by its widespread occurrence in water, soil, and groundwater systems (Bruton et al., 2013).

Advanced oxidation processes, which rely on the production of hydroxyl radicals in water have been recently found effective for the elimination of compounds that exist at low concentrations and that are difficult to eliminate by conventional methods. Ultrasonic irradiation is a novel method of hydroxyl radical generation, and combination of ultrasound with AOP's (e.g. ozonation, UV irradiation, Fenton reaction) is extremely effective in the destruction and overall degradation of recalcitrant organic compounds. The power of such combinations is based on the synergy induced by acoustic cavitation through unique chemical, physical and catalytic effects (Ince et al., 2001).

Within these perspectives, this research is aimed to investigate the degradability of three classified PPCPs, namely salicylic acid, methylparaben and caffeine using ultrasound and combinations of it with Fenton reaction, catalytic adsorption and photocatalysis. In that respect, the contents of the dissertation will be presented under the following scheme:

- Chapter 2 involves a theoretical background of AOP's, sonochemistry, adsorption and photocatalysis supported by a thorough review of the current literature. In addition, an extensive overview of PPCPs, their presence in the water environment, the risks they impose to aquatic life and humans, and the reported techniques for their elimination are presented. Moreover, a review of the theory of Experimental Design is given.
- Chapter 3 involves a detailed description of materials, methods and design of experiments.
- Chapter 4 is a list of published and "under-review" articles.
- Chapters 5 and 6 involves presentation of the background information and results of the published articles
- Chapters 7, 8 and 9 involves presentation of the background information and results of the "under-review" articles.
- Chapter 10 is a summary of all findings, concluding remarks and suggestions for future work.

2. BACKGROUND AND LITERATURE REVIEW

2.1. Advanced Oxidation Processes (AOPs)

Chemical oxidation processes are widely practiced in water and wastewater treatment operations despite the kinetic limitations that the oxidants of these systems are object to. As such, more effective oxidation processes and technologies have been developed to convert complex and toxic organic compounds to less hazardous, and more biodegradable forms without kinetic restrictions (Ince et al., 2000). The most effective of all is the so called "Advanced Oxidation Processes" (AOPs) that are capable of in-situ production of hydroxyl radicals, as recognized with non-selectivity and strong oxidizing capacity most which are stronger than all conventional oxidizing agents. In that respect, the efficiency of AOPs is directly related to the rate of OH radical generation within a limited period (Legrini et al., 1993). Table 2.1 lists comparative reaction rate constants of O_3 and •OH with some selected groups of organic chemicals.

Table 2.1. Relative reaction rate constants (L mol^{-1} s^{-1}) of some organic pollutant groups with ozone and the hydroxyl radical (Mandal., 2018).

Compounds	**O_3**	**•OH**
Chlorinated Alkenes	10^{-1} to 10^{3}	10^{9} to 10^{11}
Phenols	10^{3}	10^{9} to 10^{10}
N-containing Organics	10 to 10^{2}	10^{8} to 10^{10}
Aromatics	1 to 10^{2}	10^{8} to 10^{10}
Ketones	1	10^{9} to 10^{10}
Alcohols	10^{2} to 1	10^{8} to 10^{9}
Alkanes	10^{-2}	10^{6} to 10^{9}

2.1.1. Homogenous AOPs

Homogeneous AOPs include ozonation, ozonation with peroxide, ozonation with UV-light and the UV-peroxide processes. Ozonation alone is an AOP only if the process is operated at highly alkaline pH, at which O_3 decomposes to produce OH radicals. At low pH, ozone is in molecular form and reacts selectively through direct electrophilic reactions (Soares et al., 2006).

The reaction of ozone with OH^- ions is given below (Mandal., 2018):

$$2O_3 + H_2O \xrightarrow{OH^-} \bullet OH + 2O_2 + HO_2 \quad (2.1)$$

Generation of •OH in O_3/H_2O_2 and O_3/UV processes proceed via the interaction of ozone with H_2O_2, and the photolysis of ozone, respectively, as presented in Eq (2.2) and (2.3). The rate of H_2O_2 photolysis in these systems is directly related to the incident power or intensity of light and the dose of H_2O_2, while that of organic matter degradation is a function of the quantity of O_3 and •OH available in solution (Muruganandham et al., 2014).

$$O_3 + H_2O_2 \rightarrow \bullet OH + O_2 + HO_2 \quad (2.2)$$

$$O_3 + hv + H_2O \rightarrow 2\bullet OH + O_2 \quad (2.3)$$

In UV/H_2O_2 process hydrogen peroxide is activated by UV light and hydroxyl radicals (•OH) are generated by the photolysis of hydrogen peroxide (Eq. 2.4). H_2O_2 photolysis rate directly depends on the incident power or intensity. In addition, the dosage of H_2O_2 needs to be optimized, since excess H_2O_2 may scavenge hydroxyl radical.

$$H_2O_2 + hv \rightarrow 2\bullet OH \quad (2.4)$$

2.1.2. Heterogeneous AOPs

Another important class of AOPs is based on the use of solid catalysts. Most common heterogeneous AOPs are heterogeneous photocatalysis and advanced Fenton reactions. The former is discussed within this section whereas the latter is described in Section 2.3.1.

Heterogeneous photocatalysis is an effective option for treatment of pollutants from water and wastewater. The method is based on “photo-excitation” of a solid semiconductor as a result of absorbing electromagnetic radiation. In these processes metal semiconductors are commonly used to treat pollutants by means of light induced reactions. TiO_2 as a non-toxic and inexpensive semiconductor is the most widely used photocatalyst. Less common photocatalysts are ZnO, Fe_2O_3, CuO, SiO_2, MgO, WO_3, CdS. ZnO, considered as the best alternative of TiO_2, is recognized with good opto-electronic, catalytic and photochemical properties and used successfully in photocatalytic degradation of organic pollutants in water (Sakthivel et al., 2003; Khodja et al., 2001). The literature

conveys that ZnO is more efficient than TiO_2 in the decomposition of diverse organic contaminants in aqueous solution (Sun et al. 2009; Yu & Yu 2008; Behnajady et al. 2006; Daneshvar et al. 2007; Daneshvar et al. 2004; Lizama et al. 2002; Gouvea et al. 2000; Dindar & Içli 2001). However, due to its high tendency to corrode under extreme pH conditions, it attracted less attention than TiO_2 despite its larger absorption of the solar spectrum (3.37 eV) (Khataee et al. 2015).

When photon energy absorbed by TiO_2 is equal to or greater than its band gap width, conduction band electrons and valence band holes are produced. The combination of the electron in the conduction band and the hole in the valence band is referred to as an electron-hole pair and this mechanism proceeds as follows (EPA, 1998):

$$TiO_2 + hv \rightarrow e^-_{CB} + h^-_{VB} \quad (2.5)$$

Electron-hole pair subsequently migrates to the semiconductor surface and initiates chemical reactions. At the TiO_2 surface, the holes react with either H_2O or OH^- to form •OH as follows:

$$h^+_{VB} + H_2O \rightarrow \bullet OH + H^+ \quad (2.6)$$

$$h^+_{VB} + OH^- \rightarrow \bullet OH \quad (2.7)$$

The formation and availability of •OH are maximized by addition of oxidants (H_2O_2, O_3). Nevertheless, commercial TiO_2 is made of small particles that easily agglomerate in aqueous solutions, leading to decreased photocatalytic activity and ineffective recovery (Khalfaoui-boutoumi et al., 2013). The disadvantages have been partly overcome by modifying the surface or bulk properties of TiO_2 via doping, code positioning of metals, surface chelation and combining two semiconductors (Bandara et al., 2004; Kutty and Avudaithai, 1990). More recently, synthesis of nanocomposites made with various support materials has attracted great attention for the improvement of the efficiency of TiO_2 in photocatalysis.

2.2. Sonochemistry

Sonochemistry is a field, which studies the enhancement of chemical reaction and mass transfer rates under various ultrasonic conditions. Ultrasound is defined as any sound wave at a frequency above the normal hearing range of human ear (i.e. above 16 kHz) as depicted in Figure 2.1. The mechanism causing sonochemical effects in liquids is the phenomenon of acoustic cavitation. When ultrasound waves propagate in a liquid medium, they generate a repeating pattern of compressions

and rarefactions to supply energy to the liquid phase. Compression and rarefaction cycles exert a positive and negative pressure on the liquid pushing or pulling the molecules together or away from one another, respectively (Suslick, 1990).

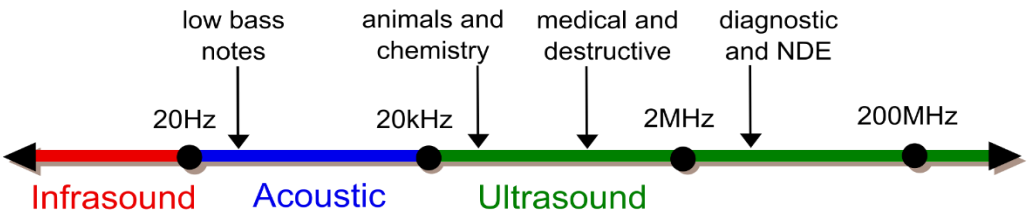

Figure 2.1. Ultrasound Range Diagram.

The phenomenon called acoustic cavitation consists of three successive stages: i) nucleation, ii) bubble growth (expansion), iii) implosive collapse as depicted in the Figure 2.2 (Suslick, 1990). In the first stage, microbubbles trapped in microcrevices of small particles within the liquid form cavitational nuclei, where cavities are generated depending on the type and purity of the liquid. (Suslick, 1990; Reisse, 1995).

In the second stage, the micro bubbles once formed grow and expand depending on the intensity of the applied sound, and when the intensity is too high, a small cavity may grow rapidly through inertial effects (Suslick, 1990). When the acoustic intensity is low, the cavity grows by rectified diffusion and lasts many more acoustic cycles before expansion (Suslick, 1990).

The third stage of cavitation occurs when the cavity is so overgrown that it can no longer absorb energy to sustain itself, and the surrounding liquid rushes in to lead to a violent implosion as a catastrophic collapse (Mason and Peters, 2002; Mason 1990; Suslick et al. 1990). At this point, the extremes of temperatures and pressures create an unusual environment or high-energy micro-reactors that enable molecular fragmentation of the entrapped gases in the collapsing cavities (Ince et al.,2001).

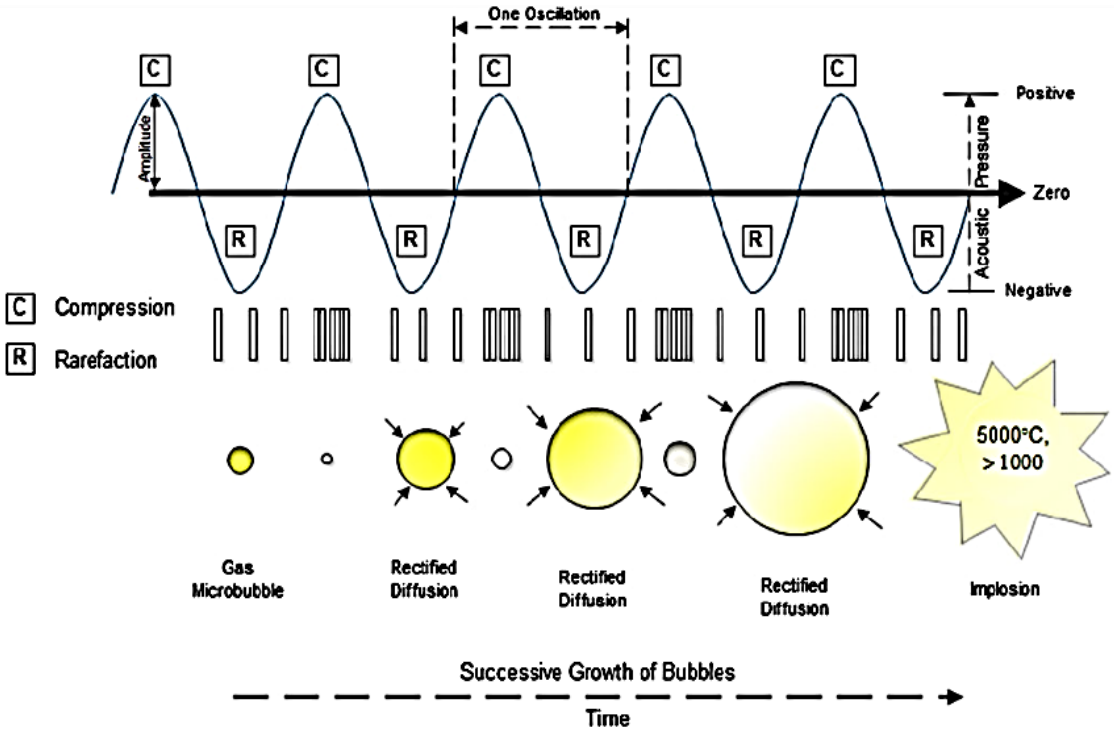

Figure 2.2. Stages of acoustic cavitation process (Abbas et al., 2013).

The reactions of hydroxyl radicals generated by sonication are shown in the following equations (Ince et al., 2001; Lorimer and Mason, 1991; Fischer et al., 1986):

$$H_2O +))) \rightarrow \bullet OH + \bullet H \text{ (pyrolysis)} \tag{2.8}$$

$$\bullet OH + \bullet H \rightarrow H_2O \tag{2.9}$$

$$2\bullet OH \rightarrow H_2 + O_2 \tag{2.10}$$

$$2\bullet OH \rightarrow H_2O_2 \tag{2.11}$$

$$2\bullet H \rightarrow H_2 \tag{2.12}$$

Chemical reactions in homogenous sonolysis proceed via radical intermediates (Ameta et al., 2018). It means that, homogenous sonochemistry is induced directly by the extreme conditions in collapsing microbubbles (Ince et al., 2001). Although many organic compounds can be degraded by homogenous sonication, the decomposition rates might still be slow for practical uses (Okitsu et al., 2005). Thus, considerable efforts have been made to accelerate the decomposition rates of organic contaminants in water by ultrasound. Previous studies found that the introduction of heterogeneous

surfaces increases the extent of interfacial cavitation. Thus, addition of solid particles serves as an additional nucleus increasing the numbers of cavitation events and accelerating the rate of decomposition (Bokhale, 2014; Xiao 2012; Khataee et al., 2018).

In heterogeneous sonochemical systems, enhancement of chemical reactivity is associated with the physical effects of ultrasound such as heat and mass transfer, surface activation, and disruption of the solid by the jetting phenomenon (Suslick, 1990). On the other hand, the solid particles may scatter the ultrasonic wave in water, weaken the energy dissipation into water, pertibute bubble distribution and decrease the removal efficiency. Therefore, understanding the effect of solid particles on sonolysis is important as their presence may exhibit different influences on degradation kinetics. In Section 2.2.2.6. more detailed information on the effect of solid particles on sonolysis is given.

Another consequence of acoustic cavitation in a liquid is the emission of light from the collapsing bubbles. Hence, in addition to driving chemical reactions, ultrasonic irradiation of liquids can also produce light and this phenomenon is called sonoluminescence (SL). Two types of SL are multi-bubble sonoluminescence (MBSL) and single-bubble sonoluminescence (SBSL) (Hilgenfeldt et al., 1999). MBSL is the light emission that occurs from a cloud of cavitating bubbles, whereas SBSL occurs from a single cavitating bubble. Due to increased sphericity of the collapse, which arises from the isolation of the bubble from perturbations, much higher temperatures and pressures are thought to be generated during SBSL compared to MBSL (Brenner et al., 2002).

Cavitational collapse produces “sonoluminescence”, i.e. an intense UV irradiation of a wide wavelength range (200–500 nm) (Suslick et al., 1999). The wavelengths shorter than 375 nm can excite the surface of TiO_2 just like in photocatalytic processes (Eren and Ince, 2010). The explanation for this phenomenon is the hot spot theory, which basically states that when a bubble collapses sufficiently fast, its contents are strongly compressed to lead to an adiabatic temperature rise for light emission in the form of short flashes (Suslick et al., 1999). The flash duration (and intensity) depends on several details of bubble collapse (such as frequency, sound pressure amplitude, type of liquid and the gas inside the bubble) (Bogdan et al., 2017).

2.2.1. The Reaction Sites in Acoustic Cavitation Processes

In homogenous sonochemistry there are three main reaction sites: the cavitation bubble, the interface between gas bubbles and the surrounding liquid, and the bulk solution, as schematized in Figure 2.3 (Adewuyi, 2001; Ince et al., 2001). The decomposition of organic molecules takes place either inside the bubble if they are highly volatile, or at the bulk liquid and the gas-liquid interface (Weavers et al., 1998). Oxidation reactions in the bulk solution are limited by the number of available, uncombined, free radicals migrated from the collapsing cavities and the interface into the bulk (Ince et al., 2001). Hydrophilic compounds with low volatility are not expected to migrate towards the bubble or the interfacial region, but rather remain in the bulk solution. Hydrophobic compounds that are highly volatile readily diffuse into the cavitation bubbles, where pyrolysis and oxidation with the OH radical are the predominant phenomena. Finally, the gas-liquid interface is the most probable reaction site for water contaminants, and owing to the high concentration of •OH (relative to that in the bulk solution) and sufficient pressure gradients and temperatures, the reactions proceed at considerably high rates.

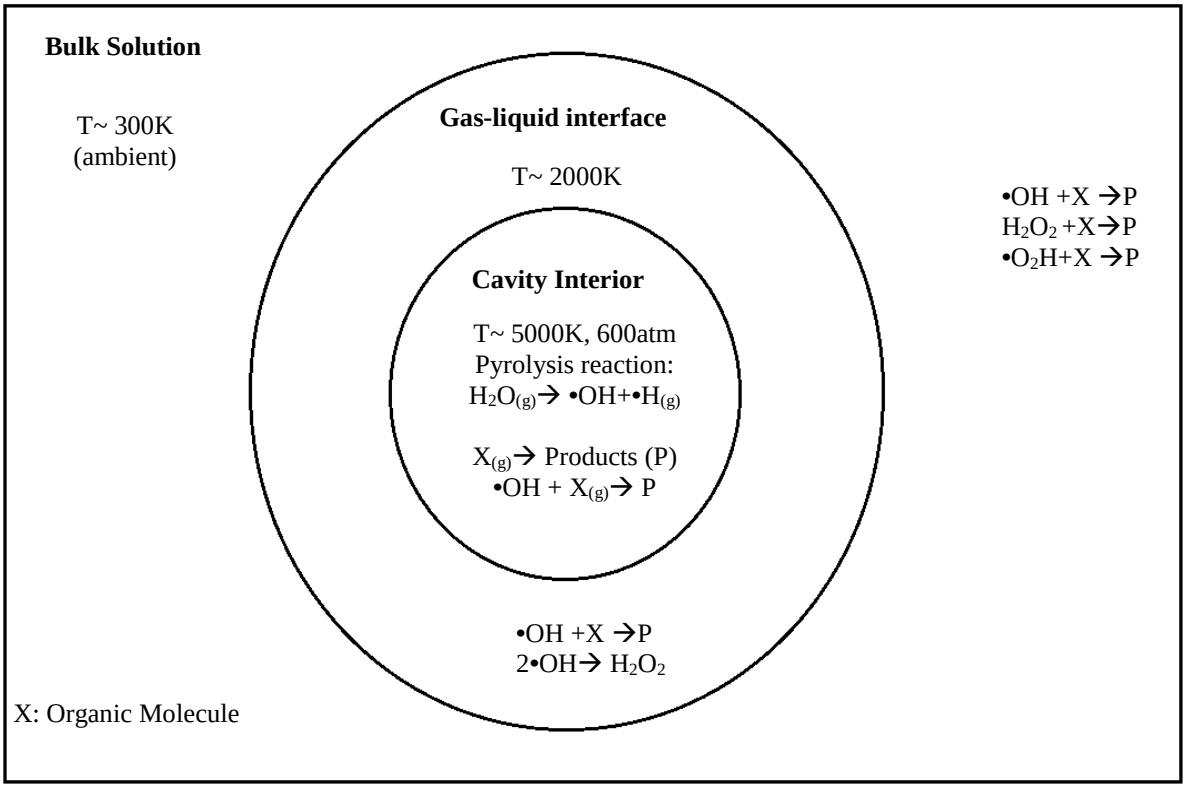

Figure 2.3. Main reaction sites in homogenous sonochemistry (Adewuyi, 2001; Ince et al., 2001).

The fate of highly soluble water contaminants in the bulk solution is related to the rate of •OH radical transfer from the bubble interior (and its interfacial sheath) into the solution bulk, which in

turn is a function of the lifetime and collapse duration of cavities, the intensity of the pressure, the geometry of the reactor and the frequency of the applied ultrasound waves (Lorimer and Mason, 1987; Mason and Peters, 2002). Some of these parameters are described in the following section.

2.2.2. Parameters Affecting Sonochemical Reactions

The main parameters affecting the sonolytic degradation efficiencies are the frequency of ultrasonic waves, properties of the target solute, power intensity, applied bubbling gas, temperature, physicochemical properties of the pollutant and addition of solids as catalysts to the system.

2.2.2.1. Frequency. Frequency has a very important role in sonication and three ranges are reported: (i) low frequency (20–100 kHz), (ii) medium frequency (300–1000 kHz), and high frequency (2-10 MHz) (Ince et al., 2001).

During low frequency sonication, a large number of compressions and rarefactions takes place which delays the collapse stage and allows volatile compounds move into the gas phase. Therefore, low frequency sonication might successfully decompose hydrophobic compounds as they easily diffuse into cavity bubbles and undergo pyrolysis inside the bubble or hydoxylation and thermal decomposition the gas-liquid interface. On the other hand, the delayed growth and elongated collapse of the bubbles causes radical scavenging and recombination reactions at the interfacial sheath, and inhibits the transfer of hydroxyl radicals into the bulk solution (Barbier and Petrier, 1996). When medium frequency ultrasound is applied larger energies are released into the liquid as a result of more rapid and violent collapse in “transient” cavitations (Suslick, 1994). As a result of the very short-lived bubbles and rapid collapse, radical scavenging hardly takes place in the gas phase and the interface. Therefore, medium frequencies are highly effective for advanced oxidation processes, which are aimed to destroy non-volatile organic pollutants in the liquid medium via free radical effects (Lepoint and Mullie, 1994; Petrier et al, 1992; Barbier and Petrier, 1996).

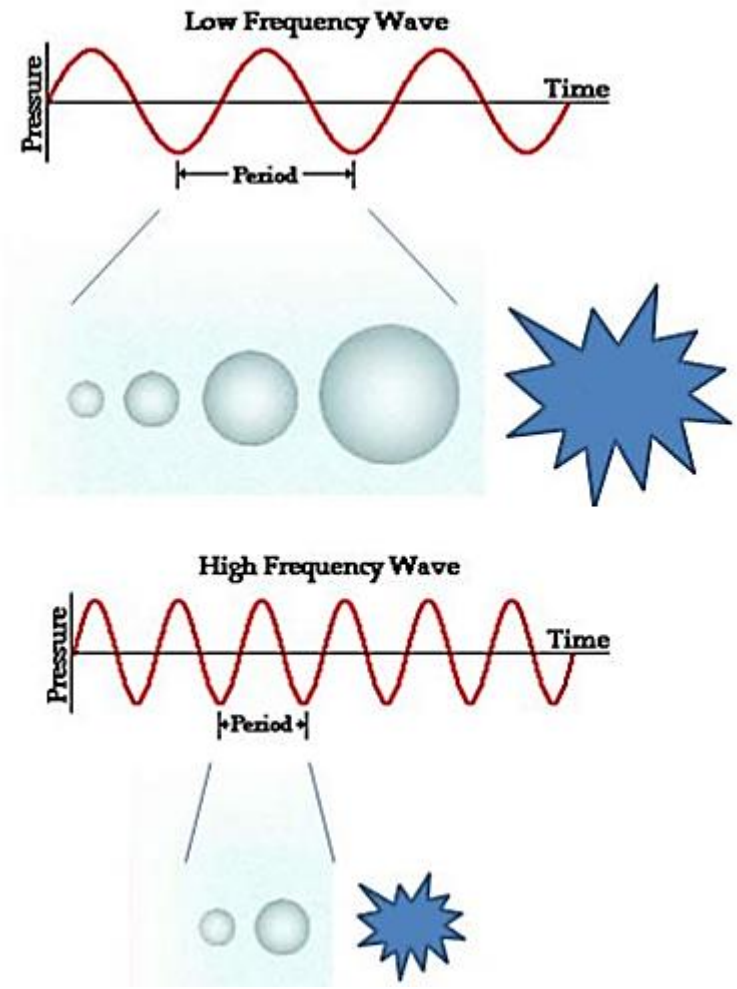

Figure 2.4. Effects of frequency (a) low-frequency ultrasound, (b) high-frequency ultrasound (Newman and Bettinger, 2007).

2.2.2.2. Power Intensity. The sonochemical reactions strongly depend on the intensity of the sound waves. In most cases, with increasing power, the reaction rate increases too. When high ultrasonic power is applied, a great number of cavitation bubbles are generated in the solution. However, many of these bubbles will come together to form larger, longer lived bubbles which will act as a barrier to the transfer of acoustic energy through the liquid which is known as the cushion effect (Mason, 1990). Therefore, it must be realized that intensity cannot be increased indefinitely.

2.2.2.3. Properties of Saturating Gas. During sonication dissolved gas bubbles serve as nuclei for cavitation. However, if gas flow is ended the solution will rapidly be free of dissolved gases as the first effect of cavitation is degassing (Mason, 1999). Therefore, in order to maintain a constant gas flow into the bubbles and sustain the "extreme" collapse conditions the liquid is continuously bubbled with a gas throughout the sonication (Ince et al., 2001). Employing gases with large polytropic ratio values are known to enhance the adiabatic conditions in the collapsing bubble and improve

sonochemical effects. For this reason, monatomic gases (He, Ar, Ne) are used in preference to diatomic gases (N_2, air, O_2). It was found that halogenic compounds are more efficiently broken down under argon, and the others (without halogens) are more efficiently degraded under air (Rooze et al., 2013). When air is selected as the bubbling gas, H_2O_2 generation is accompanied by the formation of nitrous and nitrogenous ion and larger yields are obtained due to the reaction of nitrogen with molecular oxygen to form nitric acid and radical species such as •OH, •NO_2, and •NO_3 accelerating the oxidation process (Mason and Lorimer, 2002; Kidak and Ince, 2006). Sonochemical reactions in the presence of air are as follows (Ullerstam et al., 2000):

$$2N_2+O_2 \rightarrow 2N_2O \tag{2.13}$$

$$2N_2O + H_2O \rightarrow 2HNO_2+2N_2 \tag{2.14}$$

$$\bullet H + N_2O \rightarrow N_2+\bullet OH \tag{2.15}$$

$$\bullet OH + N_2O \rightarrow 2NO + \bullet H \tag{2.16}$$

$$HNO_2+H_2O_2 \rightarrow HNO_3+H_2O \tag{2.17}$$

$$HNO_3 +))) \rightarrow \bullet OH + \bullet NO_2 \tag{2.18}$$

$$HNO_3 +))) \rightarrow \bullet H + \bullet NO_3 \tag{2.19}$$

2.2.2.4. Temperature. Due to increases in the surface tension or viscosity with decreasing temperature or due to decrease in the vapor pressure the threshold limit is reported to increase with decreasing temperature (Mason and Lorimer, 2002). Moreover, as the temperature increases the effects from cavitational collapse are reduced.

2.2.2.5. Physicochemical Properties of the Pollutant. Physicochemical properties of the compound are also very important as it determines the sonochemical reaction site. Hydrophobic compounds move into the gas bubble itself or the bubble-liquid interface (Alegria et al., 1989; Kontronarou et al., 1991; Drijivers et al., 1999). Therefore, power ultrasound at low frequencies (which generates long-lived “stable” cavities) is more effective for the pyrolytic destruction of such compounds (Ince et al., 2001; Kontronarou et al., 1991). Hydrophilic compounds (with low vapor pressures and low concentrations), on the other hand, tend to remain in the bulk solution due to the repulsive forces

between the compound and the slightly hydrophobic bubble surfaces. Therefore, their destruction depends on the quantity of hydroxyl radicals ejected to the liquid medium which is maximum during medium frequency sonication (where collapse is "transient") (Ince et al., 2001; Drijvers et al., 1999). Thermal decomposition of such non-volatile compounds may also occur at the bubble-liquid interface, but hydroxylation in the bulk medium is much more effective.

2.2.2.6. Addition of Solids. Solid catalysts, such as ceramic disks, Al_2O_3, SiO_2, talc and glass beads are widely used to enhance cavitation effects in the reaction medium. In pure liquids, cavity bubbles are spherical during collapse because its surroundings are uniform. In the presence of a solid surface, the cavity collapse dynamics change dramatically. Approaching to a solid boundary, cavity collapse is very asymmetric and generates high-speed jets of liquid (Suslick, 1994). Liquid jets drive into the heterogeneous surfaces with velocities of roughly 400 km h^{-1} and cause severe damage at the point of impact producing newly exposed, highly reactive surfaces (Suslick, 1994). The physical and chemical effects of heterogeneous cavitation are represented in Figure 2.5.

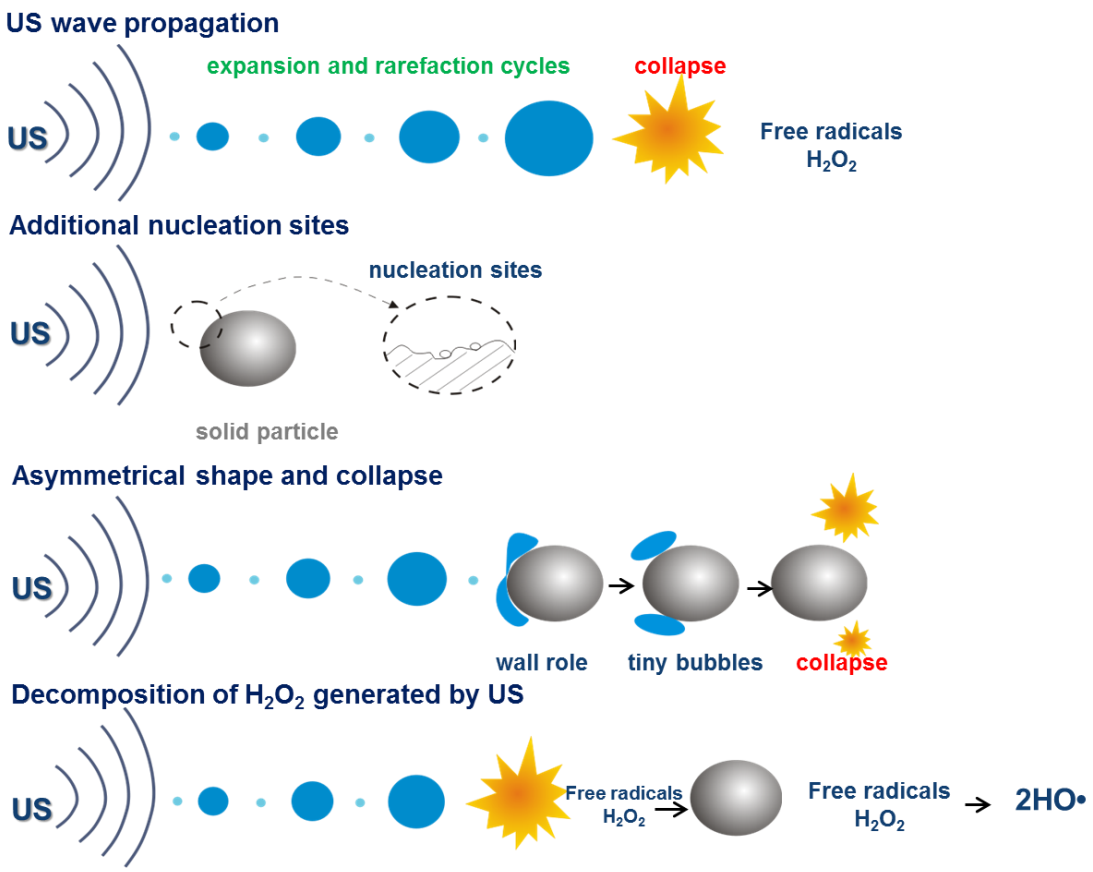

Figure 2.5. The physical and chemical effects of heterogeneous cavitation.

2.2.3. Application of Ultrasound in Water Decontamination

In the last two decades, considerable interest has been shown in the application of ultrasound as an AOP for water decontamination. As described in the section 2.2, sonication of water leads to extreme reaction conditions leading to thermal decomposition of water to produce hydroxyl radicals. Under these conditions all organic pollutants including chlorinated solvents, herbicides, substituted ethers, natural organic matter, surfactants, textile dyestuff, endocrine disrupting compounds (EDCs), pharmaceuticals and personal care products (PPCPs) are decomposed by reactions with these radicals and direct pyrolysis.

Many researchers investigated the effect of ultrasonic irradiation as a pre-treatment operation to reduce the toxicity and to improve the biodegradability in untreated effluents prior to secondary treatment (Gonze et al., 1999). Moreover, a large number of studies have been conducted on the application of ultrasound as a post-treatment technique for destruction of refractory compounds in effluent streams (Naddeo et al., 2010). It was concluded that ultrasound is not only a highly effective pre-treatment tool to improve biodegradability but also an effective post-treatment option for elimination of refractory compounds from water. However, much of the experiments of ultrasonic treatment were carried out at laboratory scale.

Advantages of ultrasound in water treatment are low maintenance requirements and low energy efficiency of alternative methods (e.g., ozonolysis, UV photolysis). Furthermore, ultrasound waves have the ability to be transmitted perfectly through opaque systems, unlike that of ultraviolet light (Ince et al., 2001). Therefore, in contrast to many other processes which are negatively affected when suspended solids of effluent increase, in ultrasonic processes efficiency may even improve by increase of turbidity or suspended solids (Mahvi, 2009; Mason and Lorimer 2002). If the reaction mechanism is pyrolysis, cavitational intensity and efficiency can be increased by the addition of solid particles, gases and adjustment of other parameters discussed in the previous section. If the main reaction mechanism is free radical attack, combination of ultrasound with other advanced oxidation process (hydrogen peroxide, ozone and photocatalysis) is reported to successfully improve the system (Kidak and Ince, 2007).

2.2.4. Sonochemical Synthesis of Nanoparticles

One of the most important applications of sonochemistry has been the synthesis of nanoparticles. Among a variety of methods, ultrasonic techniques have received special attention via their ability to provide very small dimensions as 2-50 nm. (Caruso, 2002). Some of these fine particles, owing to their massive surface area are demonstrated to act as excellent catalysts in water chemistry. Sonolytic production of nanoparticles involves the reduction of metals by primary and secondary radicals, which generate during the formation, growth and violent collapse of acoustic cavity bubbles. (Zhang et al., 2008; Mizukoshi et al., 1999). The chemical reactions describing the process are as follows (Mizukoshi et al., 1999):

$$H_2O \rightarrow \bullet OH + \bullet H \tag{2.20}$$

$$\bullet H + \bullet H \rightarrow H_2 \tag{2.21}$$

$$\bullet H + \bullet OH \rightarrow H_2O \tag{2.22}$$

$$RH + \bullet OH \text{ (or } \bullet H) \rightarrow \text{reducing species} + H_2O \text{ (or } H_2) \tag{2.23}$$

$$RH + H_2O \rightarrow \bullet R + \text{unstable products} \tag{2.24}$$

$$M^{+n} + \bullet H/H_2/\bullet R \rightarrow M^0 \tag{2.25}$$

where: M^{n+} corresponds to a metal ion and RH to an organic additive

Reactions 2.20 and 2.21 show the formation of reducing agents: (i) •H from pyrolysis of water inside the collapsing cavity bubbles, (ii) H_2 from the reaction of RH with •OH or •H. Reaction 2.24 show the formation of secondary radicals (•R) from pyrolysis of the organic additive. In the presence of these species the metal salt is readily reduced to the zero-valent form (M^0), which is then converted to M^0_{n+1} via adsorption onto M^0_n. The organic additives, which function as stabilizers are generally alcohols, surfactants and water soluble polymers.

Preparation of metallic nanoparticles by sonochemical techniques is closely related to the ambient and applied conditions, such as temperature, contact time, metal concentration, frequency, and organic additives (Caruso et al., 2002; Brotchie et al., 2008). For example, the particle size is inversely proportional to the concentration of the stabilizer (e.g. an alcohol) and the alkyl chain length

due to the fact that alcohols adsorbed on the surface of metal nuclei restrict the enlargement of particle size via stabilization (Caruso et al., 2002; Bang and Suslick, 2010). The type and concentration of dissolved gases in solution also effects the rate of reduction and faster rate are achieved in the presence of monoatomic gas molecules (due to higher collapse temperatures) (Okitsu, 2018). Applied frequency also plays a critical role in controlling particle size (Okitsu et al., 2005). The effect of frequency is based on the fact that sonochemical reactors are subject to standing waves, i.e. the number of active cavitating bubbles is a function of the frequency and reaction volume (Okitsu et al., 2005).

The synthesis of nanoparticles by sonochemical methods may be an alternative as a green reductant source for green chemistry if combined with natural eco-friendly starting materials and stabilizing agents. The distinctive advantages of this method over all chemical methods (e.g. sodium borohydride, hydrogen, alcohol) are: i) no chemical addition (except the stabilizer); ii) reasonably fast reaction rates; and iii) production of ultra-fine particles (Zhang et al., 2008).

2.3. Other Processes and Reactions Related to the Study

2.3.1. Fenton and Advanced Fenton Reactions

The oxidation processes utilizing Fe^{+2} salts to activate H_2O_2 are referred to as classical Fenton‘s reactions (Dewil et al., 2005). In classical Fenton process, reaction between dissolved Fe^{2+} and H_2O_2 in acidic aqueous solution leads to oxidation of Fe^{2+} to Fe^{3+} and formation of the highly reactive •OH.

$$Fe^{2+} + H_2O_2 \rightarrow Fe^{3+} + \bullet OH + OH^- \text{ (chain initiation)} \quad (2.26)$$

$k_1 \approx 70\ M^{-1}\ s^{-1}$ (Rigg et al., 1954)

$$\bullet OH + Fe^{2+} \rightarrow OH^- + Fe^{+3} \text{ (chain termination)} \quad (2.27)$$

$k_2 \approx 3.2 \times 10^8\ M^{-1}\ s^{-1}$ (Buxton and Greenstock, 1988)

The newly generated ferric ions may also react with hydrogen peroxide and decompose it into water and oxygen. Moreover, ferrous ions and $HO_2\bullet$ radicals are formed during the reactions. The reactions are shown in the following:

$$Fe^{3+} + H_2O_2 \leftrightarrow Fe^{2+} + HO_2\bullet + H^+ \quad (2.28)$$

$k_3 \approx 0.001\text{-}0.01\ M^{-1}\ s^{-1}$ (Walling and Goosen, 1973)

$Fe\text{-}OOH^{2+} \rightarrow HO_2\bullet + Fe^{2+}$ (2.29)

The reaction of hydrogen peroxide and ferric ions is known as the Fenton-like reaction.

$Fe^{2+} + HO_2\bullet \rightarrow Fe^{3+} + HO_2^-$ (2.30)

$k_4 \approx 1.3x10^6\ M^{-1}\ s^{-1}$ (at pH=3) (Bielski et al., 1985)

$Fe^{3+} + HO_2\bullet \rightarrow Fe^{2+} + O_2 + H^+$ (2.31)

$k_5 \approx 1.2x10^6\ M^{-1}\ s^{-1}$ (at pH=3) (Bielski et al., 1985)

$\bullet OH + H_2O_2 \rightarrow H_2O + HO_2\bullet$ (2.32)

$k_6 \approx 3.3x107\ M^{-1}\ s^{-1}$ (Buxton and Greenstock, 1988)

As seen in the reactions (2.26) and (2.32), H_2O_2 is both an initiator and an •OH scavenger, particularly when its concentration is high. The generated •OH radical can react effectively with a variety of organic compound (RH) as follows:

$RH + \bullet OH \rightarrow H_2O + R\bullet$ (chain propagation) (2.33)

$R\bullet + H_2O_2 \rightarrow ROH + \bullet OH$ (2.34)

$R\bullet + O_2 \rightarrow ROO\bullet$ (2.35)

The radicals (R•) produced in reaction 2.33 may then react with Fe^{3+} (oxidation) and Fe^{2+} (reduction) as shown in the following reactions:

$R\bullet + Fe^{3+}$- oxidation$\rightarrow R^+ + Fe^{2+}$ (2.36)

$R\bullet + Fe^{2+}$- reduction$\rightarrow R^- + Fe^{3+}$ (2.37)

Reactions (2.26), (2.27), (2.33) and (2.36) constitute the general sequence of Fenton's reaction chain (Neyens and Baeyens, 2003). According to Deng and Englehardt (2006), although Fe^{3+} can be reduced to Fe^{2+} through reaction (2.31), the rate is several orders of magnitude slower than that of Fe^{2+} - Fe^{3+} conversion through reaction (2.27). And the formed Fe^{3+} may precipitate to iron oxyhydroxides, particularly as pH is increased.

The application of the classical Fenton process depends on the amount of ferrous ion in the solution and limited by the system's ability to regenerate it. Advanced Fenton process utilizes zero-valent iron (ZVI) (which is the solid form of iron) for the generation of hydroxyl radicals from zero-valent iron/Fe^{2+} recycling (Devi et al., 2009). When zero-valent iron is used as the catalytic source of iron, the surface of the metal iron corrodes producing insitu ferrous ions which react with hydrogen peroxide and generate hydroxyl radicals. Catalytic activity of ZVI depends on the reactivity of iron to initiate surface reactions. A simplified reaction scheme occuring in water during advanced Fenton oxidation is the following (Güyer and Ince, 2010):

$$Fe^0(s) + 2H_2O(aq) \rightarrow Fe^{2+}(aq) + 2OH^-(aq) + H_2(g) \quad (2.38)$$

$$Fe^0 + H_2O_2 \rightarrow Fe^{2+} + 2OH^- \quad (2.39)$$

$$Fe^{2+} + H_2O_2 \rightarrow Fe^{3+} + \bullet OH + OH^- \quad (2.40)$$

$$Fe^{2+} + \bullet OH \rightarrow Fe^{3+} + OH^- \quad (2.41)$$

$$Fe^{3+} + H_2O_2 \rightarrow Fe^{2+} + \bullet OOH + H^+ \quad (2.42)$$

One major advantage of using iron powder instead of iron salts is the avoidance of loading aquatic systems with counter anions. Moreover, in comparison to the classical Fenton process significantly lower concentrations of ferrous ion and ferric ion are achieved in wastewater treated by advanced Fenton process. In addition, recycling of ferric iron at the iron surface speeds up the process through the following reaction:

$$2Fe^{3+} + Fe^0 \rightarrow 3Fe^{2+} \quad (2.43)$$

2.3.2. Adsorption by Sepiolite

Adsorption is a powerful technique for removing organic and inorganic contaminants from water. The process is defined as the adhesion of atoms, ions or molecules from a gas, liquid or dissolved solid to a surface (adsorbent). The most common adsorbents for aqueous solutions and industrial wastewater are activated carbon, natural or modified biochar, and clay minerals with their unique surface properties. The most commonly used clay minerals in adsorption processes are montmorillonite, hectorite, sepiolite, laponite, saponite, rectorite, vermiculite, zeolite, kaolinite, and

chlorite (Han et al., 2019). The performance of all in adsorption is related to their surface area, porosity and pH, while the efficiency of adsorption is also a matter of the pollutant type. Clay minerals are very special not only due to their unique surface properties, but also via the presence of reactive groups on them to promote oxidative and reductive decomposition of the adsorbed species in the surface.

Sepiolite is a natural clay mineral found widely in Eskişehir. It is a hydrated magnesium silicate with a needle-like structure, high specific surface area (>300 m^2/g), a slightly negative charge (low cation exchange capacity), and considerable hydrophilicity (due to the high density of silanol (-SiOH) groups in its composition). The structure of sepiolite is presented in Figure 2.6. The chain-like structure produces needle-like particles that are arranged in such a way to form loosely packed and porous aggregates with an extensive capillary network associated with the high porosity (~0.4 cm^3/g) and light weight of the mineral.

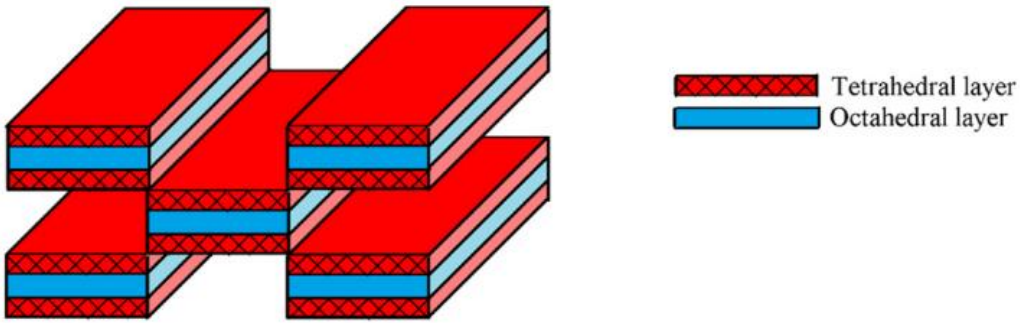

Figure 2.6. The structure of sepiolite (Cecilia et al., 2018).

Most clay minerals including sepiolite are originally land materials and require surface modification before using as catalysts. All of the modification techniques are based on creation of secondary pores and extending of the external surface area to enhance the adsorption capacity (Mabovu 2011). The modification is carried out in one of three ways namely: i) acid activation, ii) traditional ion exchange, iii) sonolytic polymerization/intercalation.

During activation of sepiolite by acidification the magnesium octahedral sheet dissolves, leading to an increase in the porosity and the surface area of the adsorbent with simultaneous opening of the inaccessible sites and formation of longer channels within the clay structure (Perez-Pariente et al. 1988; Rodriguez et al. 1994; Dekany et al. 1999; Sabah and Majdan 2009; Rodriguez et al. 1995). It has been reported that the discontinuous octahedral sheets of sepiolite provide available open tunnels with edges of broken bonds at either side (Watanabe et al. 2000; Garcia-López et al. 2010). The amount and type of acid sites can be increased if more tunnels, edges and broken bonds are created

by proper acidic activation (Rodriguez et al. 1995), and this enhances both the porosity and the specific surface area (Ahlrichs et al. 1975; Celdeira et al. 2014). Finally, the acid-activation of sepiolite results in the loss of about half of the zeolites and hydroxyl water from the structure, as a consequence of which the micropores plug and the crystal structure collapses (Ruiz-Hitzky 2001).

Cation exchange method is commonly used usually to remove ions from the structure of clay material and to convert it to the homo-ionic form (Semmens and Martin 1988). Modification of sepiolite by the cation exchange method with sodium chloride provides two advantages if the solid is used as a support material to TiO_2: i) it enhances the formation of TiO_2 particles on the surface of sepiolite, ii) it increases the adsorption capacity of the semiconductor (Khalaf et al. 1997). Once, the sodium form of sepiolite (Na-Sepiolite) is obtained, ion exchange by any other alkali or transition metal is very easy (Corma et al. 2004).

Sepiolite and other layered silicate clays are naturally hydrophilic such that they are not suitable for mixing and interacting with polymeric matrices (Giannelis 1996). Hence, making a composite out of untreated clay is not feasible unless the surface is treated to enhance its ability of interaction with the matrix. The use of sonication as a method of particle size reduction is very popular owing to the unique properties of cavitational collapse that leads to the formation of microjets and shock wave impacts on the surface together with interparticle collisions. As such, sonication of clay solutions delaminates and reduces the particle size (Pérez-Rodriguez et al. 2002; Wiewióra et al. 2003; Franco et al. 2004), while increasing the surface without altering the amount of micropores (de Haro et al. 2005). Sonication also prevents agglomeration of nano-fillers in the polymeric matrix, which is the primary challenge in preparing nanocomposite materials (Jordan et al. 2005). Sonication is also effective for hydrogel production in the absence of any chemical initiators via generation of free radicals during cavity collapse (Teo et al. 2010; Cass et al. 2010; Shirsath et al. 2011; Sandhya et al. 2013; Kumar et al. 2002; Khaled et al. 2007).

2.3.3. Photocatalysis with immobilized TiO_2

As described in Section 2.1.2., photo-excitation of TiO_2 with light of an energy greater than its band gap energy generates electron-hole pairs and initiates heterogeneous photocatalytic reactions. However, due to its limited photo response range (<380 nm) TiO_2 shows low efficiency under UV-visible region. Furthermore, small specific surface area, easily corroded surface, rapid recombination of electron-hole pairs and low adsorption ability are other drawbacks associated with the use of non-modified TiO_2 (Asahi et al., 2001; Zhang et al., 2008). To overcome these limitations, various

strategies such as doping with various transition metal ions, metal coating, surface sensitization and semiconductor coupling have been adopted (Li and Li, 2002; Huet al., 2003; Sivalingam et al., 2003; Arana et al., 2004; Carp et al., 2004).

Since heterogeneous photocatalytic reactions occur on the photocatalyst surface, adsorption of the target contaminants is important for their degradation. Therefore, immobilization of TiO_2 onto porous solids is a promising tool in the development of effective and high-quality photocatalysts. The value of the method rises from the formation of nanocomposite materials with high specific surface area and porosity that enable reactions on and at the surface boundaries (Akkari et al., 2018).

Research with clay-supported TiO_2 nanocomposites has demonstrated the suitability of this modification for all kinds of applications. Sepiolite is a natural inexpensive and widely available clay mineral with reactive surfaces, so that it is a very attractive support material for immobilizing TiO_2 nanoparticles. It has been reported that sepiolite-TiO_2 composites have high adsorption capacity and photoactivity relative to TiO_2 (Chen and Dionysiou 2008; Dvininov et al., 2009). In addition, sepiolite is reported to facilitate the migration of oxygen species to and away from the surface of the immobilized catalyst (Suarez et al., 2006; Guisasola et al., 2005). Moreover, embedding of TiO_2 nanoparticles within the structure of sepiolite has been demonstrated to avoid the formation of macroscopic aggregates of photoactive particles, protect the erosion of the semiconductor surface and decrease the band gap energy of TiO_2 (Zhang et al., 2014; Kibanova et al., 2009).

In summary, the use of sepiolite as a support material, particularly after surface modification, brings a positive synergy to the catalytic performance of the TiO_2 (Rytwo et al., 1998; Alkan and Dog, 2005; Zhang et al., 2011; Shi and Yang, 2009; Suárez et al., 2008; Aranda et al., 2008). The schematic illustration of mechanism of the activation of photocatalytic activity sepiolite/TiO_2 is given in Figure 2.7.

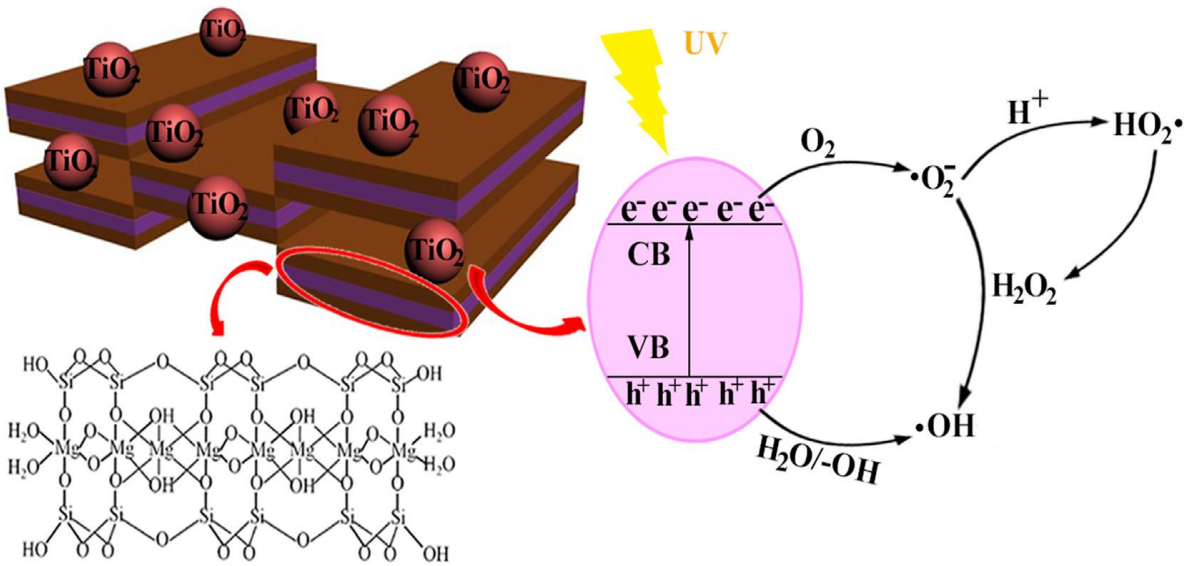

Figure 2.7. The schematic illustration of immobilized TiO_2 (Liu et al., 2017).

2.3.4. Methods of Sepiolite-TiO_2 Nanocomposite Synthesis

The most common means of producing sepiolite-TiO_2 nanocomposites are the "sol-gel", "surfactant-tinplating colloidal", "potassium pyrosulfate melting", "mild solid-state sintering" and "boiling reflux" (Zhang 2014; Karamanis et al. 2011, Aranda et al. 2008, Shi & Wang 2009, Liao et al. 2016, Wang et al. 2006). The most common of all is the "sol–gel" method using an alkoxide precursor followed by calcination treatment (Danks et al., 2016). Even though sol-gel is a very popular technique it has its own disadvantages such as high cost of precursors, shrinkage of a wet gel upon drying and weak bonding inside the product. Moreover, formation of gel is a slow process, which makes sol gel a time consuming technique compared to other methods such as ultrasound. The use of ultrasound for synthesizing sepiolite-semiconductor nanocomposites is rare, but very attractive due to the unique advantages of ultrasound and its performance as a green technology.

Ultrasonic techniques are attractive for intercalation of noble nanoparticles into separated silicate layers of sepiolite to enable a drastic decrease in the reaction time and an increase in the interlamellar space (Belova et al., 2009). Hence, cavitation facilitates the dispersion and penetration of TiO_2 nanoparticles into the interlayer spacing of layered structures (Wetzel et al., 2003; Cho et al. 2006; Belova et al. 2008; Morgan & Harris 2004; Jokar et al. 2017). The advantages of ultrasound over conventional methods of sepiolite-semiconductor synthesis are as follows (Jokar et al. 2017; Katdare et al. 2000; Sonawane et al. 2008):

1) acceleration of the diffusion of the intercalating pillaring species
2) enhancement of mechanical properties
3) increasing the number of nano-clay clusters
4) reducing the size of nano-clay clusters
5) improving the adsorption capacity
6) increasing the micro-porosity
7) reducing the reaction times
8) increasing the yields

2.4. Introduction to Pharmaceuticals and Personal Care Products (PPCPs) and Their Elimination from Water

Pharmaceuticals and Personal Care Products (PPCPs) comprise a large group of chemicals and are defined as products used for personal health (prescription and non-prescription drugs), cosmetic reasons (cosmetics, fragrances, soaps, lotions, toothpastes and sunscreens) and agribusiness (veterinary medicines). These compounds are washed of human body, excreted, or directly disposed to the sewage system. Hence, huge amount of PPCPs are dispersed every year. As many PPCPs are stable against biodegradation they are only partially eliminated when passing through conventional wastewater treatment plants (WWTPs) (30–90% efficiency) (Pietrogrande and Basaglia 2007). Residuals either end up in receiving waters or adsorbed in sewage sludge that might be used in fertilizers. It is well established that PPCPs enter surface water mainly through insufficiently treated effluents of WWTPs. These compounds can also enter into the soil environment and groundwater through reuse of wastewater on agricultural lands. Sources and pathways of PPCPs in the environment is shown in Figure 2.8.

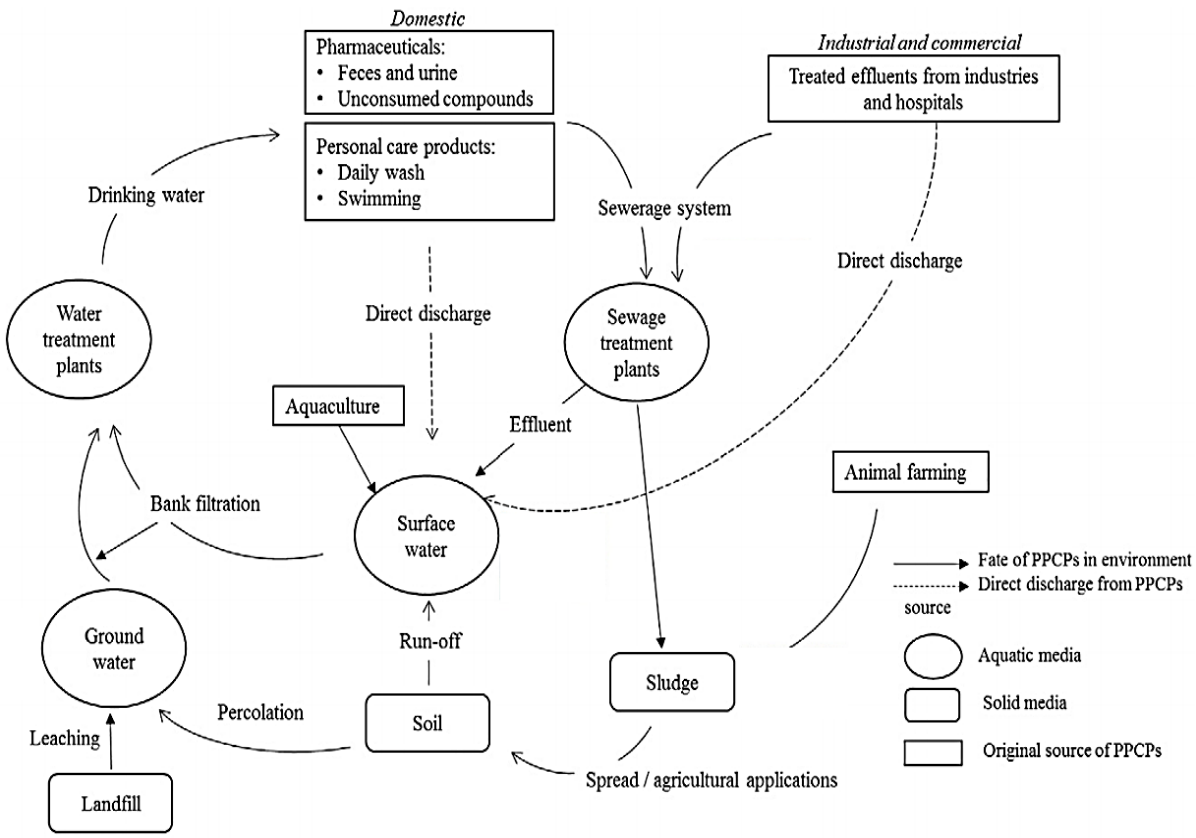

Figure 2.8. Sources and pathways of PPCPs (Yang et al., 2017).

Since a variety of PPCPs have been detected in the environment at concentrations reaching µg/L, many countries have concerned about the adverse health effects on humans, other living organisms and ecosystem (Ashton et al., 2004; Calamari et al., 2003; Glassmeyer et al., 2005; Bendz et al., 2005; Gros et al., 2006; Moldovan, 2006; Hummel et al., 2006; Zuccato et al., 2008). Moreover, compounds of a low persistence might even cause unwanted effects in the environment due to synergic effects through combined parallel action (Fent et al., 2006). List of some PPCPs identified in environmental samples and their potential risks are shown in Table 2.2.

Table 2.2. PPCPs identified in environmental samples and their potential effects (Yang et al., 2017; Zhang et al., 2019; Dev et al., 2019).

PPCP Class	Compound Name	Use/Origin	Potential Risks
Antibiotics	Sulfonamides, trimetoprim, fluoroquinolones, chlortetracycline, lincomycin, erythromycin, oxytetracycline, tetracycline, roxithromycin, tylosin	To treat bacterial infections in both humans and animals	Antibiotic resistance
Analgesics/non-steroidal anti-inflammatories (NSAIDs)	Acetaminophen, ibuprofen, diclofenac, naproxen ketoprofen, indomethacine, phenazone	Analgesic, anti-inflammatory and antipyretic	Chronic toxicity to non-targeted organism under prolonged exposure
Antiepileptics	Carbamazepine	To stop, prevent, or control seizures	Persistence in the environment
Hormones	Estradiol, 17-Ethinyl Estradiol, Testosterone, Progesterone	To regulate specific body functions in the absence of naturally produced hormones	Bioaccumulation within aquatic organisms
Musks fragrances	Nitromusks, tonalide, polycyclic musks, galaxoline	Commonly used in perfumery	Bioaccumulation within fish

2.4.1. Current methods of PPCP Destruction in Water

2.4.1.1. Biochemical Degradation Processes. Activated sludge biological treatment is the most commonly used and the cheapest available technology for removal and degradation of contaminants. However, in the case of PPCPs, these micropollutants are only partly removed by activated sludge sewage treatment (Johnson et al., 2011). Table 2.3 presents the removal efficiency of PPCPs in the WWTPs. Even though long sludge retention times improved the removal of some PPCPs by activated sludge treatment, only a few of the PPCPs were completely degraded and most existing WWTPs are not designed for such long sludge retention times (Katsoyiannis et al., 2006; Oulton et al., 2010; Carballa et al., 2004).

Table 2.3. Presence of PPCPs in the Environment and Their Elimination by WWTPs.

PPCP	Surface Water	Groundwater	WWTP Influent	WWTP Effluent	References
		(ng L^{-1})			
Antibiotics					
Sulfamethazine	164	252	7400	110	Yang et al., 2017
Tetracycline	44.9	141	257	152	Chen et al., 2018, López-Serna et. al., 2013, Yang et al., 2017
Ofloxacin	7.1-630	367	1020	980	Chen et al., 2018, López-Serna et. al., 2013, Fick et al., 2009, Yang et al., 2017
Antiepileptic drugs					
Carbamazepine	1075	390	15780	7570	Heberer et al., 2002, Yang et al., 2017
β-Blockers					
Propranolol	3060	-	638	388	Beale et al., 2010, Yang et al., 2017
Hormones					
Estrone	170	-	41	2.5	Kolodziej and Sedlak 2007, Yang et al., 2017
17β-Estradiol	93	6-66	8.6	1	Ying et al., 2009, Yang et al., 2017
Estriol	8	-	13	10	Lei et al., 2009, Yang et al., 2017
NSAIDs					
Diclofenac	380	121	1660	430	López-Serna et. al., 2013, Yang et al., 2017
Ibuprofen	37000	1500	2800	720	Yang et al., 2017
Bactericides/disinfectants					
Triclosan	2300	2110	892	202	Chalev and Halden 2009, Stuart et al., 2012, Yang et al., 2017
Triclocarban	2506750	12-36.2	1150	49	Chalev and Halden 2009, Montes-Grajales et al., 2017, Yang et al., 2017
Preservatives					
Butylparaben	14	-	15-27	3	Carmona et al., 2014,
Methylparaben	2600	5000	290-10000	6-334	Carmona et al., 2014, Stuart et al., 2012, Yang et al., 2017
Propylparaben	145	5500	520-2800	2-210	Carmona et al., 2014, Stuart et al., 2012, Yang et al., 2017

Table 2.3. Presence of PPCPs in the Environment and Their Elimination by WWTPs (cont.).

PPCP	Surface Water	Groundwater	WWTP Influent	WWTP Effluent	References
		(ng L^{-1})			
Sunscreen UV filters					
2-Ethyl-hexyl-4-trimethoxycinnamate	10-2013	-	462	150	Bratkovics and Sapozhnikova 2011, Yang et al., 2017
Other PPCPs					
Caffeine	194-517	16-164	5860	108	Reif et al., 2006, Karnjanapiboonwong et al., 2011, Sui et al., 2011, Yang et al., 2017
Salicylic Acid	4100	43.7-2014.7	640-2000	140	Ternes et al., 1998, Heberer et al., 2000, Yang et al., 2017

PPCPs removal by activated sludge process is a combined effect of volatilization, adsorption and biodegradation (Li et al., 2015; Suarez et al., 2010). Usually, volatilization occurs during aeration and its contribution to PPCPs removal is usually less than 10%. Adsorption of PPCPs to activated sludge depends on the physicochemical properties of the pollutant and environmental conditions. Biodegradation is the main PPCP removal mechanism in activated sludge process. Therefore, biological acclimation and bioaugmentation of pure or mixed culture (capable of removing PPCPs) can be used for enhancement of PPCPs removal in biological treatment process (Wang et al., 2016).

Pure cultures isolated from activated sludge, sediment or wastewater, have been used successfully in a number of studies for PPCPs removal (Popa et al., 2014; Reis et al., 2014; Hu et al., 2013; Almeida et al., 2013; Zhang et al., 2013; Zhou et al., 2014). Moreover, some pure cultures isolated from the activated sludge does not only degrade a specific PPCP but a wide range of PPCPs (Reis et al., 2014). Mixed cultures are easier to achieve than pure cultures and they also have capacity to remove PPCPs (Khunjar et al., 2011). In some instances, activated sludge poorly removes PPCPs and in order to improve the efficiency addition of mixed culture into the activated sludge has been reported (Zhou et al., 2014). Moreover, by mixed culture higher biodegradation rates were achieved in removing the mixed PPCPs compared to removing individual PPCPs (Vasiliadou et al., 2013). This is attributed to the use of some PPCPs as carbon and energy source by mixed culture, promoting the decomposition of other PPCPs.

2.4.1.2. Physical Methods. Adsorption is one of the main processes often used for removal PPCPs in the environment. Carbon-based adsorbents, such as activated carbon, graphene and carbon nanotubes

have been widely studied for PPCP removal. Activated carbon as a traditional adsorbent is reported to remove some PPCPs (Wang and Wang 2016). The charge and hydrophobicity of the compound determines the adsorption capacity of activated carbon (Rodriguez et al., 2016). Other important factors for PPCP removal using activated carbon are contact time (Nam et al., 2014), pH (Mestre et al., 2007) and structure of activated carbon (Mestre et al., 2007). However, with the increase of operation time two problems were reported: decrease of adsorption capacity and deterioration of activated carbon in the complex wastewater systems (Wang and Wang, 2016). Moreover, activated carbon has a low adsorption capacity for macromolecular substance which is attributed to the steric effect of micropores. In the study of Westerhoff et al. (2005) after a 4-hour contact time with powdered activated carbon (1, 5 and 20 mg L^{-1}), about 90% removal of the initial concentration (ranging from 10 to 250 ng L^{-1}) of PPCPs was achieved. However, according to Xiao (2012) a 4-hour contact time of PAC with PPCPs is too long and cannot be applied to large water treatment plants.

Due to their remarkable properties, higher specific surface area compared to activated carbon, graphene and graphene oxide attracted the attention for PPCPs removal. The removal efficiency by graphene and its oxide depends mainly on the physiochemical properties of PPCPs, pH and contact time (Yang and Tang, 2016; Kyzas et al., 2015). However, the high cost of graphene limits its applicability. Therefore, more studies are needed for its relatively low cost production.

Carbon nanotubes with their large specific surface areas, and high chemical and thermal stabilities, are attractive adsorbents in wastewater treatment. Many studies showed that carbon nanotubes have high PPCP adsorption capacity but it depends on the surface chemistry, properties of carbon nanotubes and the physiochemical properties of the PPCP (Jung et al., 2015). In addition, it is important to develop simple and effective production methods (Wang and Wang, 2016).

Although adsorption of PPCPs onto the activated carbon, graphene, graphene oxide and carbon nanotubes are reported to be a promising technique, attention should also be paid to the recycle and regeneration of the adsorbents and to the environmental fate and toxicity of these co-existent adsorbents and PPCPs.

The application of nanofiltration (NF), reverse osmosis (RO) and other membrane processes in water treatment plants are reported to be effective for organic micropollutant removal. Many studies were conducted and in some cases 95% PPCP removals were achieved (Bruggen et al., 2003; Nghiem et al., 2004).

2.4.1.3. Chemical and Advanced Oxidation. Various chemical treatment technologies (e.g. UV, ozone oxidation, coagulation, lime softening, chlorine,) were tested for PPCP elimination in bench-scale studies. The results of these studies show that processes such as coagulation–flocculation with aluminum or iron salts and UV irradiation could not achieve high levels of PPCPs removal. On the other hand, in some cases it was possible to remove 90% of some PPCPs using chlorine or ozone oxidation (Adams et al., 2002; Mullroy et al., 2001). The removal efficiency of PPCPs by chlorination was 90%, but chlorine reacts with natural organic matter (NOM), generating toxic disinfection byproducts (DBPs) (Westerhoff et al., 2005; Xiao, 2014). Therefore, development of high efficiency and green technologies for PPCPs removal from water has lately received great attention.

Advanced Oxidation Processes (AOPs), which are recognized with onsite generation of OH radicals in the reaction medium seem to be promising alternatives for the destruction of recalcitrant organic pollutants such as PPCPs in water (Esplugas et al., 2007). Figure 2.9 shows the distribution of AOPs tested for PPCPs.

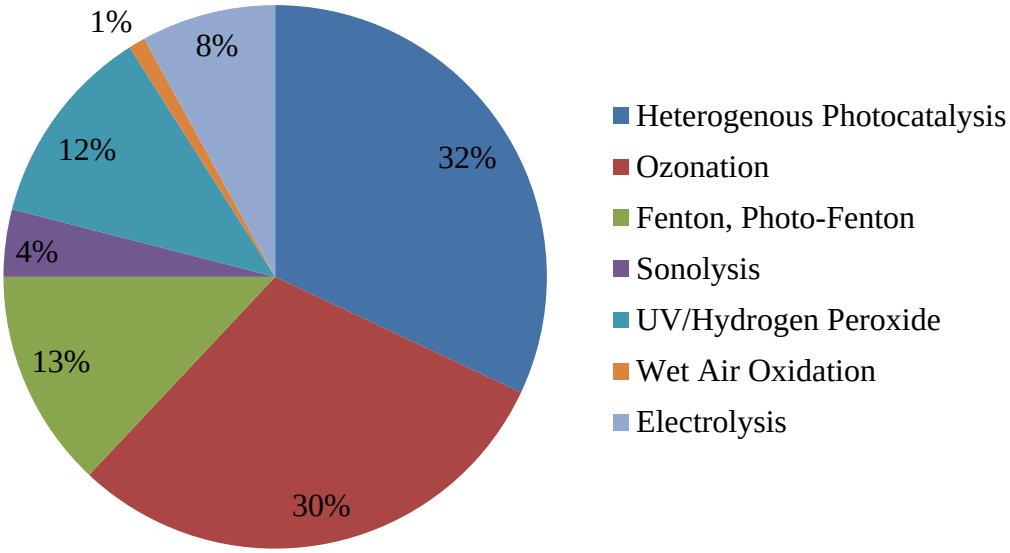

Figure 2.9. Distribution of AOPs tested for PPCP degradation (Klavarioti et al., 2009).

Among the AOPs employed for PPCP degradation, heterogeneous photocatalysis with semiconductors, ozonation and Fenton reactions are the most popular, and other processes involve wet air oxidation, electrolysis and sonolysis, as shown in Figure 2.9. Only few researchers have investigated the effect of ultrasound on elimination of PPCPs by AOP's, despite the very unique and "extreme" conditions generated by ultrasound (Ince et al., 2001; Hartmann et al. 2008; Isariebel et al., 2009; Arriaga et al., 2008, Naddeo et al., 2009).

2.5. Theory of Experimental Design

The effect of the variables on the efficiency of the processes and/or reaction kinetics can be investigated either by conventional "one-factor-at-a-time" (OFAT) method or statistical design of experiments (DOE) (Palasota and Deming, 1992; Ay et al., 2009). Since OFAT method cannot interpret the interaction between two or more variables, it leads to incomplete understanding of the behavior of the systems with multiple variables, and cannot provide an accurate prediction of the system behavior (Mohajeri et al., 2010). On the other hand, statistical DOE uses provides an experiment design which allows modeling nonlinear behaviors and interactions between the variables (Montgomery 2008).

The selection of the experimental design depends on objectives of the study and the number of factors to be investigated. There may be three different types of objectives of an experimental study. First objective type is called comparative. Comparative studies aim to compare different systems by collecting data from them. In these data collection studies with more than one experiment factors Randomized Block Design is commonly used.

Studies with the second objective type, called screening, aims to collect preliminary information about the behavior and characteristics of a system. Usually the main aim is to explore possible behaviors and interactions as much as possible without getting into causal explanations and detailed models. Screening studies are usually conducted by full or fractional factorial designs (Table 2.4). A full factorial design (FFD) includes all possible combinations of factors and levels. The total number of experiments for studying k factors at 2-levels is 2^k. Using FFD it is impossible to miss any interactions since all factor interactions are accounted for. One of the major limitations of full factorial designs is that the thoroughness makes it time- and cost-prohibitive when the number of factors is more than 4. Therefore, full factorial design is particularly useful for preliminary experiments, when the number of factors is less than or equal to 4 and when the number of factors is more than 4, one may look into fractional factorial designs. In contrast to full factorial design in fractional factorial design all possible combinations of factors and levels are systematically not tested.

The third type of objective, called Response Surface, aims to collect information that can be fed into a detailed descriptive model of the system. Response surface methodology (RSM) is considered as the most effective for modeling, analysis and optimization of multivariable systems. A response surface model provides an approximation for the system response (e.g., percent yield of a reaction) for given values of each factors or variables that are included to the study and has a potential to have

an influence on the response (e.g., temperature and pressure). Although a response surface model can include higher order terms of independent variables, a full second-order polynomial empirical model is usually adequate for describing a wide variety of multifactor chemical systems (Hartley 1959; Deming 1987). The structure of a second order response surface model is given in Equation 2.44 below:

$$Y = \beta_0 + \sum_{i=1}^{k} \beta_i x_i + \sum_{i=1}^{k} \beta_{ii} x_i^2 + \sum_{i \geq j}^{k} \sum_{i=1}^{k} \beta_{ij} x_i x_j \quad (2.44)$$

where stands for predicted response, β_0 is intercept, β_i first order term for factor i, β_{ii} is the second order term for factor i and, represents the interaction effect. x_i and x_j are factor values in the experiment (e.g., pH, sonication time). The interaction term is a measure of how much the dependent variable, with respect to one factor, changes as the other factor increases or decreases (Palasota et al., 1992).

The most common experimental design which is suitable for RSM is central composite design (CCD) (Myers et al., 2009). CCD is an efficient and flexible design method which provides sufficient data on the effects of variables and overall experiment error with a minimum number of experiments. Furthermore, it offers useful data about direct, pairwise interaction and curvilinear variable effects (Mohajeri et al., 2010). The quality of information obtained from multifactor experimental designs, such as the central composite design, gives the researcher a broader understanding of the chemical system being investigated. It also gives a richer basis for asking further questions about the behavior of the system. Other design methodologies that can be used in response surface studies are Box-Behnken design (BBD), which is a special 3-level RSM design. The number of experiments (N) required for BBD is defined as:

$$N = 2k(k - 1) + C_0 \quad (2.45)$$

where k is number of factors and C_o is the number of central points.

These designs are useful for avoiding experiments performed under extreme conditions, as it does not contain any points at the vertices of the experiment region. For the situations where the responses at the extremes are important BBD should not be used because unsatisfactory results might occur. Table 2.4 gives an overview of the three types of objectives and appropriate statistical designs for them.

Table 2.4. Guideline for design selection depending on the experimental objectives (Natrella, 2010).

	Objective		
Number of Factors	Comparative	Screening	Response Surface
1	One-factor completely randomized design	-	-
2-4	Randomized block design	Full or fractional factorial	Central Composite or Box-Behnken
≥5	Randomized block design	Fractional factorial or Plackett-Burman	Screen first (Screening designs) to reduce number of factors

Statistical design is also used in computerized experiments in which simulations or numeric analysis methods are used to obtain outputs from a computer model. However, the design of computer experiments is different from the design of physical experiments, because mathematical models are used for experiments and the output might not subject to random variations (Sacks et al. 1989). If there is no randomness in the output, replications are not required. In addition, computer experiments are usually much cheaper compared to the physical experiments in a laboratory thanks to increased computation power of today's computers. Therefore, computer experiments can be designed using a Latin Hypercube Design (LHD) which projects an n-point design on to any factor resulting in n different levels for that factor (McKay et al, 1979). LHD requires a large number of experiments compared to other statistical designs. The schematic representation of experimental designs discussed above are given in Figure 2.10.

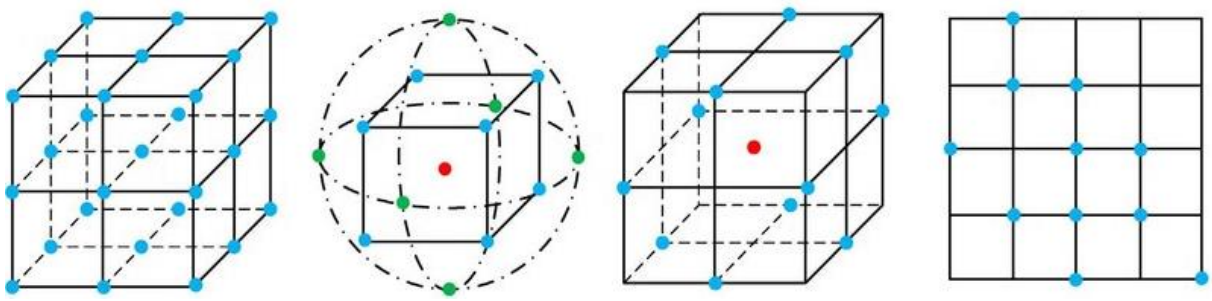

(a) (b) (c) (d)

Figure 2.10. The schematic representation of experimental designs: a) full factorial design; b) central composite design (CCD); c) Box-Behnken design; d) latin hypercube design.

Response Surface Methodology can be used in different problem settings. In simulation of complex systems, RSM can be used to model output variable based on the parameter values of a particular simulation run. Especially in case of large simulation models, which takes a long period of time to run, RSM can be used to guide the optimization/calibration process efficiently. In such applications, ranges of model parameters as well as their probability distributions within those ranges are entered into the simulation model as input. The simulation model runs repeatedly by using a different parameter value at each replication. Output values obtained from all simulation replications indicate the distribution of output variable as a result of uncertain model parameters. This approach is known as Monte Carlo Simulations in the literature. Latin Hypercube Design can be considered as an example to probabilistic experimental design procedure. In our study, experimental factors are determined using central composite design, which is a well-known fractional factorial design in the statistics literature. This approach implicitly assumes that experiment factors have a uniform distribution within their range and all parameter space must be considered equally in order to understand the output behavior comprehensively.

3. MATERIALS AND METHODS

3.1. Materials

3.1.1. Test Compounds

Salicylic acid (SA), Methylparaben (MP) and Caffeine (CAF) were purchased from Sigma-Aldrich, with >99% purity. The chemical and physical properties of the test compounds are given in Table 3.1.

Table 3.1. Psychical/chemical properties of salicylic acid, methyl paraben and caffeine (Kamaya et al. 2005; Yalkowsky and Dannenfelser 1992; Hansch and Leo 1995).

Property	SA	MP	CAF
Molecular Weight (g moL^{-1})	138.1	152.2	194.19
pKa	2.97	8.50	14.0
Water Solubility at 25 ^{o}C (mg L^{-1})	2240	2500	21600
EC_{50} (mg L^{-1}) (*D. Magna*)	870	41.10	182

3.1.2. Reagents

The reagents potassium dihydrogen phosphate (KH_2PO_4, Merck), sodium hydroxide (NaOH, Merck), sodium bicarbonate ($NaHCO_3$, Merck), sulfuric acid (H_2SO_4, Merck), hydrogen peroxide (H_2O_2, Merck), potassium hydrogen phthalate (KHP, Merck), sodium dihydrogen phosphate (NaH_2PO_4, Merck) were all reagent grade. Finisterre C18 SPE cartridges were purchased from Finisterre, Istanbul. Air, argon and oxygen gases were obtained from Ozvarislar, Istanbul with >99% purity. HPLC grade acetonitrile, methanol and phosphoric acid were purchased from Merck (Istanbul). ZVI (45-150µm) and hydrogen peroxide were obtained from Hepure (USA) and Merck (Istanbul), respectively. Sepiolite was obtained from Sigma Aldrich in powder form (d=5 µm). TiO_2 nanoparticles (30-40 nm) were obtained from Evonik. Microtox acute reagent (*Vibrio fischeri* bacteria), reconstitution solution and diluent were purchased from Azur.

3.2. Methods

3.2.1. Experimental

3.2.1.1. Ultrasonic Reactors.

- 20 kHz Probe-Type (Reactor 1). The system was made of a low-frequency horn connected to a 180W generator and a piezoelectric transducer (1.13 cm^2) emitting at 20 kHz. The solution volume was 150 mL and the power density was estimated as $0.19 WmL^{-1}$. The horn is submerged 3 cm from the top of the cell, which has an effective volume of 80 mL. The reactor was cooled by water circulation to maintain constant temperature.

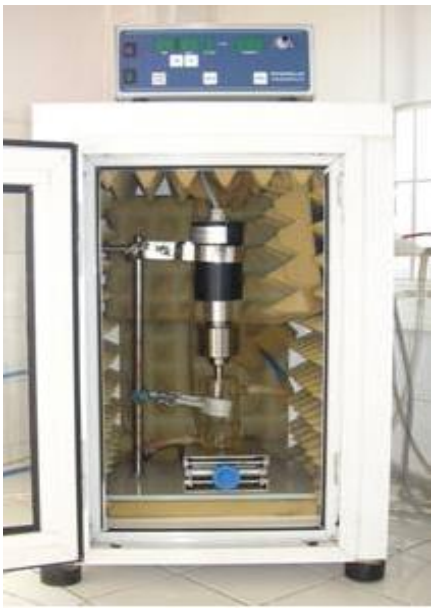

Figure 3.1. Reactor 1.

- Multi-Frequency (Reactor 2). The system consisted of a plate-type reactor with a 500-ml glass cell and a 120W generator connected to three piezoelectric transducers (22 cm^2) emitting at 572, 856 and 1164 kHz (Ultraschall/ Meinhardt, Germany). The reactor was surrounded by a water-cooling jacket to keep the solution at constant temperature (25 ± 0.5 °C) The reaction volume was optimized at 250 mL, and the power density in it was estimated by calorimetry as $0.21 WmL^{-1}$.

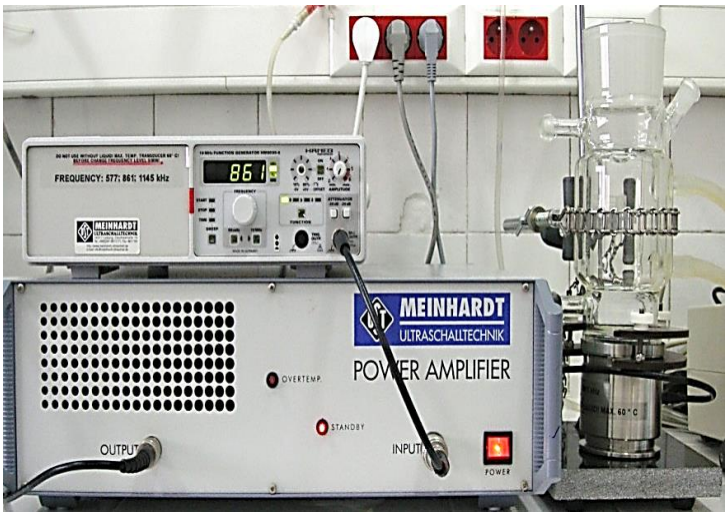

Figure 3.2. Reactor 2.

- <u>200 kHz Ultrasonic Bath (Reactor 3).</u> The system was made of a high-frequency ultrasonic bath connected to a 100W generator emitting at 200 kHz (Kaijo Quava Mini QR003, Japan). A water circulation system was used to keep the solution at constant temperature (25±0.5 ºC).

Figure 3.3. Reactor 3.

<u>3.2.1.2. The Photo Reactor.</u> The system consisted of a xenon lamp (MAX-301, 300 W; Asahi Spectra Co. Ltd.) equipped with a purpose-built mirror module (350–500 nm; Asahi Spectra Co. Ltd.) was used.

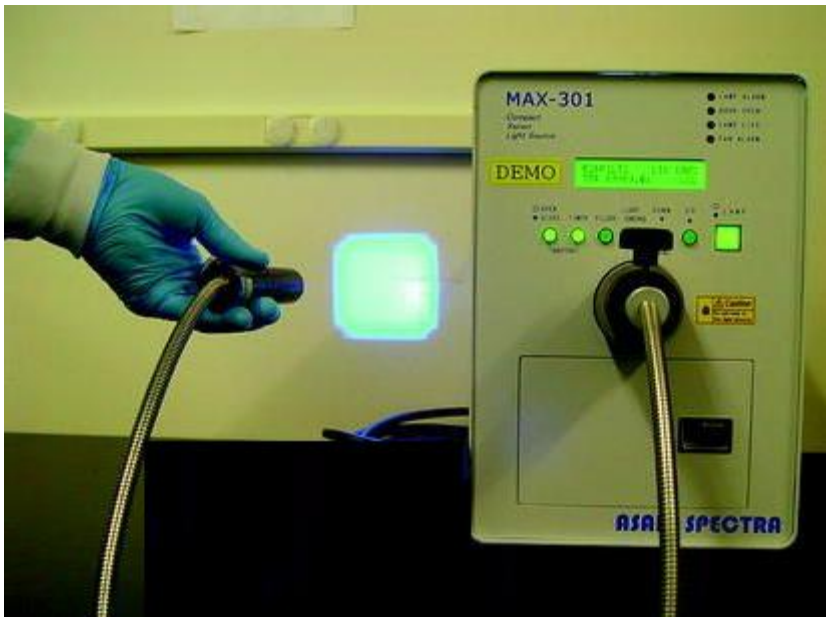

Figure 3.4. The Photo Reactor.

3.2.2. Procedures

3.2.2.1. Adsorption. Batch adsorption tests with raw and modified forms of ZVI, sepiolite, TiO_2 and their nanocomposites were carried out at concentrations of 2.5-50 mg L^{-1} of ZVI, 0.025-8.0 g L^{-1} of sepiolite, 0.25-1.0 g L^{-1} TiO_2 and 0.25-1.0 g L^{-1} of the nanocomposites in a shaker at a mixing rate of 125 rpm.

3.2.2.2. Sonolysis & Sonocatalysis.

- Salicylic acid: The reactor contents were sonicated for 45-min, during which samples were collected periodically for the analysis of SA, DOC/ TOC and UV absorption. The optimum pH, frequency, initial solute and ZVI concentrations were selected based on the efficiency of mineralization.

- Methylparaben: The ultrasonic device used in homogeneous and heterogeneous sonolysis of MP was Reactor 2 and the power. The experimental method involved sonication of MP without sepiolite addition to select the optimum concentration, frequency, injected gas, power and pH. Samples were monitored periodically to analyze the concentrations of MP and TOC. The tests were repeated in the presence of sepiolite at optimized conditions to reconfirm the same conditions and to select the optimum sepiolite concentration.

- Caffeine: The reactor contents were sonicated in Reactor 2 for 30 min at natural pH. Samples were collected periodically for the analysis of caffeine and DOC/TOC. The optimum frequency was selected based on the efficiency of mineralization.

3.2.2.3. Photolysis and Photocatalysis. These processes were applied only to caffeine. Samples were exposed to 30 min photolysis under UV-VIS irradiation (300-600 nm) by a Xenon lamp in the presence and absence of catalysts (TiO_2, Sepiolite, TiO_2/Sepiolite) at three pH levels (3, 6 and 9). The effluents were monitored for the concentration of CAF and TOC. Some of the samples were exposed 856 kHz US in Reactor2 at pulse mode (1 s on 1 s off) to investigate the effect of post-sonication on the degree of C-mineralization.

3.2.2.4. Post-Sonication. Commercial TiO_2 and lab-made nanocomposites were added to PPCP containing solutions and irradiated for 15-min with the photo reactor, followed by pulse mode sonication for 30 and 60 minutes using R2.

3.2.2.5. Sonolytic Synthesis of Nanoparticles and Nanocomposites.

- Sepiolite/SDS-intercalates: The procedure was adopted from the literature reporting the synthesis of surfactant/clay nanocomposites (Belova et al., 2009). Accordingly, a 0.04 g of raw sepiolite was mixed with 250 mL distilled water for 24 h. A 40-ml portion of 0.5% solution of SDS was added to the swollen clay and the mixture was sonicated in Reactor 3 (R3). The intercalation process was terminated after 20, 40 and 60-min, after which the suspensions were centrifuged, filtered and dried at 160°C for 24-h.

- Sepiolite/TiO_2 nanocomposites: Immobilization was performed by dispersion of the sepiolite powders in water, followed by addition of TiO_2 (Degussa-P25) and sonication for 30-min in Reactor 3. The Sepiolite/TiO_2 weight ratio was 1:1. The powders were separated by filtration through 0.2 µm membranes (Milipore, OmniPore) washed and dried at constant temperature (60°C) for 12 hours (Todorova et al., 2014).

3.2.3. Analytical Methods

3.2.3.1. Calorimetric Determination of Ultrasonic Power in Solution. Some of the energy transferred to solution during US is lost as heat, and only the remaining part produces cavitation (Mason, 1999). Hence, the power output of the ultrasonic generator can be significantly different from the power delivered into the solution. Among available methods to measure the amount of ultrasonic power

entering a sonochemical reaction medium, the most common and easiest is calorimetry (Mason, 1999). The method involves measurement of the temperature increase against time during a fixed period, which is then fitted to a polynomial to estimate the quantity dT/dt. The ultrasonic power (P) is then estimated by substituting the value of dT/dt into Equation 3.1 (Mason and Cordemans, 1998):

$$P_d = (dT/dt) x C_p x M \quad (3.1)$$

where: P_d= power dissipated in the system (W), (dT/dt)= the temperature rise at certain time interval (ºC/sec), Cp= heat capacity of water (4.1840 J g^{-1} $ºC^{-1}$) , and M= mass of water in the reaction vessel (g). The power thus found is then used to determine the efficiency of the system in units of energy per unit emitting area-intensity (W cm^{-2}), or energy per unit volume-density (W mL^{-1}).

3.2.3.2. High Pressure Liquid Chromatographic (HPLC) Determination of PPCP concentrations. Concentrations of SA, MP and caffeine were analyzed by a Shimadzu LC-20AT HPLC with a 20A UV–vis photo diode array detector equipped with Inertsil ODS-3V (C18) (Hypersil BDS), 250 × 4.6 mm, 5 µm particle size column. The conditions of each analysis are ad described in Table 3.2.

Table 3.2. The operation conditions of HPLC for analysis of SA, MP and CAF.

Compound	**Detection Wavelength (nm)**	**Mobile Phase**	**Injection Volume (µL)**	**Flow rate (mL/min)**
SA	254	20 mM phosphoric acid (pH 2.0 unadjusted) and acetonitrile (50:50)	10	1
MP	250	Water/Acetonitrile/Phosphoric acid (70/30/0.35)	10	1
CAF	272	Water/Methanol (50/50)	5	1

3.2.3.3. Determination of Total Organic Carbon. The analyses of organic carbon (TOC) was done using a Shimadzu TOC-V CSH analyzer operating in the non-purgeable organic carbon (NPOC) mode. The instrument was calibrated by standard solutions of potassium hydrogen phthalate (1-10 mg L^{-1}). All samples were measured in triplicate.

3.2.3.4. Determination of Hydrogen Peroxide. Hydrogen peroxide concentration was analyzed using a Unicam Heλios Alpha/Beta double beam spectrophotometer with a 1 cm quartz cell followıng the potassium iodide method described by Klassen et al. (1994). The method is based on the reaction of iodide (I^-) with H_2O_2 to form triiodide ion (I_3^-), which has a strong absorbance at 351 nm.

3.2.3.5. Determination of Microtox Toxicity. The acute toxicity of the solutions before and during sonolysis was determined using a Microtox-500 Toxicity Analyzer and the related software (Azur Environmental, USA). The data were reported as 15-min EC50 that is equivalent to the percentage of the initial solution that renders 50% light inhibition in time.

3.2.3.6. Identification of the Oxidation Byproducts. The oxidation byproducts were identified by LC/MS/MS-QTRAP with an ionization tandem mass spectrometry (LC-ESI-MS-MS), which provided the structure of the products. The 100-fold diluted samples were analyzed by direct infusion into the ESI source via a syringe pump at a flow rate of 10 µL/min. Enhanced Mass Scanning (EMS) and Enhanced Product Ion (EPI) scan modes were used to acquire information on parent compounds and their fragmentation patterns, respectively. The mass spectrometer was operated under the following conditions: ion source temperature: 500ºC; curtain gas: 20 psi; nebulizer gas: 40 psi; heater gas: 60 psi; CAD gas: Low; IS pos: +5500 V. The EMS spectra of the samples were obtained by scanning over the m/z range 55-155 at a scan rate of 10000 Da/s using collision energy (CE) at 10 V, declustering potential (DP) at 70 V and entrance potential (EP) at 10 V. All data were acquired and processed using the Analyst 1.6.2. Software.

3.2.3.7. SEM Analysis of the Catalysts or Nanoparticles. The structure, morphology and size of raw and SDS-intercalated nanoparticles of sepiolite were analyzed by environmental scanning electron microscope (ESEM)-Philips XL30 ESEM-FEG/EDAX.

4. PUBLICATIONS

Two research articles have already been published from the research, two are under review and one is ready for submission, as given in the following:

Published

Savun-Hekimoğlu, B. & Ince, N. H. (2017). Decomposition of PPCPs by ultrasound-assisted advanced Fenton reaction: A case study with salicylic acid. *Ultrasonics Sonochemistry, 39*, 243-249. **(SCI-A, Impact Factor: 6.012)** *https://doi.org/10.1016/j.ultsonch.2017.04.013*

Savun-Hekimoğlu, B. & Ince, N. H. (2019). Sonochemical and sonocatalytic destruction of methylparaben using raw, modified and SDS-intercalated particles of a natural clay mineral. *Ultrasonics Sonochemistry, 54, 233-240.* **(SCI-A, Impact Factor: 6.012).** *https://doi.org/10.1016/j.ultsonch.2019.01.034*

Under Review

Savun-Hekimoğlu, B. & Ince, N. H. (2019). Optimization of Methylparaben Degradation by Sonocatalysis *Ultrasonics Sonochemistry (Submitted, Under revision).*

Arslan, E., Savun-Hekimoglu, B., Agopcan-Cinar, S., Ince, N.H., Aviyente, V. (2019). Hydroxyl radical-mediated degradation of salicylic acid and methylparaben: An experimental and computational approach to assess the reaction mechanisms. *Environmental Science and Pollution Research (Submitted, Under revision).*

To be Submitted

Savun-Hekimoğlu, B. & Ince, N. H. (2019). Photocatalytic Degradation of Caffeine on Sepiolite Supported-TiO_2.

The following chapters present word documents of the “published”, “under-review” and “to-be submitted” articles

5. DECOMPOSITION OF PPCPS BY ULTRASOUND-ASSISTED ADVANCED FENTON REACTION: A CASE STUDY WITH SALICYLIC ACID

The most commonly employed lab-scale AOPs for removing salicylic acid (SA) from water are photocatalysis with TiO_2, electrochemical, Fenton, and wet air oxidation, and rarely ultrasonication (Guinea et al., 2008; Scheck and Frimmel, 1995; Adán et al., 2006; Rao et al., 2009; Goi et al., 2008). As discussed in more detail in Section 2.2.3 the application of ultrasound in heterogeneous reactions provides unique advantages (enhancement of mass transfer and chemical reaction rates, improvement of the catalyst surface, reducing of chemical consumption and sludge generation) (Eren and Ince 2010). A very common sonocatalyst is zero-valent iron (ZVI) with its very reactive surface and ability to release Fe species in solution, thus initiating Fenton or Advanced Fenton reactions. A unique advantage of ultrasound in these systems is that one of the components of Fenton reagent (H_2O_2) is in-situ generated via combination of two hydroxyl radicals that form upon water pyrolysis in the collapsing cavity bubbles (Ince et al., 2001).

The operation of sono-Fenton reaction requires consideration and optimization of the that critical process parameters, namely pH, the dose of ZVI and H_2O_2 (if external addition is necessary), and the initial concentration of the reactants. In the past, the effect of these variables on the efficiency of the process and/or reaction kinetics have been investigated with focus on conventional “single-factor-at-a-time” method (Arslan-Alaton et al., 2009). However, the method is inadequate with incomplete understanding of the behavior of the system, which is affected by multiple variables (Palasota and Deming, 1992; Ay et al., 2009). In addition, the “single-factor-at-a-time” method does not show the effect of interactions between parameters, and therefore cannot provide an accurate prediction of the system behavior (Mohajeri et al., 2010). The confusion may be avoided with the use of well-designed experimental systems and adequate multifactor models such as the “response surface methodology” (RSM), which is widely used to develop empirical models that accurately describe process behaviors and interactions between the variables (Montgomery, 2010). No scientific work has been so far published on the use of RSM in the experimental design of a sonocatalytic reaction system to be used the degradation of PPCPs by advanced Fenton reactions.

This present study was aimed to investigate the degradability of salicylic acid in water by advanced sono-Fenton reaction using zero-valent iron to predict the individual and interactive effects

of process parameters on the efficiency of carbon mineralization. The method of prediction was based on the RSM methodology and multiple regression analysis. The reactions were run in a high-frequency reactor at various preset values of ZVI, H_2O_2, electrical power and pH, which were selected as the independent variables of the model. The response of the system to variations in these variables was selected as the reduction in total organic carbon (TOC), which is the dependent variable reflecting the efficiency of the system.

5.1. Experimental Procedures

Batch adsorption tests were carried out at 10 mg L^{-1} SA and varying concentrations of ZVI (2.5, 5, 10, 30, 50 mg L^{-1}) in a shaker at pH 3.5 and a mixing rate of 125 rpm for 60-min to assess the effect of catalyst dose on the degree of SA adsorption. The ultrasonic devices were R1 (a low frequency horn) and R2 (multifrequency plate-type). The reactor contents were sonicated for 45-min, during which samples were collected periodically for the analysis of SA, DOC/TOC and UV absorption. The optimum pH, frequency, initial solute and ZVI concentrations were selected based on the efficiency of mineralization.

5.2. Factorial Design and Data Analysis

Values of the model factors were selected using the central composite technique with a 4-factor-5-level inscribed composite, and the design matrix was generated by MATLAB 11.2. The open source R Gui software was used for the statistical analysis of results and validation of the regression model.

5.3. Results and Discussion

5.3.1. Control Experiments

Batch adsorption data collected during 60-min contact of SA with ZVI in the absence of ultrasound showed that the compound weakly adsorbed on the metal surface and the degree of adsorption increased with increased concentrations of the adsorbent. Maximum SA adsorption was 13% at the highest dose of ZVI, while the percentage of DOC removed from solution under equivalent conditions was slightly larger (16.4%) as the evidence of oxidative degradation in the bulk solution or at the reactive metal surfaces. The data are presented in Figure 5.1.

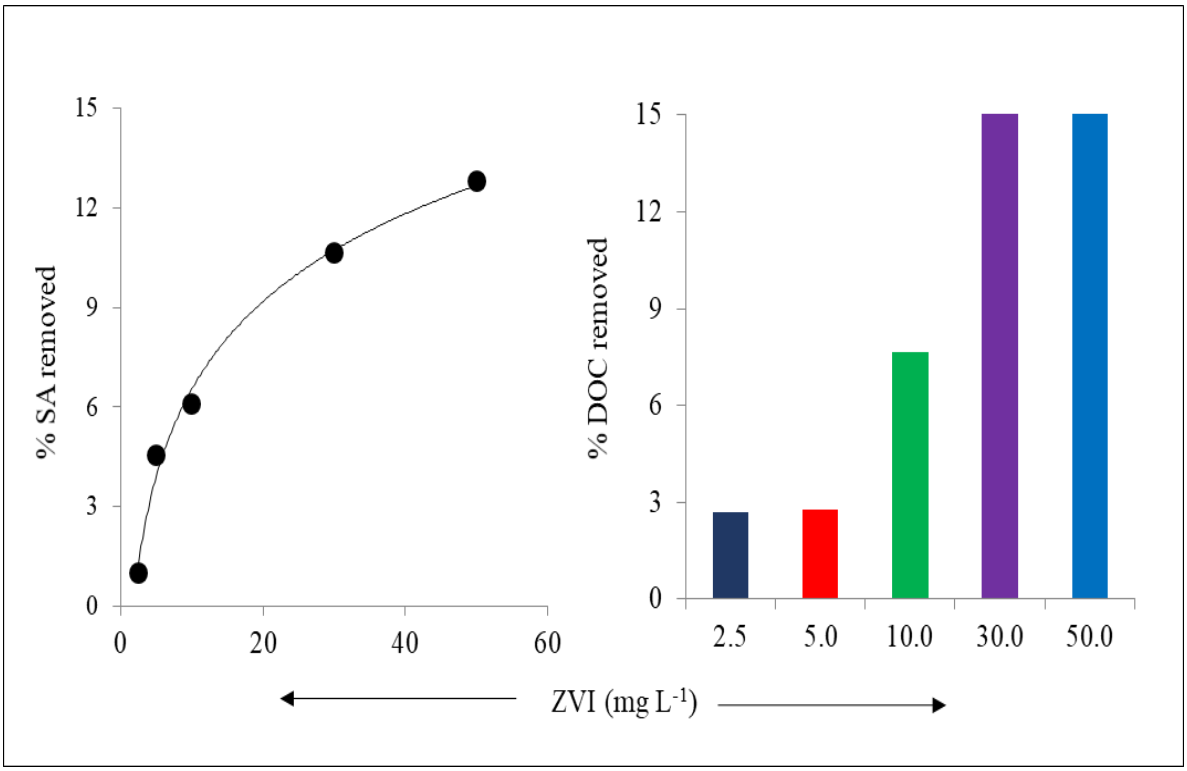

Figure 5.1. The effect of ZVI concentration on the adsorption of SA (C_0=10 mg L^{-1}) at pH 3.5 and the corresponding DOC removal from solution.

The second set of control experiments were those carried out in the absence of ZVI to select the optimum values of pH, C_0 and frequency. The data were generated at three pH levels (3.5, 5.0, 9.0), four concentrations (2.5, 5, 8.75, 10 and 15 mg L^{-1}) and three frequencies (20 kHz, 572 kHz, 856 kHz). We found that the optimum SA concentration was 10 mg L^{-1}, and low frequency irradiation (20 kHz) was considerably ineffective, as it provided almost no reduction in SA and TOC (data not given). The lack of sonochemical reactions under 20 kHz is related to the long collapse duration of cavity bubbles that facilitates radical combination reactions, which in turn reduces the incidence of bubble collapse and the rate of OH• ejection to the bulk solution.

Figure 5.2 presents time-rate of SA decomposition and DOC decay observed during high frequency irradiation of 10 mg L^{-1} SA at the test pH levels. The data show that the rate of oxidation was a maximum at the acidic pH (3.5) and there was no significant difference between irradiation at 572 kHz and 856 kHz. Higher reactivity at acidic pH is based on the low pKa of the compound (2.97), above which it exists in anionic form. As such, the compound is only slightly anionic at pH 3.5 and may partly diffuse to the gas-liquid interface, which is a very effective reaction site containing high concentrations of radical species released from collapsing cavity bubbles. We also found that at prolonged reaction time (60-min) SA was completely decomposed, with however, no improvement in mineralization. The finding is in good agreement with the literature, showing the reaction

mechanism of SA decomposition by •OH, and the formation of dihydrobenzoic acid and catechol, which are more hydrophilic and less reactive with •OH than the parent compound (Gogate et al., 2014; Arrojo et al., 2007; Amin et al., 2010; Martinez-Tarifa et al., 2010). Note also that high-frequency irradiation was considerably more effective than low (20 kHz), due to a larger number of oscillations (i.e. transient cavitation) and more frequent occurrence of efficient bubble collapse (25-fold) that favor free radical transfer to the bulk liquid (Eren and Ince 2010). As such, 572 kHz was selected as the operating frequency for the rest of the experiments.

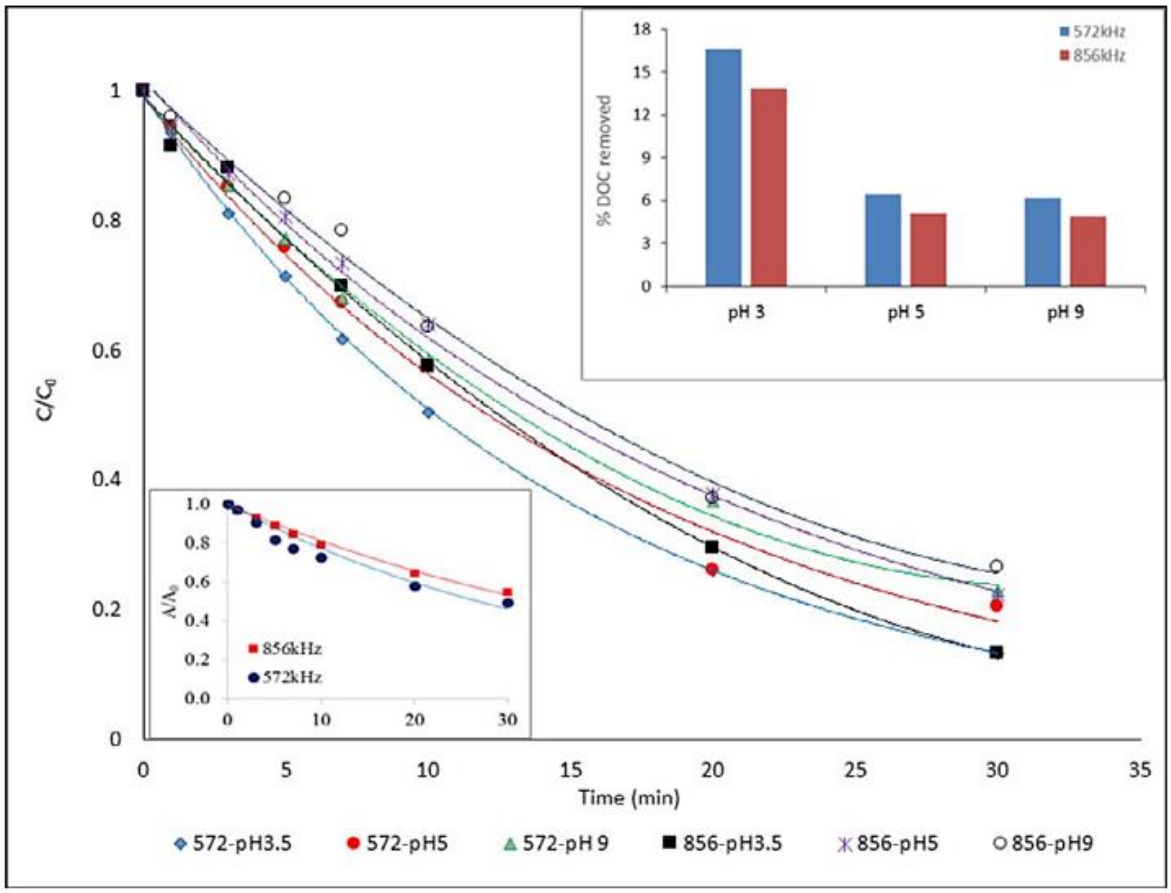

Figure 5.2. The effect of pH and frequency on the rate of SA decomposition (C_0 = 10 mg L^{-1}) and mineralization. Estimated values of pseudo-1st order reaction rate constants were: 572 kHz-0.067, 0.056, 0.049 min^{-1}; 856 kHz-0.066, 0.050, 0.046 min^{-1}, for pH 3.5, 5 and 9, respectively. The inset at the bottom left shows relative decay of the absorbance of the sample solution at 297 nm by sonolysis at 572 and 856 kHz at pH 3.5.

5.3.2. Sonocatalysis and the Effect of H_2O_2 Addition

Prior to modeling, we ran some experiments with 7.5-50 mg L^{-1} ZVI and 0-300 mg L^{-1} H_2O_2 to determine the optimum regions of factor space keeping all other conditions the same as selected in control experiments. The results of sonolysis with ZVI alone (no H_2O_2) are presented in Figure 5.3, which shows that the rate of SA decomposition is closely related to the quantity of ZVI, the excess of which (>10 mg) retards mineralization via the reaction of Fe^{2+} with •OH, as depicted in Eq (5.1).

$$Fe^{2+} + \bullet OH \rightarrow Fe^{3+} + OH^- \quad (5.1)$$

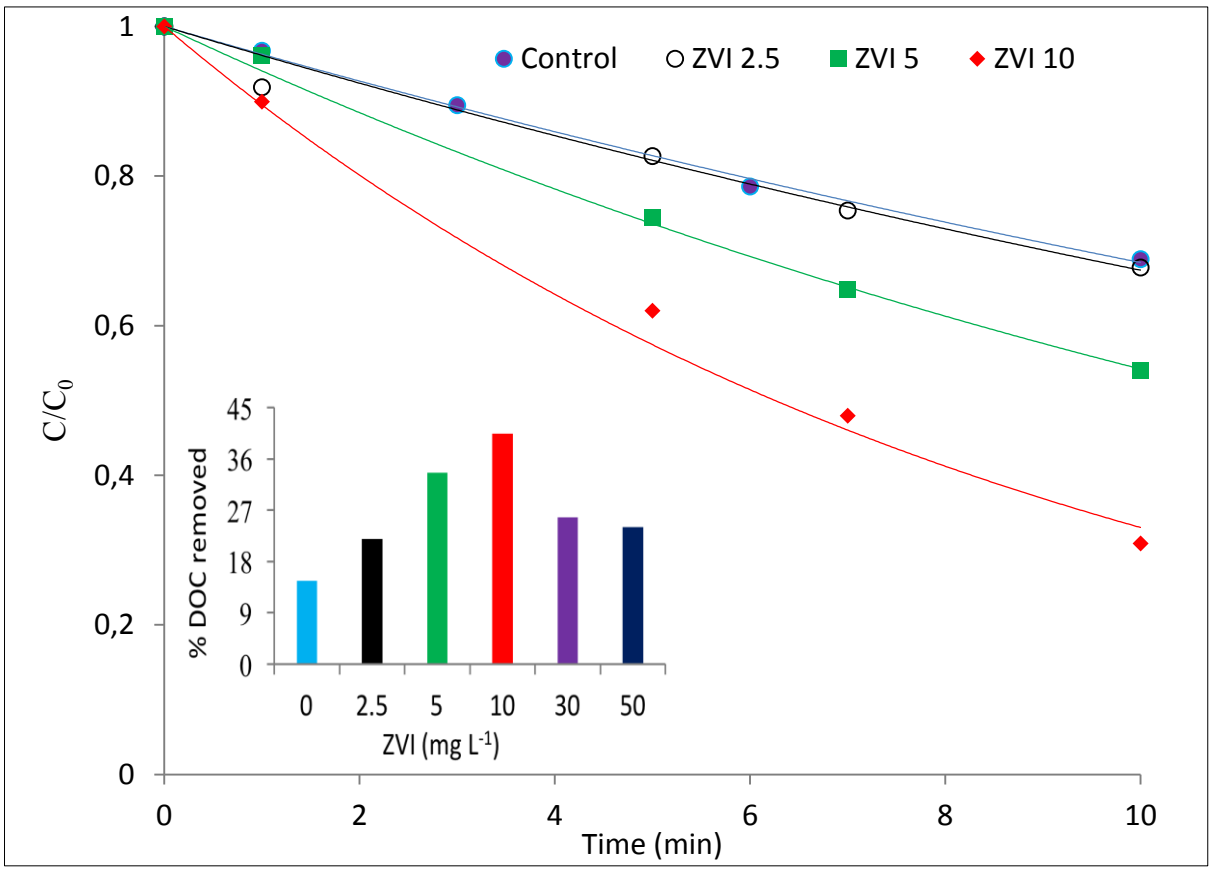

Figure 5.3. Sonocatalytic decomposition and mineralization of SA in relation to the quantity of ZVI added. Reaction conditions were: C_0=10 mg L^{-1}, pH 3.5, f=572 kHz, Ps=0.21WmL^{-1}. "Control" refers to US alone, reaction time for SA and DOC decay were 10-min and 45-min, respectively.

We also found that SA is sufficiently decomposed in the absence of ZVI if there is sufficient H_2O_2 in the reactor, but mineralization is considerably low. The efficiency of TOC decay was improved by the addition of a properly-selected dose of the two, as depicted in Figure 5.4. We found that the "best" molar ratio of H_2O_2: ZVI was 13.13, under which the reaction was most rapid with a rate constant of 0.49 min^{-1}. Note that percentage of mineralization by the addition of 10 mg L^{-1} ZVI

and no H_2O was higher than that in the presence of the "best" H_2O_2: ZVI ratio. The finding is the evidence of rate inhibition via excess •OH consumption by accumulation of H_2O_2 (after complete depletion of SA), and the production of •OH-reactive peroxyl radicals (Eq 2.42) by the reaction of Fe^{3+} with the excess peroxide, as reported in the literature (Chakma and Moholkar, 2014; Bhasarkar et al., 2013).

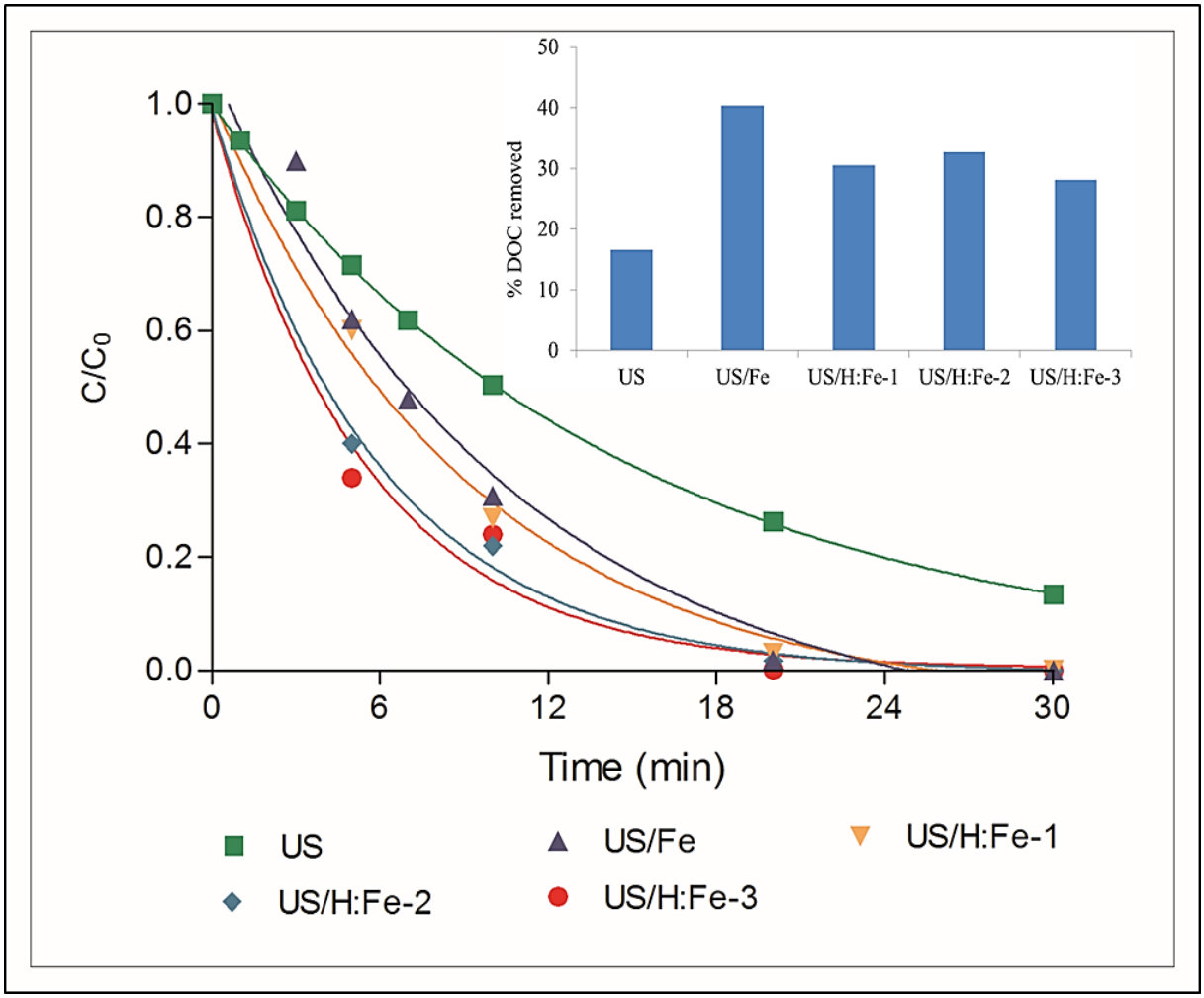

Figure 5.4. Relative rate of SA decay and percentage of C-mineralization by sonocatalysis with various molar ratios of H_2O_2: ZVI at pH 3.5. The legends US, US/^{Fe}, US/H: Fe-1, US/H: Fe-2, US/H: Fe-3 refer respectively to US alone, US/ZVI, US/H_2O_2: Fe=3.27, US/H_2O_2: Fe=6.56, US/H_2O_2: Fe=13.13. Initial conditions were C_0=10mg L^{-1}, f=572 kHz, ZVI=10 mg L^{-1}, Ps=0.21WmL^{-1}.

In the next set of experiments, we used a wider range of H_2O_2: ZVI ratio to elucidate the interactive effects of the two reagents. Estimated values of the apparent reaction rate constants and the fraction of DOC decay obtained under the applied ratios are listed in Table 5.1. The data show that mineralization was a maximum (45%) at a H_2O_2 /ZVI molar ratio of 4.4:0.9, while the rate of SA

decay was a maximum at 8.8:0.9, which was slightly less effective for the mineralization of the compound (41.7%).

Table 5.1. The impact of H_2O_2 to ZVI molar ratio on the apparent reaction rate constant and percent mineralization of SA during sonolysis at pH=3.5. Reaction times for k' and DOC were 5-min and 45-min, respectively.

H_2O_2:ZVI (mM/mM)	k' (min^{-1})	DOC decay (%)
0/0	0.031	17.1
0/0.5	0.063	32.8
4.4/0.5	0.034	31.6
8.8/0.5	0.120	18.8
0/0.9	0.060	30.3
4.4/0.9	0.160	45.0
8.8/0.9	0.350	41.7
8.8/0	0.072	17.3
4.4/0	0.034	17.6

5.3.3. Experimental Design

As pointed out previously, we used a four-factor central composite technique and MATLAB 11.2 to generate the values of the model factors for the design matrix. The factors and the restrictions on their allowed ranges were as: **pH** (2.0-3.5), **power** (60-120 Watt), **ZVI** (0-30 mg L^{-1}) and **H_2O_2** (0-40 mg L^{-1}). The matrix generated is presented in Table 5.2.

Table 5.2. Experimental design matrix and levels of independent process variables

Factor 1	Factor 2	Factor 3	Factor 4	**Fe** (mg L^{-1})	**H** (mg L^{-1})	**P_o** (W)	**pH**
-0.5	-0.5	-0.5	-0.5	7.5	10	84	2.375
-0.5	-0.5	-0.5	0.5	7.5	10	84	3.125
-0.5	-0.5	0.5	-0.5	7.5	10	108	2.375
-0.5	-0.5	0.5	0.5	7.5	10	108	3.125
-0.5	0.5	-0.5	-0.5	7.5	30	84	2.375
-0.5	0.5	-0.5	0.5	7.5	30	84	3.125
-0.5	0.5	0.5	-0.5	7.5	30	108	2.375
-0.5	0.5	0.5	0.5	7.5	30	108	3.125
0.5	-0.5	-0.5	-0.5	22.5	10	84	2.375
0.5	-0.5	-0.5	0.5	22.5	10	84	3.125
0.5	-0.5	0.5	-0.5	22.5	10	108	2.375
0.5	-0.5	0.5	0.5	22.5	10	108	3.125
0.5	0.5	-0.5	-0.5	22.5	30	84	2.375
0.5	0.5	-0.5	0.5	22.5	30	84	3.125
0.5	0.5	0.5	-0.5	22.5	30	108	2.375
0.5	0.5	0.5	0.5	22.5	30	108	3.125
-1	0	0	0	0	20	96	2.75
1	0	0	0	30	20	96	2.75
0	-1	0	0	15	0	96	2.75
0	1	0	0	15	40	96	2.75
0	0	-1	0	15	20	72	2.75
0	0	1	0	15	20	120	2.75
0	0	0	-1	15	20	96	2
0	0	0	1	15	20	96	3.5
0	0	0	0	15	20	96	2.75
0	0	0	0	15	20	96	2.75
0	0	0	0	15	20	96	2.75
0	0	0	0	15	20	96	2.75
0	0	0	0	15	20	96	2.75
0	0	0	0	15	20	96	2.75
0	0	0	0	15	20	96	2.75
0	0	0	0	15	20	96	2.75
0	0	0	0	15	20	96	2.75
0	0	0	0	15	20	96	2.75
0	0	0	0	15	20	96	2.75
0	0	0	0	15	20	96	2.75

Statistical assessment of the data in the matrix by a backward stepwise regression function provided Eq (5.2) as the predictive model of the system (Adj. R^2=0.9037):

$$\%\mathrm{DOC} = -171.15 + 1.67(\mathbf{Fe}) + 3.43(\mathbf{H}) + 1.37(\mathbf{P_o}) + 67.89(\mathbf{pH}) - 0.057(\mathbf{Fe^2}) - 9.70(\mathbf{pH^2}) - 0.46(\mathbf{Fe} \times \mathbf{pH}) + 0.002(\mathbf{Fe} \times \mathbf{P_0}) - 0.04(\mathbf{H} \times \mathbf{P_0}) - 0.24(\mathbf{P_0} \times \mathbf{pH}) \quad (5.2)$$

where: **Fe**, **H**, **pH** and **Po** refer respectively to ZVI (mg L^{-1}), H_2O_2 (mg L^{-1}), pH, and the applied power (W).

The significance of each regression term was assessed by the p value or t-statistics, which are not influenced by magnitudes of the independent variables, as is true for non-standardized regression coefficients. Note also that there are no unnecessary terms in Eq (5.2), as they were eliminated using the Akaike Information Criterion (AIC), the value of which is supposed to decrease upon each elimination. Regression diagnostic checks were performed through residual plots based on the assumption that residual terms follow normal distribution with zero mean and constant variance. The residuals of the model were found to be randomly distributed around zero with a constant spread, and the normal distribution was verified by quantile-quantile plots (Walpole and Myers 1998).

The regression model above is a complicated second order equation, which does not provide direct insight into the interactive relationships between factors and the dependent variable. Hence, we used 3-D response surface plots to shed light on the interactive relations between each two factors and the dependent variable. The plots were generated by setting two of the factors to constants and plotting the other two against the dependent variable using MATLAB. One such plot is presented in Figure 5.5 to visualize relative impacts of power and H_2O_2 on the efficiency of mineralization. The data show that the efficiency reaches its maximum (34%) when the power is increased to the upper (120 W) and H_2O_2 is kept at the lower boundaries (0 mg L^{-1}). The maximum was considerably reduced (20%) by keeping both factors at their upper boundaries, due to the inhibition caused by: i) enhanced consumption of HO• (by excess peroxide) and ii) scattering and attenuation of the incoming waves (Gültekin et al., 2009).

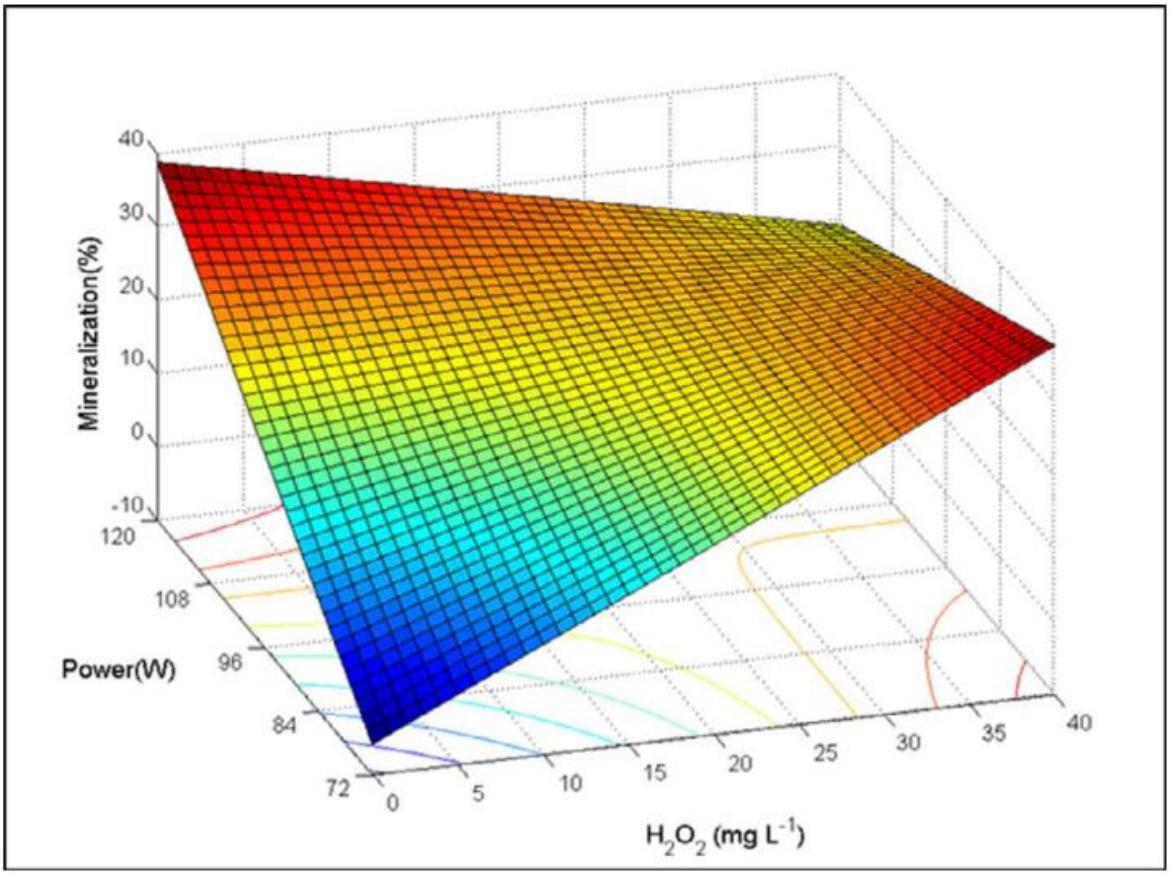

Figure 5.5. Interactive effects of ultrasonic power and H_2O_2 on carbon mineralization by advanced sono-Fenton reaction at pH=2.75 and ZVI=20 mg L^{-1}.

We also found that mineralization is a jointly concave function of pH and ZVI, as depicted in Figure 5.6 (a) and (b). The difference between the two plots is that H_2O_2 and power were fixed at 40 mg L^{-1} and 72 W, respectively in the first one; and 0 mg L^{-1} and 120 W in the second. Maximum efficiency of TOC decay under these two conditions was 40% and 45%, respectively, but the value of ZVI was almost doubled from 16 mg L^{-1} in the first case to 30 mgL^{-1} in the second. Note also that the observed maximum at 72 W is higher than that at recorded at 120 W (Figure 5.5), confirming the evidence of reduced cavitation activity or reduced rate of HO• formation at extreme power inputs.

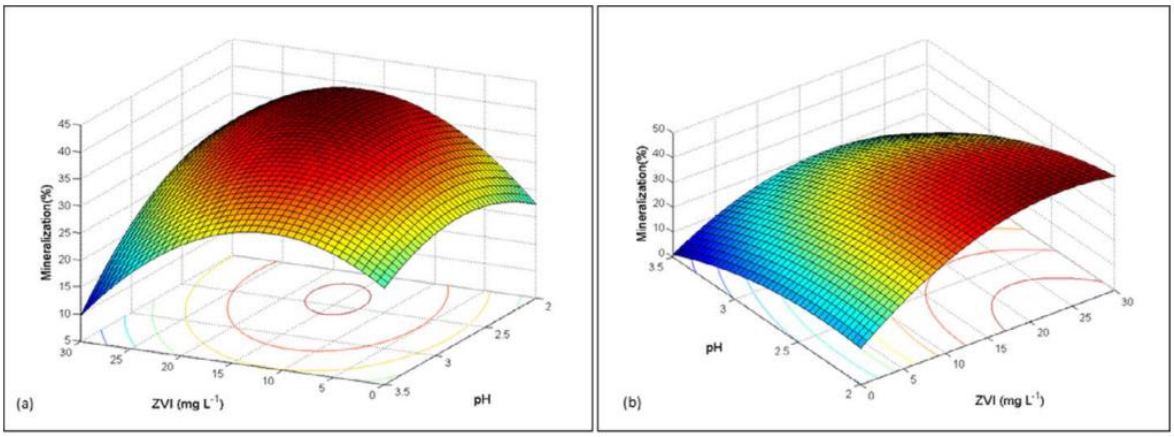

(a) (b)

Figure 5.6. Interactive effects of pH and ZVI on mineralization of SA by advanced sono-Fenton reaction at H_2O_2=40mg L^{-1}, P=72W (a), and H_2O_2=0, P=120W (b).

Another concavity of relations was established between TOC decay and variations in H_2O_2 and ZVI at pH=2.75 and P=96 W, as depicted in Figure 5.7. It was found that the efficiency of mineralization increased with increasing quantities of ZVI and H_2O_2, reached a maximum (30%) at ZVI=15 mg L^{-1} and H_2O_2=20 mgL^{-1}; and sharply declined as the concentration of ZVI was further increased. To check the impact of power on the above findings, we further predicted the efficiencies at a higher power input (120 W) keeping all other parameters the same. We found that maximum mineralization in this case was 20%, and reagent inputs were increased to 30 mg L^{-1}, and 21 mg L^{-1}, as H_2O_2 and ZVI, respectively (data not shown). Hence, it is obvious that there is a threshold power, above which the formation of excess gas bubbles scatters the incoming waves to the walls of the reactor, leading to a reduction in energy dissipation by cavitation activity (Sivakumar and Gedanken 2004). In addition, the likely coalescence of these bubbles may form bubble clouds, which will attenuate the sound waves.

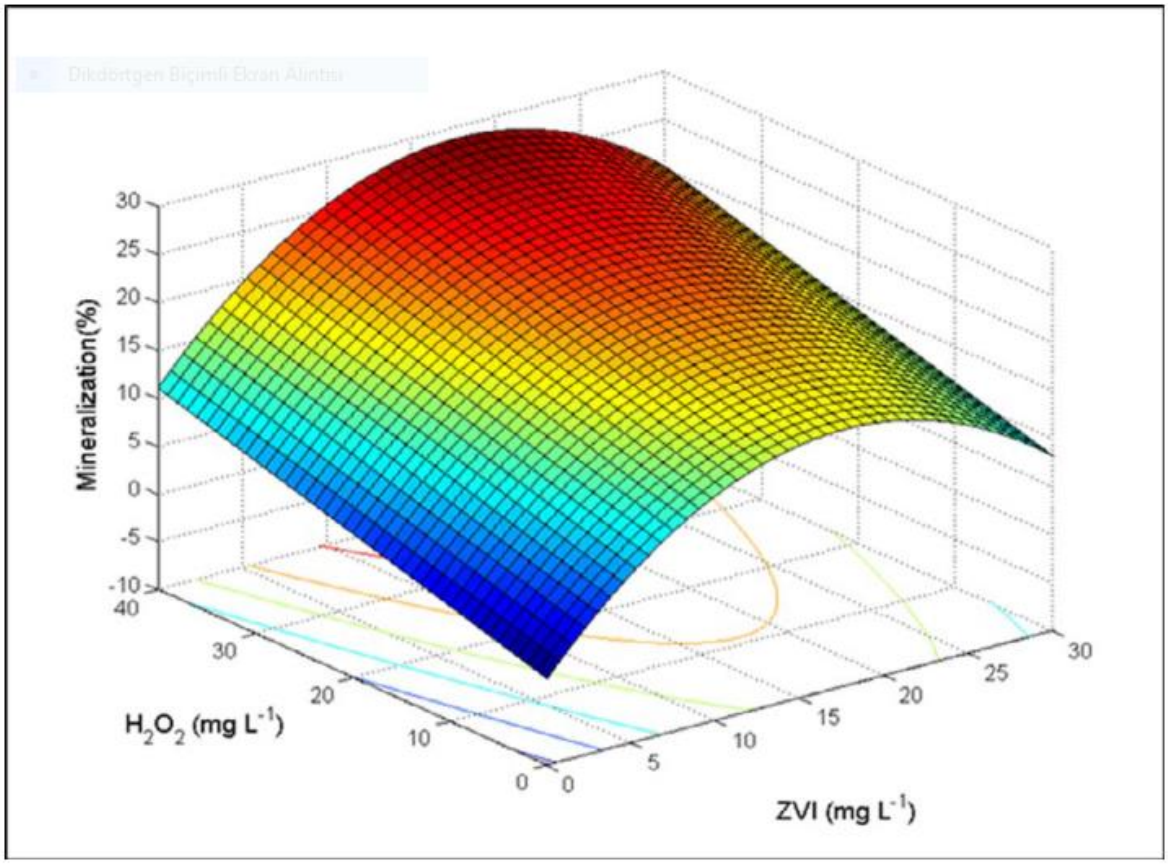

Figure 5.7. Interactive effects of ZVI and H_2O_2 on mineralization of SA by advanced sono- Fenton reaction at pH=2.75 and P=96 W.

Although many more 3-D plots could be generated to visualize the effects of two variables on the fraction of mineralization, they would not provide the necessary information about the optimal values of the system parameters. As such, we ran a numerical program (nested loops) that required the input of upper and lower bounds of each factor to predict the conditions that will yield maximum degree of TOC elimination. It was found that the efficiency of TOC decay may reach a maximum of 48% at pH=2.0, ZVI=24 mg L^{-1}, H_2O_2=0 mg L^{-1}, and P=120 W (the results are case-specific, i.e. estimated based on our laboratory conditions and sono-reactor). The striking feature of this prediction is that the maximum is achieved only at the very extreme conditions, i.e. the upper and lower boundaries. Hence, the predictions do not actually represent the optimal conditions, as they are either too low or too high requiring intensive consumption of energy and chemicals. As such, the values of control variables or model factors that are predicted by the model must be questioned and checked for technical and environmental applicability. In case they do not satisfy the applicability criteria, the numerical procedure must be repeated under one or more restrictions.

Considering the above, we restricted the mineralization efficiency to 40% and forced pH and power to constants as 2.75-3.0 and 72 W, respectively. The predicted value of H_2O_2 to ZVI ratio (by

mass) under these limitations was around 2.5-3.0. More importantly, a small sacrifice from the efficiency of the process may found to considerably improve the applicability of the model.

5.3.4. Model Validation

In k-fold cross validation, the entire dataset is divided into k equal portions at the beginning of the study. Each portion is used as test set whereas the rest of the dataset is used training set. The method of model validation was based on the "4-tuple cross-validation test" (Gültekin and Tezcanlı-Güyer, 2009) with the following procedure:

i) Splitting of the experimental data to four equal subsets and considering three subsets as the training set and the other as the test set.

ii) Replication of the procedure four times to allow the contribution of the "test set" to each subset

iii) Calculating the mean absolute percent errors (MAPE) between estimated and observed mineralization percentages by MAPE=$(E - O)/O$, where E and O represent the estimated and observed data points, respectively. The use of MAPE as the accuracy measure is due to its simplicity and provision of a good idea about the deviation of estimations from the actual data (Hyndman and Koehler, 2006).

The results of cross-validation tests as listed in Table 5.3 provided an average MAPE of 0.09 (no outliers), which means that the deviation between model prediction of TOC and the observed values is 9%.

Table 5.3. Results of cross-validation.

Replication #	MAPE
1	0.08534
2	0.10799
3	0.09834
4	0.08769

The validity of a regression model can also be tested directly by plotting the experimentally observed values of the dependent variable against predicted. The procedure required some additional experiments under the following factor ranges: ZVI=14-24 mg L^{-1}, H_2O_2=0-40 mg L^{-1}, P_o=72-120 W and pH=2.0-3.0. The plot of observed and predicted TOC decay against the experiment number that

contains information on the applied conditions is presented in Figure 5.8. The error bars showing the confidence intervals were calculated using the following expression (Walpole and Myers, 1998):

$$P = \hat{y}_i \pm t_{\alpha/2} s \sqrt{1 + x_i (X'X)^{-1} x_i}, \quad (5.2)$$

where: P is the prediction interval, $\hat{y}_i$ is the predicted value, x_i is the vector of independent variable values for the ith observation, s is the standard deviation of residuals and X is the matrix of independent variables used in multiple linear regression analysis.

The mean absolute percent error (MAPE) in this method of validation was 5.4% without excluding the outliers, and 5.0% with excluding the fourth experiment, where pH was 3.0 and H_2O_2 was at its maximum boundary. Note that the efficiency was a maximum in experiment 2 (47%), in which pH was 2.0 and H_2O_2 was 9 mg L^{-1}. The second best value (38.2) was obtained in experiment 7, where pH was 2.75 and all other values the same as in experiment 2. In summary, the data show that the regression model is valid and can be used safely as a tool for predicting the mineralization of aromatic micropollutants in a high-frequency sonoreactor operated at moderately acidic pH.

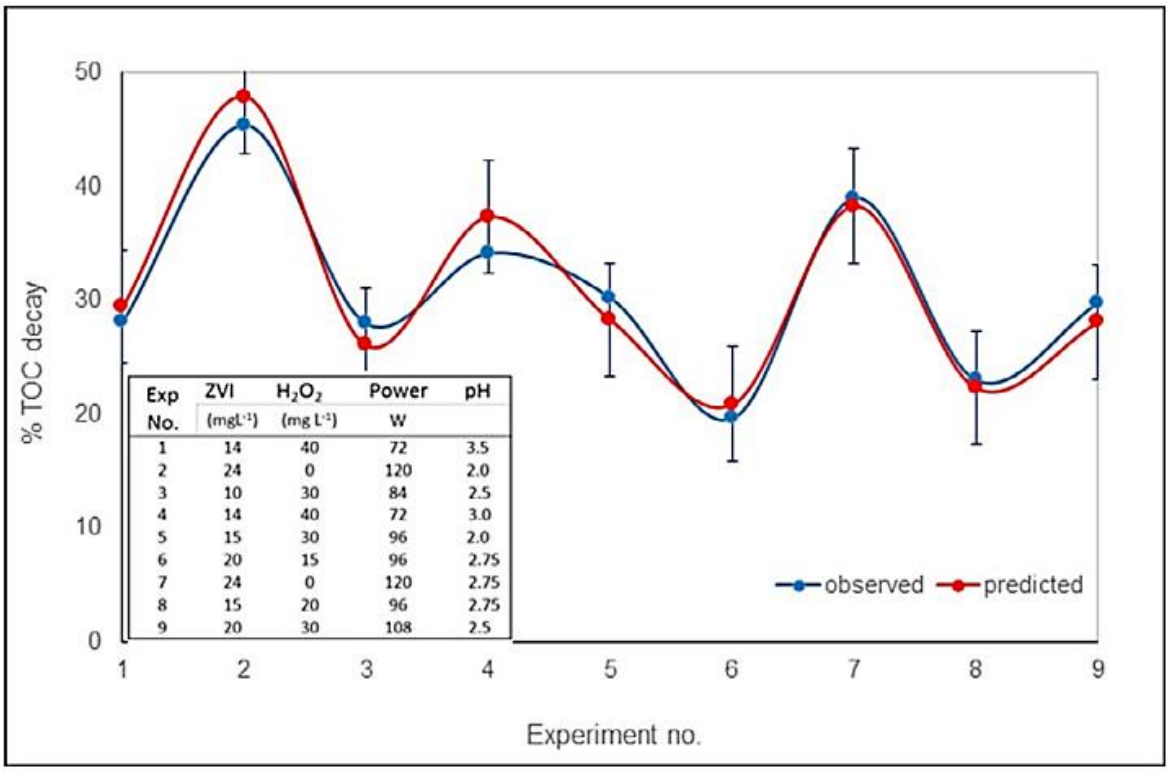

Figure 5.8. Experimental and model prediction of C-mineralization. Horizontal axis labels are as defined in the inset at the bottom left.

5.4. Conclusions

The degradation of salicylic acid in water by sonolysis and sonocatalysis using ZVI and/or ZVI/H_2O_2 was investigated to select the operating parameters (frequency, pH, concentrations of ZVI and peroxide) and to develop a predictive model that describes the interactive relationship between % mineralization and four of the control variables, namely power, pH, ZVI and H_2O_2. Preliminary experiments aimed to select the operating conditions revealed that the optimum frequency and solute concentrations were 572 kHz and 10 mg L^{-1}, respectively independent of the initial levels of pH and ZVI, but strongly dependent on the power input and H_2O_2 addition, the excess of which inhibited the mineralization of the compound.

A predictive regression model developed by "response surface methodology" provided a reliable relationship between the dependent variable (%mineralization) and the independent or control variables (pH, power, ZVI and H_2O_2). 3-D surface response plots generated from model predictions of TOC decay at varying levels of the model factors, or the control variables provided good information about the individual and interactive effects. Nevertheless, neither these plots nor a numerical search method were sufficient for selecting the optimal conditions that allow the achievement of a desired efficiency within reasonable levels of chemicals and energy consumption. The model predicted almost 50% carbon mineralization at the cost of maximum power and chemical (acid buffers) inputs, but it could also be forced to predict more feasible conditions such as 40% mineralization under 72 W, 2.75 $\leq$pH$\leq$3.0, and H_2O_2: ZVI mass ratio of 2.5-3.0.

Finally, the regression model was found valid in explaining the relationship between mineralization and the control variables of the system. Hence, it promises reliable predictions of the performance of a sonocatalytic reaction system, given sufficient experimental data generated under well-specified reactor, reagent and ambient conditions. The model can also be used in shedding light on the individual and interactive effects of these parameters on the performance or efficiency of the catalytic system.

6. SONOCHEMICAL AND SONOCATALYTIC DESTRUCTION OF METHYLPARABEN USING RAW, MODIFIED AND SDS-INTERCALATED PARTICLES OF A NATURAL CLAY MINERAL

Sonolytic destruction of methylparaben (MP) has been rarely investigated, despite the very unique and "extreme" conditions generated by ultrasound to yield a remarkably suitable medium for "high energy chemistry" (Ince et al., 2001). The only two studies related to sonochemical destruction of MP are those of Sasi et al. (2015) and Steter et al. (2014), which are related to setting of the optimum frequency and testing of the power of ultrasound in enhancing the efficiency of electrolysis, respectively. Our experience over years has shown that the major drawback of sonochemical oxidation of organic compounds is the low efficiency of carbon mineralization, which is a very crucial parameter in water treatment processes. Hence, application of ultrasound in combination with AOPs or other advanced water treatment processes (e.g adsorption, precipitation, etc.) is a promising solution to enhance the efficiency of carbon mineralization via increased rate of •OH generation and improved surface properites of the adsorbent, respectively (Ziylan and Ince, 2015). Despite its unique properties and high abundancy in Anatolia, sepiolite is rarely used for scientific or technical purposes, except as an adsorbent for the elimination of dyestuff and some organic compounds (Alkan et al., 2007). Moreover, there are no studies reporting the use of sepiolite together with ultrasound, although some clay minerals (other than sepiolite) have been lately combined with short frequency ultrasound to improve surface and film properties, to enhance food yields, to increase the efficiency of. ultrafiltration, to shorten the equilibrioıum time in adsorption, to facilitate intercalation of anionic surfactants and polymeric substances with significant reduction in size, to favor catalytic reactions, and to recover the catalyst without any changes in the crystalline structure (Chatel et al., 2016). The literature related to the elimination of PPCPs with sepiolite is limited to those studies reporting fixed bed adsorption of caffeine (Sotelo et al., 2013; Álvarez et al., 2015), adsorptive oxidation of metoprolol (a β-blocker) on sepiolite-supported ZVI (Daneshkhah et al., 2017), adsorption of salicylic acid, clofibric acid, carbamazepine and caffeine onto metal-doped sepiolite (Cabrera-Lafaurie et al., 2015), and adsorption of metronidazole on Fe-modified sepiolite (Ding and Bian, 2015). To the best of our knowledge, sepiolite has not been so far tested for adsorbing methylparaben, nor as a catalyst in sonochemical oxidation of organic compounds.

The present study aims to investigate and compare the degradation of MP by sonolysis and sonocatalysis in the presence of raw and variously modified particles of sepiolite. It also reports the oxidation byproducts of sonolysis and highlights the effect of operation parameters (e.g. pH,

MP/sepiolite concentration, frequency, bubbling gas) and particularly that of surface modification. The role of OH radicals was also tested by running the reactions in the presence of propanol and t-butanol, which are strong scavengers of •OH at the interfacial zone and the gas phase, respectively.

6.1. Experimental Procedures

6.1.1. Modification of Sepiolite

The surface of raw sepiolite after grinding was modified by:

i) **Pre-sonication**: Powders of raw sepiolite were added into pure water, mixed and shaken in a 35-kHz ultrasonic bath for **5**-min. After centrifugation, the precipitate was dried at 70°C for 6 hours. A fraction of the dried precipitate was separated and heated to 110°C to test the effect of heating on the adsorption properties of the surface (Chong et al. 2009).

ii) **Acid-activation:** Raw, grinded sepiolite was washed and stirred in a dilute solution of HCl for 10-h at 70°C. The suspension was filtered out; the filtrate was thoroughly washed (until no Cl^- remained) and dried at 70°C for 24 hours (Zhang et al., 2014).

iii) **Sonolytic intercalation**: The procedure was described in Section 3.2.2.5.

6.1.2. Silent Adsorption

Batch adsorption tests without ultrasound were carried out to investigate the adsorption capacity of raw sepiolite and the effect of surface modification and pH using 10 mg L^{-1} of MP and increasing concentrations of the mineral (1-8 g L^{-1}). The solutions were mixed at 125 rpm for 6 hours. The tests were repeated in the presence of 0.025-0.50 g L^{-1} of intercalated sepiolite.

6.1.3. Sonolysis and Sonocatalysis

The ultrasonic device used in homogeneous and heterogeneous sonolysis of MP was Reactor 2 (R2) described in the section 3.2.1.1. The experimental method involved sonication of MP without sepiolite addition to select the optimum concentration, frequency, injected gas, power and pH. Samples were monitored periodically to analyze the concentrations of MP and TOC. The tests were repeated in the presence of sepiolite at optimized conditions to reconfirm the same conditions and to select the optimum sepiolite concentration.

6.2. Results and Discussion

6.2.1. Silent Adsorption of MP on Sepiolite

Batch adsorption tests with 10 mg L^{-1} MP and various concentrations of raw sepiolite during 6-h mixing at two pH levels showed that adsorption was most favorable at pH 3, and increased substantially with increasing concentrations of sepiolite. Higher adsorption capacity of the surface at acidic pH is due to increased quantity of surface-OH_2^+ groups, while at pH>6.7, i.e. the region at which the surface is negative (pKz=6.7) there are practically no exchangeable anions at the outer surface and thus no adsorption (Sasi et al., 2015). We also found that the adsorption capacity of the mineral was slightly weakened upon pre-sonication, and considerably weakened by further treatment (heating), as depicted in Figure 6.1 (a). The output signifies the destruction of the anionic sites on the surface of the mineral, which exhibits amphoteric characteristics via substitutions within the lattice of the solid (of Si^{4+} and Mg^{2+}) and breaking of the Si–O–Si (siloxane) group during grinding (Alkan et al., 2005).

In another batch, we lowered the concentration of the mineral by forty-times and tested the activity of raw and modified particles (pre-sonicated, acidified and 60-min intercalated) under the same conditions. We found that the extent of adsorption was significantly lowered, nevertheless it was a maximum in the presence of 60-min intercalated nanocomposite at the minimum test concentration. The data are presented in Figure 6.1 (b).

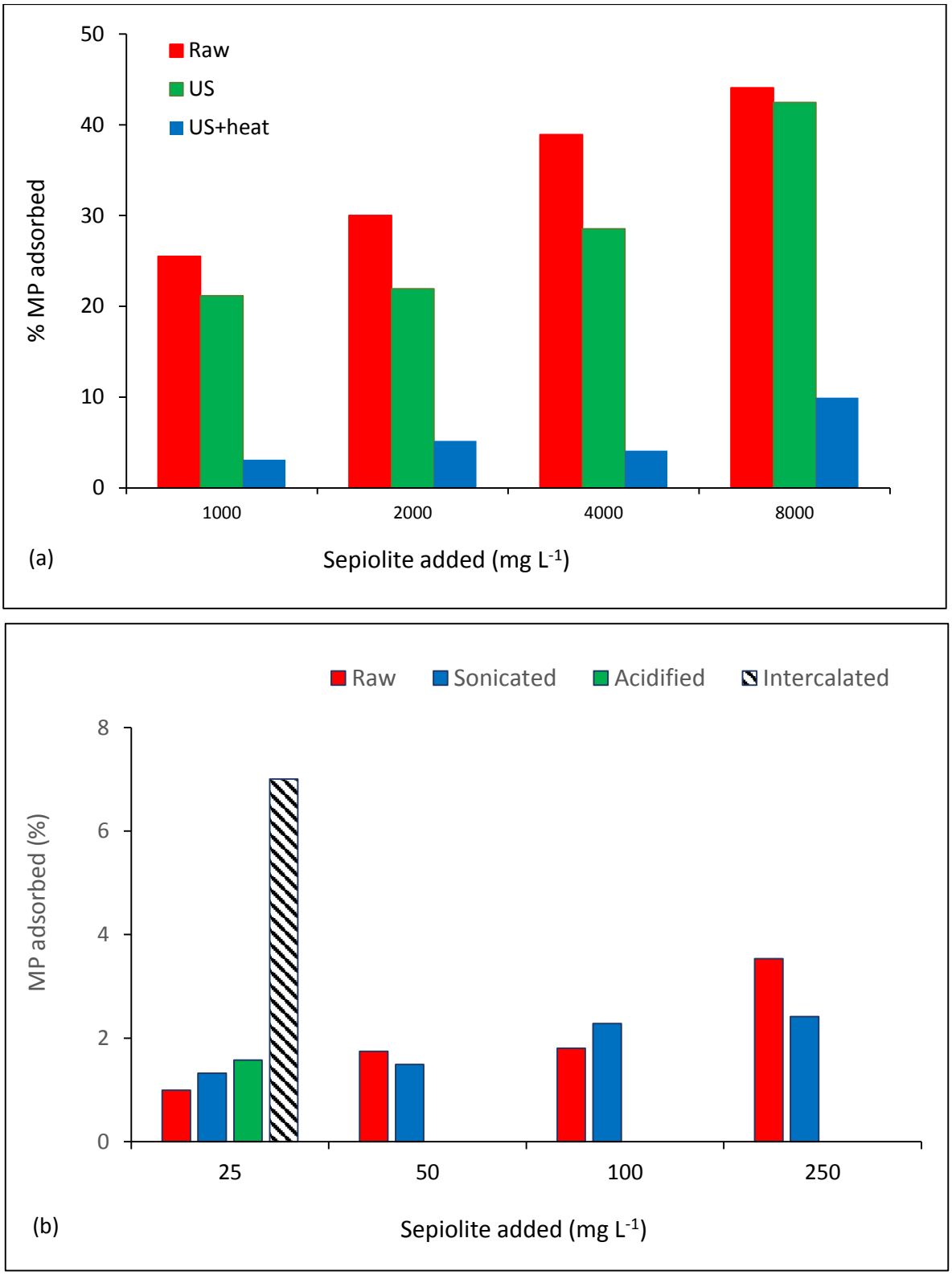

Figure 6.1. Impact of concentration and surface modification of sepiolite on the degree of MP adsorption (C_0=10 mg L^{-1}) at pH 3 after 6-h contact with the mineral.

6.2.2. Characterization of Raw and SDS-intercalated Nanoparticles of Sepiolite

SEM images of raw and SDS-intercalated particles of sepiolite are presented in Figure 6.2 (a-d), which show that the original structure (a) was highly fibrous with large voids/holes between the loosely-packed aggregates. Particles of the first nanocomposite (b), i.e. the 20-min intercalate were more closely packed and the distance between the layers was much larger than that of the raw sepiolite. More importantly, the aggregates were smoother and more porous. After longer sonication (40-min and 60-min-(c-d), however, the voids between the clusters were found to disappear and the interlayer distance was considerably shortened.

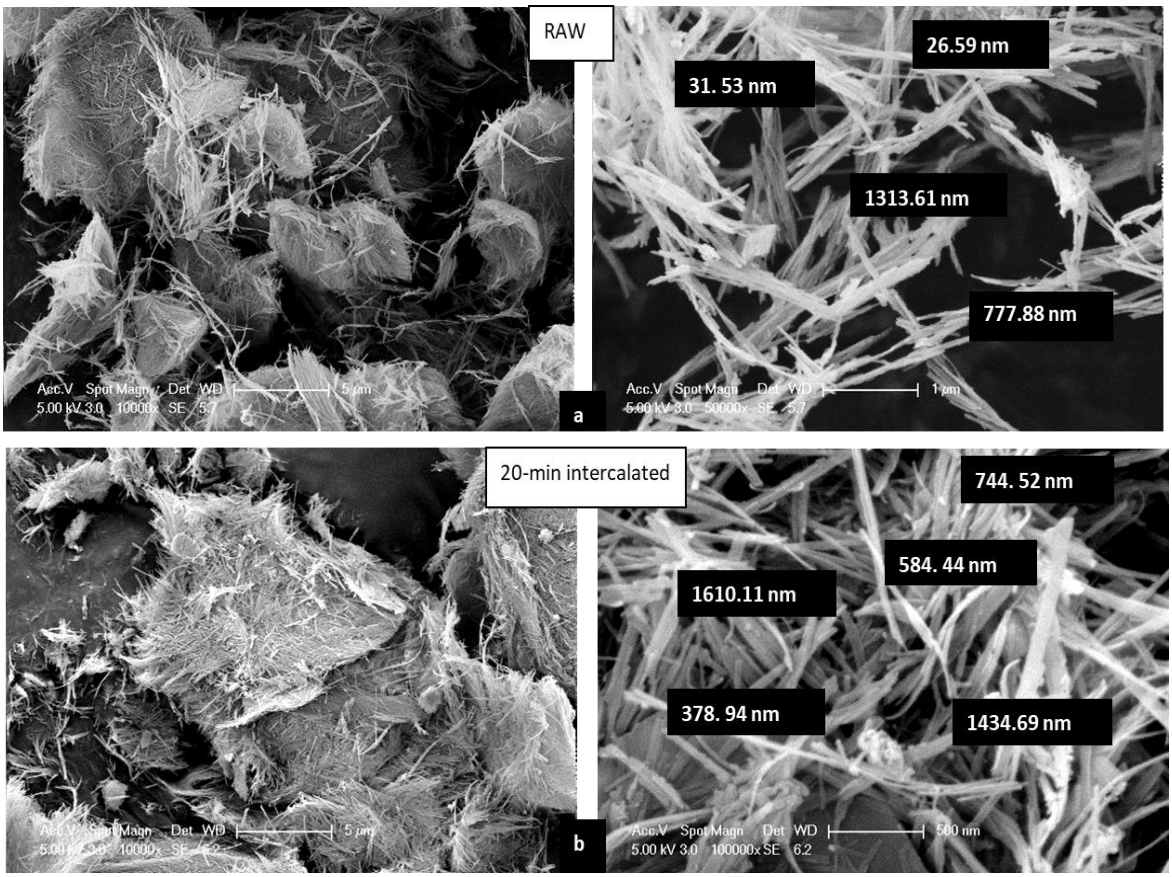

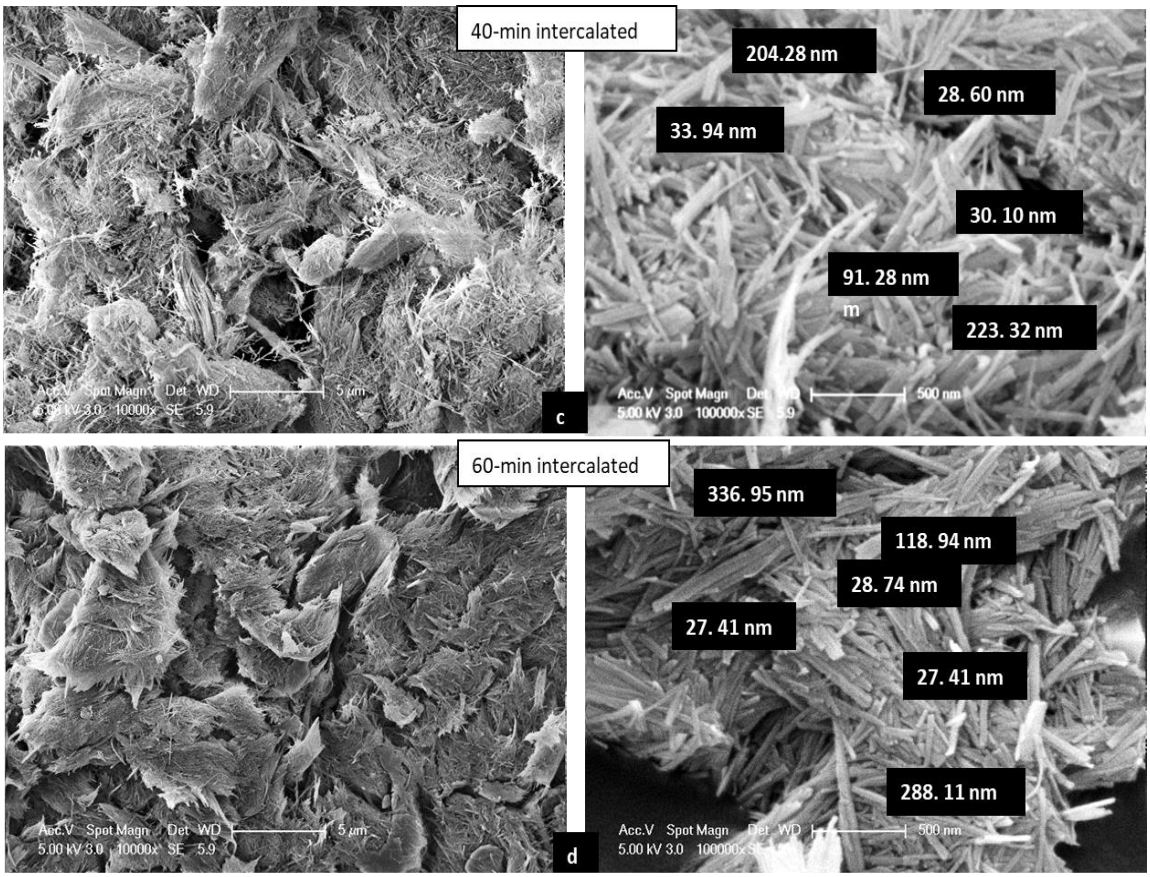

Figure 6.2 (a-d). SEM images of raw, 20-min, 40-min and 60-min SDS-intercalated particles of sepiolite

6.2.3. Sonolysis without Sepiolite

Sonication of MP to select the optimum reaction conditions showed that the rate of reaction was pseudo-first order and maximum when the initial concentration of the compound was 10 mg L^{-1}. Lower reaction rates in the presence of higher concentrations implies that the gas-liquid interface is the main reaction site, i.e. MP partitions between the liquid and the interface. The hypothesis was justified by analyzing the relation between the reaction rate and the initial concentration, as depicted in Figure 6.3. We found that the data fit perfectly to the Langmuir-Hinshelwood equation (Eq. 6.1), which is commonly used to model heterogeneous reaction kinetics based on the assumption that adsorption and desorption are in equilibrium (Okitsu 2005; Xiao et al., 2014):

$$\frac{1}{r_0} = \frac{1}{kKC_0} + \frac{1}{k} \tag{6.1}$$

where: r_0 is the initial reaction rate (mM min^{-1}), k and K are the second-order reaction rate and the equilibrium constants, respectively (mM min^{-1} and mM) and C_0 is the initial concentration of MP (mM).

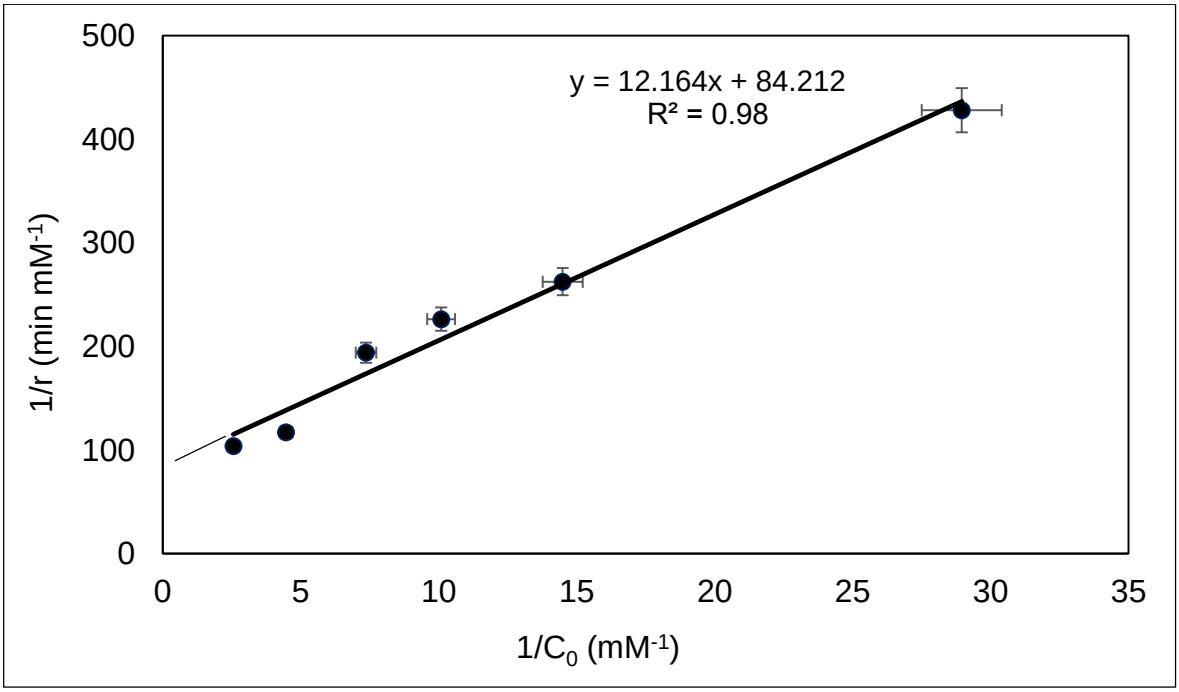

Figure 6.3. Heterogeneous kinetic modeling to show the relation between the rate of sonochemical decay and the initial concentration of MP. Reaction conditions were f=572 kHz, pH= 6.5, t=10-min, C_0=5, 10, 15, 20, 30, 60 mg L^{-1}

The apparent reaction rate constants and the corresponding degrees of TOC decay at each test concentration are listed in Table 6.1. Due to the highest rate of reaction and highest degree of TOC decay, 10 mg L^{-1} was selected as the working test concentration in all experiments.

Table 6.1. The pseudo-1st order reaction rate constants estimated for 10-min sonolysis (at 572 kHz) of increasing concentrations of MP at pH 3.0.

MP (mg L^{-1})	-k' (min^{-1})	% TOC removed
5	0.098	8.56
10	0.090	7.62
15	0.068	5.49
20	0.054	4.20
30	0.040	2.11
60	0.024	2.00

It is well known that injection of a suitable gas into sonicated liquids increases the nucleation sites and the collapse temperature of cavitation bubbles (Ince et al., 2009). Selection of the most suitable gas was based on injecting successively of air, argon and ozone into solution at equal rates

while monitoring the concentration of the target compound during sonolysis. It was found that the rate of MP decomposition was very close under each gas atmosphere, as depicted in Figure 6.4. However, the degree of TOC decay displayed variations, as it increased in the order: O_3>Ar>Air. The data are depicted in the inset of Figure 6.4, which also shows the degree of latent TOC decay, i.e. total fraction of C-mineralization 8-h after reaction. Better performance of ozone in C-mineralization is due to the production of excess reactive oxygen species as well as the likely reactivity of the oxidation byproducts with molecular ozone. On the other hand, an increase in total mineralization long after termination of the reaction under air bubbling must be due to the formation of some stable and reactive species. Sonochemical reactions occurring during air injection into water are outlined in (Eq. 2.13-2.19). Note the formation of nitrite and nitrate radicals, which are less reactive with aromatic compounds than •OH ($k=10^7$ L $mol^{-1}s^{-1}$), but more stable (Gultekin and Ince, 2008). Henceforth, we selected air as the operating bubbling gas owing to its ease of applicability, cost-effectiveness (relative to Ar and O_3) and residual effect long after the reaction ends.

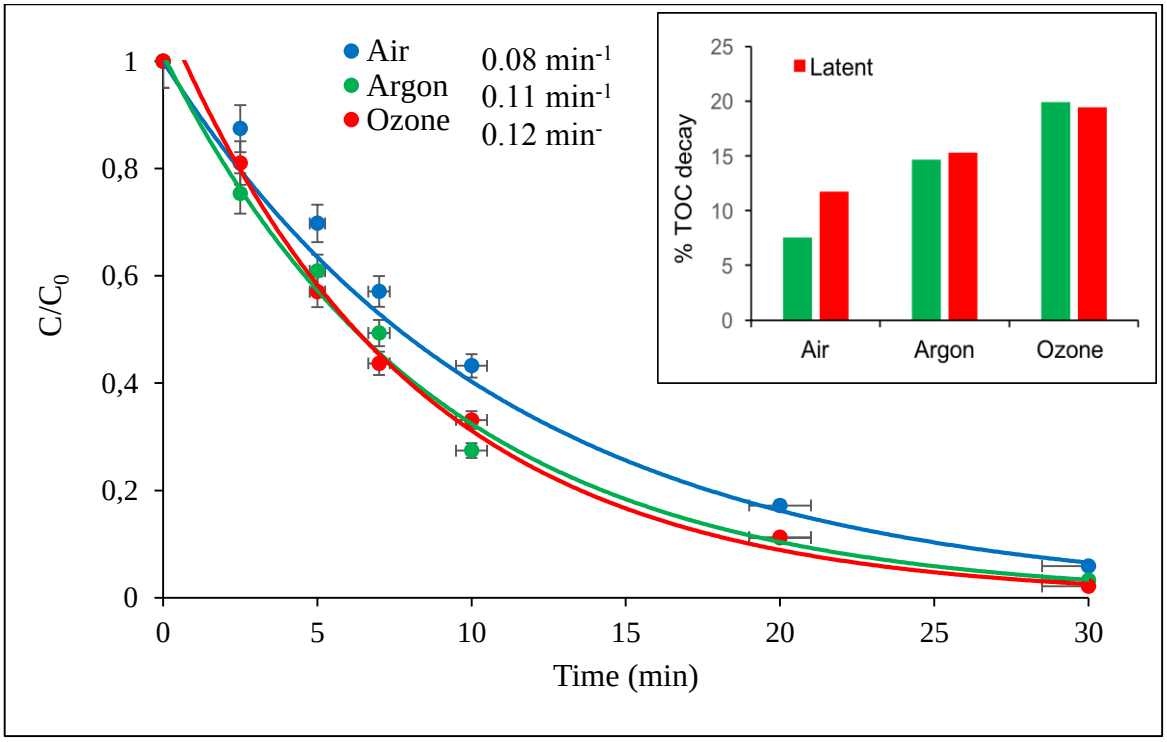

Figure 6.4. Impact of bubbling gas on the oxidation and mineralization of MP during sonolysis at 572 kHz at pH 3.0. "Latent" refers to 8 hours of silent reaction right after sonolysis.

The rest of the operational parameters were selected on the basis of reactivity of MP, low reagent consumption and cost-effectiveness. The list of findings that guided the selection process is presented in Table 6.2. Accordingly, 861 kHz and pH 6.5 were the working conditions in all experiments unless indicated otherwise. Although pH 3 was more favorable for the silent adsorption of MP and for the

reactions under 572 kHz, we preferred the neutral pH to minimize the use of chemicals and to take advantage of using the higher frequency. The selection was also justified by the marginal adsorption of MP at the test concentration of the adsorbent, regardless of pH. Finally, a higher reaction rate at 861 kHz and pH 6.5 is due to reduced resonant bubble size, leading to increased number of active bubbles and oscillations, and a larger efficiency of •OH ejection, as explained in a previous study (Gültekin et al., 2009; Ince et al., 2009).

Table 6.2. The apparent reaction rate constants of sonochemical decay of MP at varying pH and frequencies.

pH	**k' (min^{-1})**	
	577 kHz	861 kHz
3.0	0.081	0.072
4.5	0.070	0.060
6.5	0.063	0.079
9.0	0.027	0.028

Monitoring and identification of the oxidation byproducts at the selected operating conditions showed that well-defined peaks were detectable only at the 10th-min reaction (due to rapid oxidation of the compound after longer sonication, and the restrictions of the analytic device for identifying low molecular weight organic acids). Accordingly, we detected six major peaks at molecular weights of 85, 108, 110, 134, 138 and 150 g $mole^{-l}$ with 10-s relative intensities of 1.42, 0.30, 0.15, 0.50, 0.42 and 0.15, respectively. The peaks correspond successively to propionic acid, benzoquinone, catechol, maleic acid, 4-hydroxybenzoicacid and tartaric acid, some of which are in good agreement with the literature (Sasi et al., 2015). The data are presented in Figure 6.5, together with the peak for the mother compound-methylparaben.

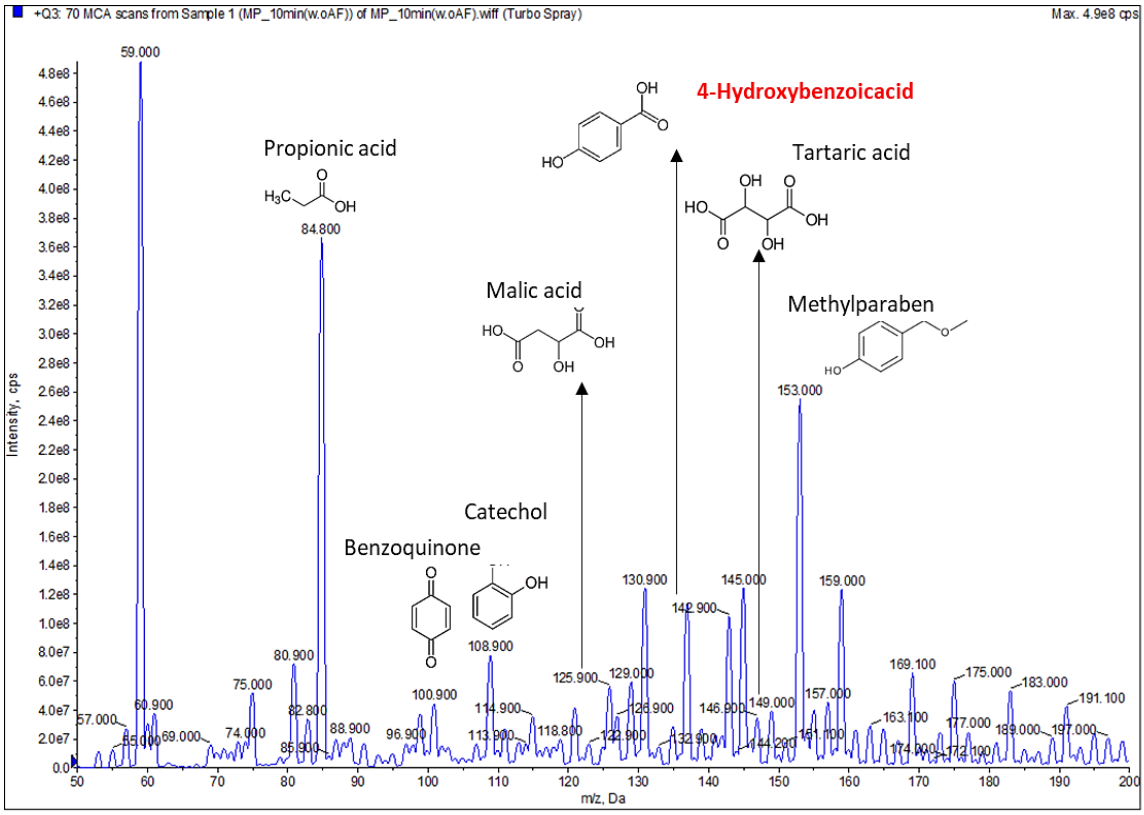

Figure 6.5. LC/MS/MS chromatogram of methylparaben sonicated at 861 kHz for 10-min.

The role of OH radicals and the potential reaction sites were assessed by 10-min sonolysis of the target compound in the presence of various doses of propanol and t-butanol, the latter being a stronger scavenger of HO• at the gas-liquid interface (Henglein and Kormann, 1985). Additionally, we sonicated the compound at pH 9.0 (adjusted successively with NaOH and $NaCO_3$) to investigate the effect of carbonates as strong scavengers of OH• in the bulk solution. We found that the reaction was considerably slow at alkaline pH (k=0.036 min^{-1}) regardless of the pH-adjusting reagent used, indicating the insignificance of carbonate species. As such, the reaction proceeded slowly only because of the alkalinity of the solution, at which the compound acquired a slightly negative charge (pK_a=8.5) and became slightly more hydrophilic. Thus, under these conditions both adsorption (on sepiolite) and diffusion to the bubble-liquid interface were partially hindered, nevertheless the major reaction site was still the bubble-liquid interface. Moreover, those reactions that took place in the bulk liquid were not governed by •OH-attack or hydroxylation, for otherwise they would proceed much slower in the presence of carbonate species. Hence, the major reaction site is the bubble-liquid interface, as justified by the larger degree of rate inhibition in the presence of t-butanol, than in that of propanol, which exists mainly in the gas phase. It was found that when the scavengers were present at a molar ratio of 5:1 (scavenger to MP), the reaction was slowed down by 11% and 23% in the presence of propanol and t-butanol, respectively, while at a dose of 50:1, the rate was slowed down by 16% and 34%, respectively. The data are presented in Figure 6.6 Note that as the concentration of

propanol increases, less •OH are ejected out from the bubble interiors. We concluded that although the degradation of MP was governed mainly by reactions with •OH at the gas-liquid interface, there were other mechanisms acting such as hydrolysis (owing to the formation of supercritical water) that has also been suggested by Sasi et al. (2015) to explain the formation of hydroxybenzoic acid during sonolysis of MP. Note also that hydrolysis has been reported as the first step in the aerobic degradation of MP (Valkova et al. 2001) and a key reaction in ultrasound-assisted enzymatic degradation of the compound (Schlittenbauer et al. 2016).

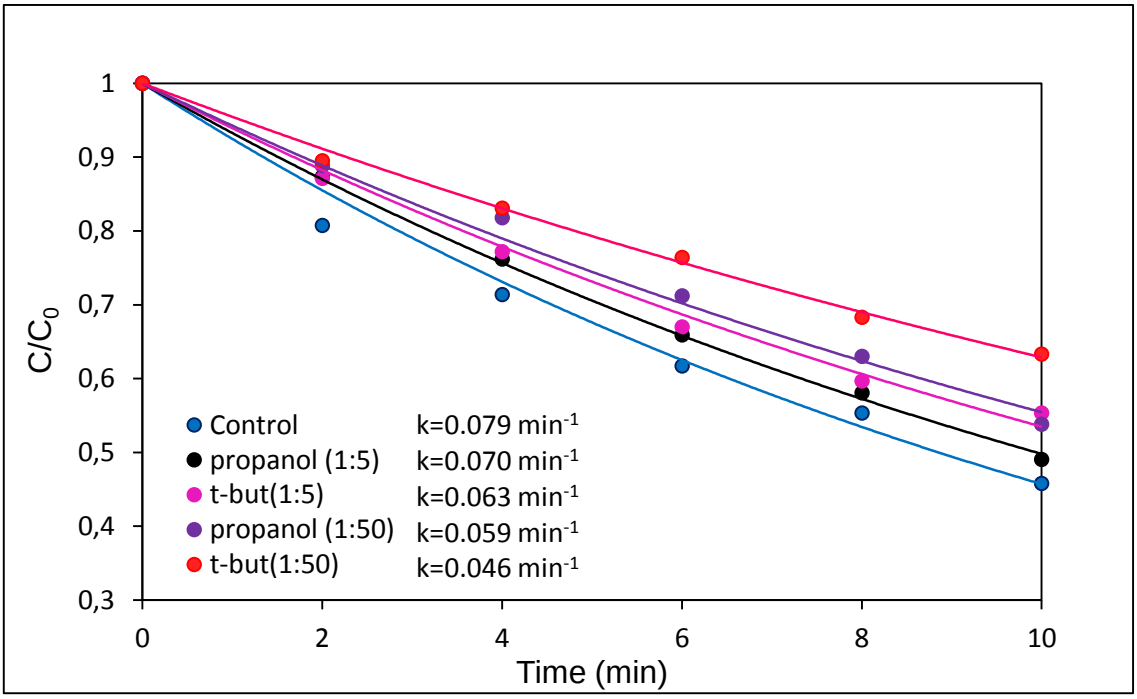

Figure 6.6. Relative impacts of propanol and t-butanol on the rate of MP decay at pH 6.5 during sonication at 861 kHz.

6.2.4. Sonocatalysis in the Presence of Raw and Surface-Modified Sepiolite

6.2.4.1. Raw sepiolite. The addition of raw sepiolite during sonolysis at 572 and 861 kHz induced only a slight increase in the rate of MP decay with respect to the corresponding control levels, as depicted in Figure 6.7 (a), while it brought a significant enhancement to the mineralization of the compound. The latter is presented in Figure 6.7 (b), which also shows that the process was inversely proportional to the concentration of sepiolite in the reactor. Accordingly, 861 kHz, 25 mg L^{-1} and 6.5 were reconfirmed as the operating conditions of frequency, sepiolite concentration and pH, respectively for the catalytic experiments.

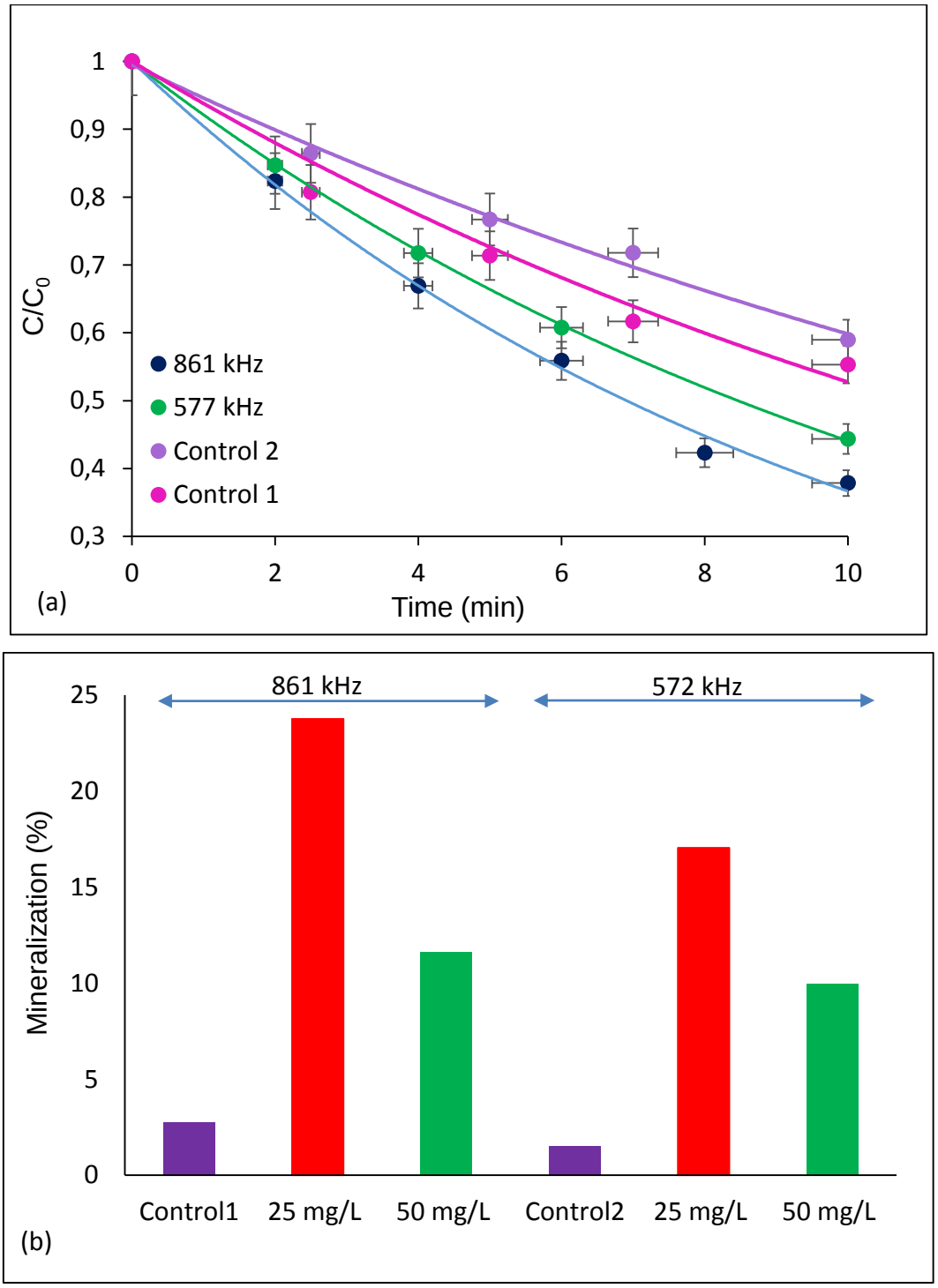

Figure 6.7. Impacts of frequency and sepiolite concentration on the rate of sonocatalytic decomposition (a) and carbon mineralization (b) of MP (C_0=10 mg L^{-1}) at pH 6.5. Control 1 and Control 2 refer to sonication without sepiolite at 861 and 572 kHz, respectively. The concentration of sepiolite in (a) was 25 mg L^{-1}.

6.2.4.2. Acid-activated and pre-sonicated sepiolite. Modification of the surface of sepiolite by acid-activation and pre-sonication was found to improve the rate of MP decay, but not necessarily the degree of carbon mineralization. The data presented in Figure 6.8 show that at pH 6.5, the initial rate

of MP reaction increased from 7.55 x10^{-2} min^{-1} (in the presence of raw sepiolite) to 8.87 x10^{-2} and 9.49 x10^{-2} min^{-1} upon sonication in the presence of acid-activated and pre-sonicated particles, respectively. On the other hand, while mineralization of organic carbon was enhanced in the presence of pre-sonicated particles (+39%), it was significantly declined in that of acid-activated sepiolite (-59%), as depicted at the bottom of Figure 6.8.

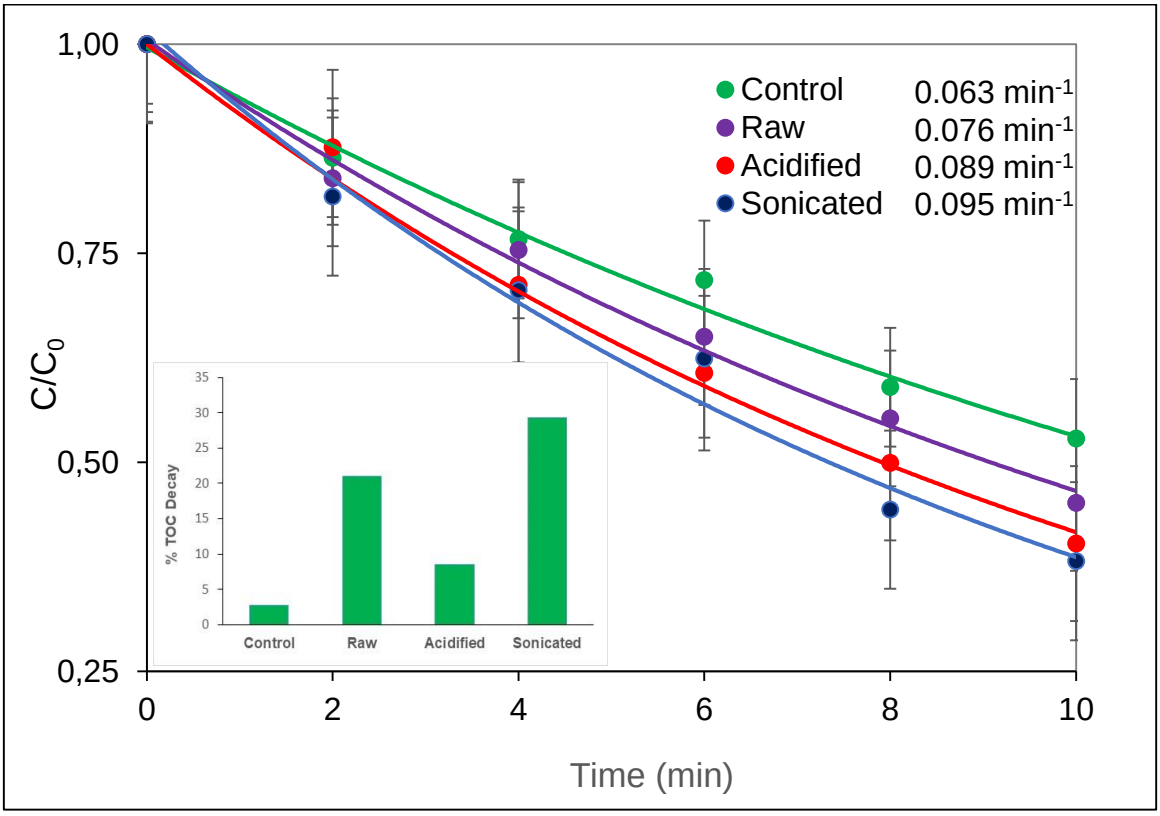

Figure 6.8. Profiles of MP decay by sonocatalysis at 861 kHz in the presence of 25 mg L^{-1} raw, sonicated and acid-activated sepiolite at pH 6.5.

The purpose of acid activation is indeed to increase the amount of acidic sites by creating excess tunnels, edges and broken bonds, which in turn improve both the porosity and the specific surface area of clay minerals (Ahlrichs et al., 1975; Celdeira et al., 2014). On the other hand, it has been reported that improper or excess acidification may result in the loss of zeolites and hydroxyl water from the structure of sepiolite, leading to plugging of the micropores and collapse of the crystal structure (Rodriguez et al., 1995). This might be the reason for the low activity of the acidified particles in the mineralization process.

6.2.4.3. SDS-intercalated nanocomposites of sepiolite. Finally, we repeated the experiments in the presence of sonolytically synthesized SDS-sepiolite nanocomposites and found surprisingly that while they were relatively inactive at the selected pH, the activity was considerably enhanced at pH

3.0. A comparative list of 10-min reaction rate constants and 30-min TOC decay fractions observed at pH 3.0 and 6.5 during sonolysis of MP at 861 kHz is presented in Table 6.3. The data clearly show that the time of sonication in the synthesis of intercalates and the level of pH in the operation of the degradation reactions are the most crucial parameters in controlling the process efficiency. Deterioration of the catalytic activity of the particles synthesized by sonication longer than 20-min is most likely due to exfoliation of the sepiolite sheets, leading to partial destruction of the layered structure. A similar interpretation is found in the literature about long-sonicated intercalates of SDS-clay composites with reduced surface area and pore diameter (Belova et al., 2009).

Table 6.3. Relative activity of raw, modified and SDS-intercalated particles of sepiolite at acidic and neutral pH. The rate coefficients and TOC decay fractions correspond to 10-min and 30-min reaction of MP (C_0=10 mg L^{-1}), respectively during sonolysis at 861 kHz.

Type of Sepiolite	k (min^{-1})		% TOC decay	
	pH 3.0	pH 6.5	pH 3.0	pH 6.5
None	7.22 x10^{-2}	6.33 x 10^{-2}	10.73	2.76
Raw	7.35 x 10^{-2}	7.55 x 10^{-2}	17.19	20.98
Sonicated	7.67 x 10^{-2}	9.49 x 10^{-2}	7.32	29.33
Acidified	7.61 x 10^{-2}	8.89 x10^{-2}	15.25	8.58
20-min NP	16.33 x 10^{-2}	6.66 x 10^{-2}	37.90	21.17
40-min NP	11.30 x 10^{-2}	4.24 x 10^{-2}	22.81	14.09
60-min NP	10.06 x 10^{-2}	3.91 x 10^{-2}	19.04	15.06

6.3. Conclusions

The widely-used PPCP-methylparaben was found to decay readily by high-frequency ultrasonic irradiation to produce phenolic and aliphatic oxidation byproducts, without however adequate carbon mineralization. The major reaction site was the bubble-liquid interface, where the governing mechanism was •OH-addition, while the reactions taking place at the bulk liquid were governed by other mechanisms. The reaction kinetics obeyed pseudo-first order rate law and followed Langmuir-Hinshelwood model, as typical of heterogeneous reaction systems.

The addition of sepiolite (a natural clay mineral recognized with its layered and porous structure) at optimized reaction conditions (861 kHz, pH 6.5, 25 mg L^{-1} clay) was found to enhance the rate of MP decomposition, but not the degree of TOC decay. Modification of the catalyst surface by pre-

sonication not only enhanced the reaction rate, but also resulted in a significant enhancement in carbon mineralization. On the other hand, acid-activated particles were only effective in accelerating the decomposition of MP, and totally ineffective for enhancing the overall degradation, or mineralization of the compound.

The catalytic activity of the particles was substantially improved upon sonolytic intercalation with an anionic surfactant (SDS), leading to a massive surface area, increased porosity, and very long interlayer distances. Nevertheless, the length of sonication time for intercalate preparation was critical, as longer sonication than 20-min led to shortening of the interlayer distance and deterioration of the layered structure. Finally, the efficiency of the degradation process using 20-min intercalates of sepiolite was a maximum at pH 3.0 yielding 38% TOC decay.

7. OPTIMIZATION OF METHYLPARABEN DEGRADATION BY SONOCATALYSIS

The present section presents the final revision of the manuscript "Optimization of Methylparaben Degradation by Sonocatalysis" that is under review in *Ultrasonics Sonochemistry*.

Ultrasonic irradiation of water bodies contaminated with refractory chemicals has lately emerged as a viable technique in water treatment operations, owing to the "extreme" conditions generated by the collapse of cavitation bubbles followed by the formation of very reactive radical species (Ince et al. 2001). Nevertheless, the method is energy-intensive and requires long reaction times to obtain appreciable degrees of carbon-mineralization. Accordingly, sonochemists have lately focused on increasing the efficiency of the process by the addition of solid particles, or by combining ultrasound with other processes such as adsorption, advanced oxidation and photocatalysis (Bokhale et al., 2014; Ince, 2018). Optimization of such complex systems, however, is very complex unless using a suitable experimental design methodology (Palasota and Deming, 1992). Among numerous methods of statistical analysis, the response surface methodology (RSM) is the most effective for modeling and analysis of processes, and for optimizing a response variable influenced by several dependent variables (Ay et al., 2009; Montgomery, 2008). The method also provides a plot of the system response (e.g. a reaction yield) against each variable that influences it. Although such models may include high order terms of independent variables, a full second-order polynomial model is often adequate for describing a wide variety of multifactor chemical systems (Montgomery, 2008).

Methylparaben (MP) is one of the most common compounds among thousands of PPCPs (pharmaceutical and personal care products) due to its wide consumption in toothpastes, cosmetics, textiles, foodstuff and beverages, as a preservative and antibacterial agent. However, the compound is classified under emerging contaminants, due to its potential contribution to the incidence of breast cancer (Zúñiga-benítez et al., 2016). Hence, elimination of MP from water has lately been a primary environmental concern, and a variety of methods comprising of biological and chemical processes have been tested. Nevertheless, sonochemical and/or sonocatalytical methods are rarely explored, and the only two studies are those reporting the selection of an optimum frequency (Sasi et al., 2015) and investigation of the synergistic effect of ultrasound on electrolytic destruction of the compound (Sterer et al., 2014).

The present study aims to explore the individual and interactive effects of the experimental parameters of MP degradation by sonocatalysis in the presence of sepiolite as the catalyst. The optimization of the experimental system was based on the data generated during sonication of varying concentrations of the compound under 572 and 861 kHz at varying pH, ultrasonic power and catalyst concentrations. The data were used to generate two factorial matrices that covered the experimental regions defined, and the corresponding axial areas. The response associated with each matrix was defined as the pseudo-first order reaction rate constant estimated by fitting the concentration-time (10-min) data to the first order rate equation.

7.1. Experimental Methods

The reactor used in all experiments was R2 as described in Section 3.2.1.1. Sample solutions were mildly aerated during sonication to maintain sufficient nuclei for cavity formation. The rate of MP decay in each set of experiment (with different initial conditions) was estimated by monitoring the concentration of the compound during reaction and fitting the data to the first order rate equation.

7.2. Factorial Design and Data Analysis

Modeling of the experimental system was based on a factorial design technique with a 4-factor-5-level (for high sepiolite concentrations), and a 2-factor 5-level (for low sepiolite concentrations) composite. The design matrices were generated by MATLAB 11.2, and statistical analysis of results and validation of the regression models were carried out using the “R Gui” software.

7.3. Results and Discussion

7.3.1. Control Experiments

The optimum conditions of sonolysis (pH, C_0, frequency) were selected based on some control experiments conducted without sepiolite. The data were generated at four pH levels (3, 4.5, 6.5 and 9), six MP initial concentrations (5, 10, 15, 20, 30 and 60 mg L^{-1}) and two frequencies (572 and 856 kHz). The results are presented in Figure 7.1 (a-b) and Figure 7.2.

Analysis of the MP in samples withdrawn from the reactor within 2-min intervals showed that the rate of reaction was pseudo-first order and faster at acidic pH, regardless of the operating frequency (Figure 7.1 (a-b)). Slowing down of the reactions with increases in pH to the alkaline level

is due to ionization of the compound (pKa=8.5), leading to enhanced hydrophilicity and reduced likelihood of diffusion to the bubble-liquid interface, where the concentration of HO• is a maximum (Gültekin and Ince 2008).

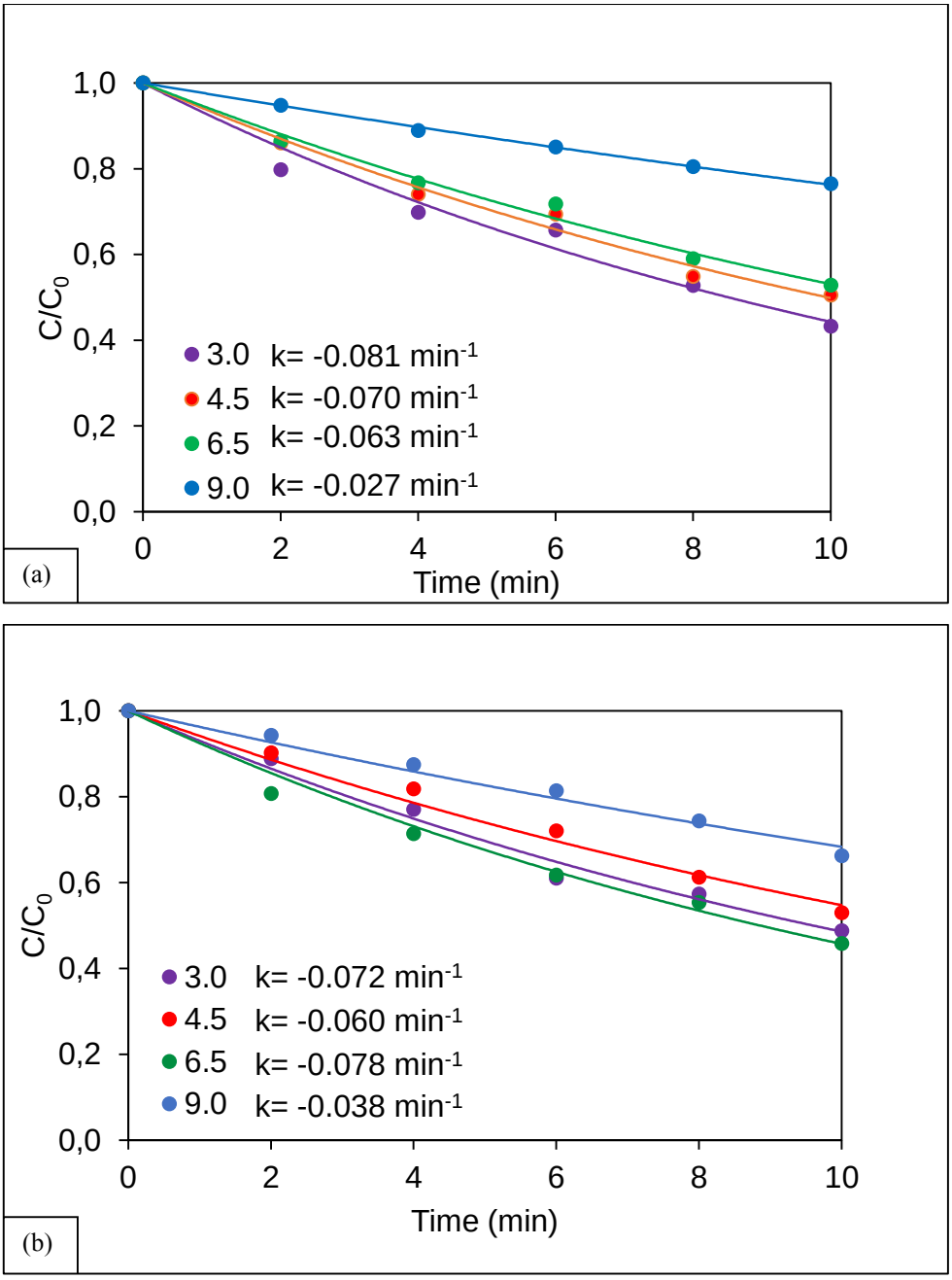

Figure 7.1. Effect of pH on the rate of MP decay by sonolysis without sepiolite at 572(a) and 856 kHz (b).

The rate of reaction also slowed down with increases in the initial concentration of MP (Figure 7.2), which is typical of sonochemical reactions in concentrated solutions of hydrophilic compounds (Kidak and Ince 2006; Serpone et al. 1994; Gültekin and Ince 2008). Note also that the reaction was most rapid at the lowest test concentration, while the degree of TOC decay was a maximum at the

next lower concentration (10 mg L^{-1}), most likely due to the more rapid formation of organic acids in the former. In another set of control experiments we monitored the concentration of H_2O_2 (data not given) during sonolysis at the two test frequencies, as an indicator of the efficiency of HO• formation. The data showed that the rate of formation was zero-order at both frequencies, but larger at the higher one. The finding is consistent with the literature reporting increased efficiency of HO• formation at higher frequencies via more frequent oscillations and higher incidence of cavitation collapse (Gogate and Pandit 2000).

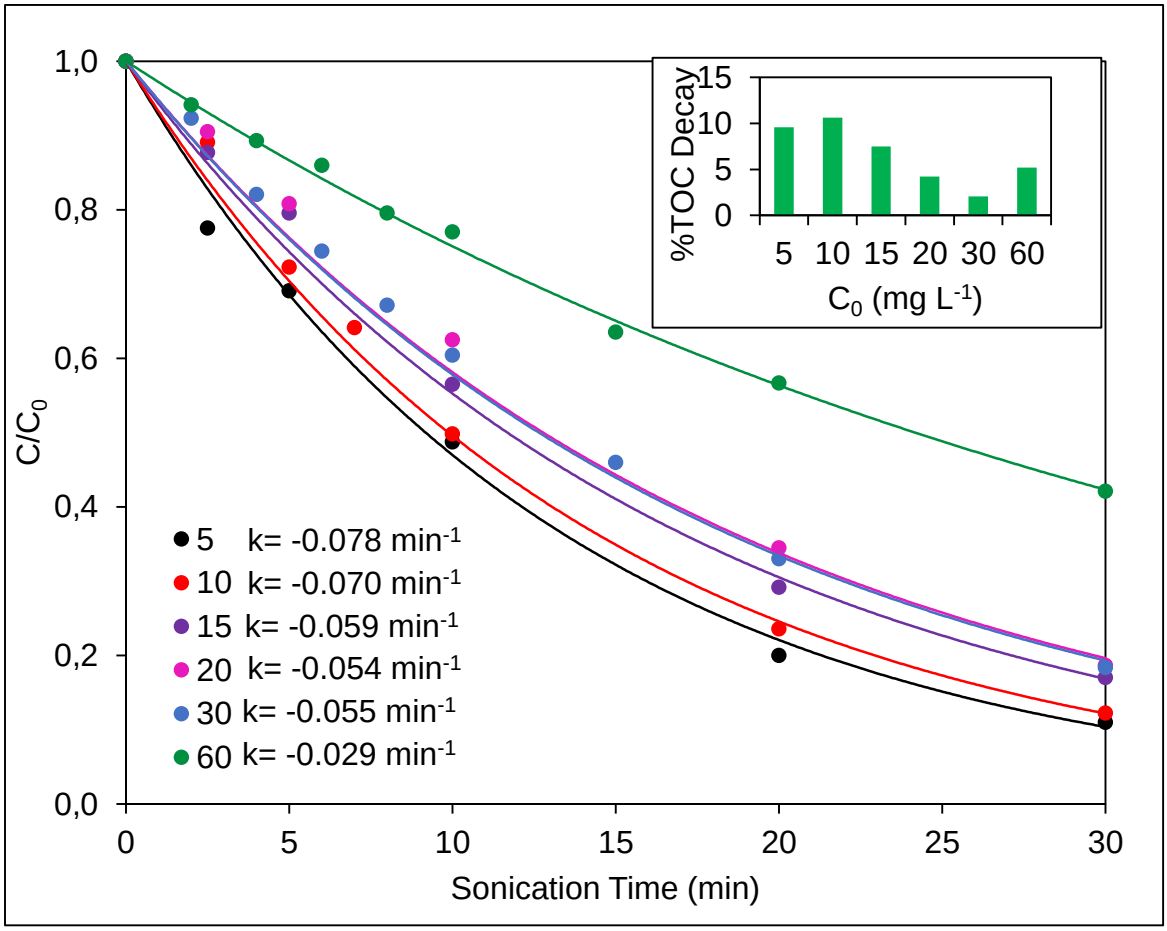

Figure 7.2. Effect of initial concentration on the apparent (10-min) rate of MP decay at 572 kHz and pH=6.5.

Microtox analysis of the reaction aliquots showed that after 30-min sonication at 572 kHz, pH 6.5 and C_0=10 mg L^{-1}, the toxicity was considerably reduced, improving from the "toxic" to the "non-toxic" level in accordance with the %EC50 scale provided in the literature (Chang et al. 2013). The data are presented in Table 7.1 as 15-min EC_{50}.

Table 7.1. Microtox toxicity and the corresponding classification of MP before and after 30-min sonication at 572 kHz.

Time (min)	% EC50	Classification
0	13.12	Toxic
30	171.90	Non-toxic

7.3.2. Sonocatalysis and Experimental Design

Preliminary experiments of sonocatalysis were initiated by adding 25 mg L^{-1} sepiolite to the reactor containing 10 mg L^{-1} MP, followed by sonication at two pH levels (3.0 and 6.5) and two frequencies (572 kHz and 861 kHz) for 10 and 30-min. Analysis of the data for the reaction rate constants and TOC decay provided the results presented in Table 7.2. Using these and the rest of the results obtained with higher and lower sepiolite doses, we made two experimental designs: to cover high (0.1-4.0 g L^{-1}) and low sepiolite concentrations (0.01-1.0 g L^{-1}). The response variable in each design was selected as the apparent reaction rate constant corresponding to 10-min reaction of MP at various pH and two frequencies.

Table 7.2. The impact of sepiolite addition on the initial rate of MP (C_0=10 mg L^{-1}) decay and TOC mineralization at two pH levels and two frequencies.

Sepiolite (mg L^{-1})	k x10^{-2} (min^{-1})				%TOC decay			
	572 kHz		856 kHz		572 kHz		856 kHz	
	pH 3.0	pH 6.5	pH 3.0	pH 6.5	pH 3.0	pH 6.5	pH 3.0	pH 6.5
0	8.11	6.33	7.22	6.33	7.52	10.61	10.73	2.76
25	8.90	8.20	7.35	7.55	17.20	20.98	17.19	21.92

7.3.2.1. Design 1: High Sepiolite Doses. Factors of the design and the restrictions on their allowed ranges were: sepiolite concentration (0.1-4.0 g L^{-1}), pH (3.0-9.0), sonication time (10-60 min) and power (70-100% of maximum). The model developed showed that the main parameters affecting the rate of MP decay were initial concentration, frequency, sepiolite dose, pH, power, and sonication time. Due to the complexity of such a multi-factor system, we reduced the number of factors by

setting the values of frequency and initial concentration to 572 kHz (faster rate of degradation at acidic pH) and 10 mg L^{-1} (largest TOC decay efficiency), respectively.

Table 7.3. Experimental design matrix and levels of independent process variables.

X_1	X_2	X_3	X_4	Catalyst (g L^{-1})	pH	Time (min)	Power (%)
-0.5	-0.5	-0.5	-0.5	1.0	4.5	22.5	77.5
-0.5	-0.5	-0.5	0.5	1.0	4.5	22.5	92.5
-0.5	-0.5	0.5	-0.5	1.0	4.5	47.5	77.5
-0.5	-0.5	0.5	0.5	1.0	4.5	47.5	92.5
-0.5	0.5	-0.5	-0.5	1.0	7.5	22.5	77.5
-0.5	0.5	-0.5	0.5	1.0	7.5	22.5	92.5
-0.5	0.5	0.5	-0.5	1.0	7.5	47.5	77.5
-0.5	0.5	0.5	0.5	1.0	7.5	47.5	92.5
0.5	-0.5	-0.5	-0.5	3.0	4.5	22.5	77.5
0.5	-0.5	-0.5	0.5	3.0	4.5	22.5	92.5
0.5	-0.5	0.5	-0.5	3.0	4.5	47.5	77.5
0.5	-0.5	0.5	0.5	3.0	4.5	47.5	92.5
0.5	0.5	-0.5	-0.5	3.0	7.5	22.5	77.5
0.5	0.5	-0.5	0.5	3.0	7.5	22.5	92.5
0.5	0.5	0.5	-0.5	3.0	7.5	47.5	77.5
0.5	0.5	0.5	0.5	3.0	7.5	47.5	92.5
-1.0	0.0	0.0	0.0	0.0	6.0	35.0	85.0
1.0	0.0	0.0	0.0	4.0	6.0	35.0	85.0
0.0	-1.0	0.0	0.0	2.0	3.0	35.0	85.0
0.0	1.0	0.0	0.0	2.0	9.0	35.0	85.0
0.0	0.0	-1.0	0.0	2.0	6.0	10.0	85.0
0.0	0.0	1.0	0.0	2.0	6.0	60.0	85.0
0.0	0.0	0.0	-1.0	2.0	6.0	35.0	70.0
0.0	0.0	0.0	1.0	2.0	6.0	35.0	100.0
0.0	0.0	0.0	0.0	2.0	6.0	35.0	85.0
0.0	0.0	0.0	0.0	2.0	6.0	35.0	85.0
0.0	0.0	0.0	0.0	2.0	6.0	35.0	85.0
0.0	0.0	0.0	0.0	2.0	6.0	35.0	85.0
0.0	0.0	0.0	0.0	2.0	6.0	35.0	85.0

0.0	0.0	0.0	0.0	2.0	6.0	35.0	85.0
0.0	0.0	0.0	0.0	2.0	6.0	35.0	85.0
0.0	0.0	0.0	0.0	2.0	6.0	35.0	85.0
0.0	0.0	0.0	0.0	2.0	6.0	35.0	85.0
0.0	0.0	0.0	0.0	2.0	6.0	35.0	85.0
0.0	0.0	0.0	0.0	2.0	6.0	35.0	85.0
0.0	0.0	0.0	0.0	2.0	6.0	35.0	85.0

Using the matrix generated (Table 7.3), we obtained a complex quadratic equation to explain the relation between the response variable (k) and the operation parameters of interest. The equation was simplified by eliminating some of the terms in reference to the Akaike Information Criterion (AIC) (Hand 2007) to obtain the following expression (adj. R^2=0.8907):

$$k = -0.22-(0.021\ \mathbf{S}) -(0.0027\ \mathbf{pH}) - (0.00034\ \mathbf{t}) + (0.0041\ \mathbf{P}) + (0.0043\ \mathbf{S}^2) + (0.00005\ \mathbf{t}^2) + (0.0016\ \mathbf{S \times pH}) - (0.00017\ \mathbf{S \times t}) - (0.000037\ \mathbf{t \times P}) \qquad (7.1)$$

where: **k** (min^{-1}), **S** ($g\ L^{-1}$), **t** (min), and **P** (%) are the apparent reaction rate constant, the concentration of sepiolite in the reactor, time of sonication and the percentage of maximum generator power, respectively. The significance of the regression terms in Eq. 7.1 was assessed by p-value or t-statistics, neither of which are influenced by the magnitude of the independent variables.

The diagnostics of the model based on residual analysis showed that there were no severe indications of non-normality, nor any evidence of heteroscedasticity (i.e. residual variance was constant for all values of the dependent variable with a non-zero mean). Accordingly, the regression model defined in Eq. 7.1 is a good predictor of the pseudo-first order degradation rate constant of methyl paraben under sonocatalysis, and it describes the investigated system sufficiently well within the defined experimental range. Model prediction of the factors influencing the reaction rate constant in decreasing order of significance are: ultrasonic power, sepiolite dose, pH and the interaction of sepiolite dose with pH and time.

To visualize these interactions, we generated 3-D surface plots by setting two of the factors to constant values, and plotting the other two against the response variable **k**. One such output is presented in Figure 7.3, which shows clearly the interactive effects of time and pH on the apparent reaction rate constant. Accordingly, k is a convex function of sonication time, i.e. it decreases during the first 35-min and increases thereafter. The decrease is most likely due to the rapid production of

some oxidation byproducts that compete with MP for the active adsorption sites and OH radicals. Indeed, LC/MS/MS analysis of the solution after 5 and 10-min sonolysis (data not reported) showed that 4-hydroxybenzoic (HBA) acid was the main product that formed readily upon sonication, as also reported in the literature (Sasi et al. 2015). Moreover, the second order reaction rate constants of MP and HBA with HO• are 4.2×10^{9} and 6.8×10^{9} $M^{-1}s^{-1}$ (Lindsey and Tarr 2000; Tay et al. 2010), respectively, justifying the competition. Increasing of the reaction rate constant after extended sonication, therefore, must be due to the oxidative destruction or depletion of HBA.

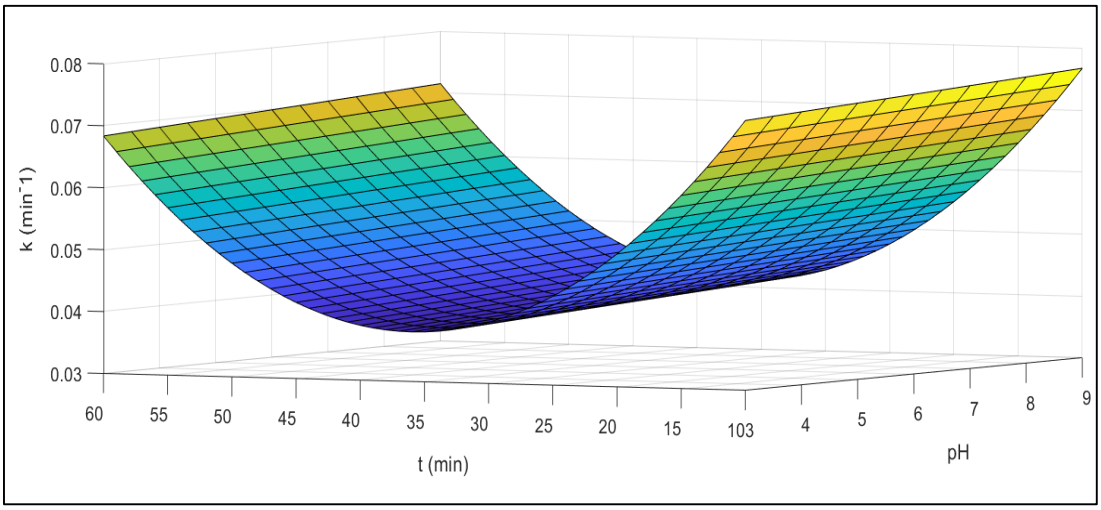

Figure 7.3. Relative impacts of **t** and **pH** on the response variable **k** at **P**=85% and **S**=2 g L^{-1}.

Another 3-D plot to shed light on the interaction of time and sepiolite concentration is presented in Figure 7.4. Like the previous one, the reaction rate constant was found to vary as a convex function of the two variables, reaching a maximum either at their lowest or at the highest values. In other words, k was a maximum either at the longest sonication time and the smallest concentration of sepiolite; or at the shortest sonication time and the highest sepiolite dose. The inverse relationship between time and the catalyst dose may be explained by potential agglomeration of sepiolite particles at high concentrations, leading to attenuation of the ultrasonic field and reduction of the energy transmission efficiency. The effect becomes more drastic when sonication time increases and the particles form larger flocs, leading to bubble coalescence and reduced collapse violence (Ziylan et al. 2013).

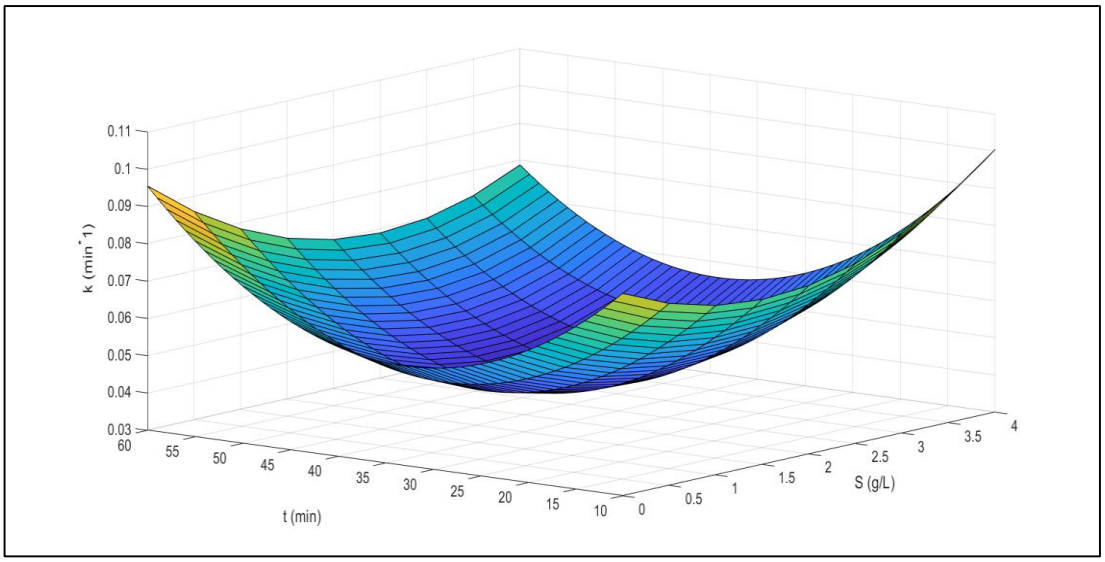

Figure 7.4. Relative impacts of **t** and **S** on the response variable **k** at **pH** 6 and **P**=85%.

Finally, the interactive effect of pH and sepiolite dose on k is presented in Figure 7.5. It was found that when the concentration of sepiolite was considerably reduced (within the defined range), the rate constant increased with decreasing pH. The explanation for this is the improvement in the dispersion of particles with increases in the ratio of MP to sepiolite and the acidity of the solution. A similar conclusion was deduced in the literature for the enhancement in the adsorption of organic molecules on low concentrations of sepiolite via the interaction of silanol groups at the outer surface of the mineral with the surrounding water, leading to better dispersion of the particle-organic molecule suspensions (Shichi & Takagi 2000).

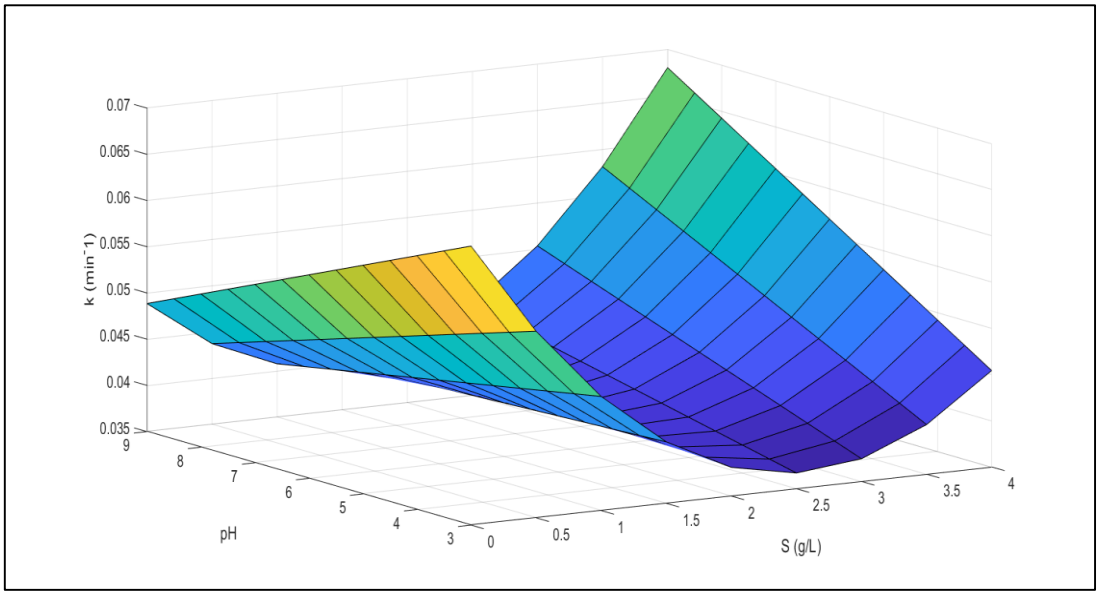

Figure 7.5. Interactive effects of **pH** and **S** on the response variable **k** at **P**=85% and **t**=35-min.

Figure 7.5 also shows that at considerably high concentrations of sepiolite, the reaction rate constant increased with increasing pH, which can be explained by variations in the zeta potential of the mineral with pH. It has been reported that in most cases, the zeta potential of sepiolite is negative above pH 7.0 (Tunç et al. 2008; Alkan et al. 2005; Sabah et al. 2007), leading to deprotonation of the surface and an increase in the number of negatively charged sites. At pH larger than 8.4, MP also acquires a negative charge, but the data show that its adsorption is favored under these conditions. The explanation for more favorable adsorption at alkaline pH is the strong Van der Waals attraction forces between the solid surface and the anionic sites on the molecule. In conclusion, the increase in k at high pH and high concentrations of sepiolite must be due to enhanced adsorption of the compound via a combination of Van der Waals forces and hydrogen bonding. The latter is consistent with the literature reporting enhanced adsorption of anionic polymers onto sepiolite at alkaline pH via H-bonding (Tunç et al. 2008) and more favorable adsorption of organic molecules on sepiolite via strengthening of hydrogen bonding interactions (Brown et al. 2002).

Optimization of the model was based on a numerical program (nested loops), which required the input of upper and lower bounds of each factor to predict the conditions that provide the highest values of k. Accordingly, we found that the optimum conditions that provide maximum yield **(**0.17 min^{-1}) are **t**=10 min, **pH**=9, **S**=4.0 g L^{-1}, **P**=100% of capacity. The method used for validation was the same as reported in our previous work on sonocatalytic decay of salicylic acid in the presence of ZVI (Savun-Hekimoglu and Ince, 2017). The mean absolute percent errors (MAPE) of the four subsets (0.268, 0.189, 0.127 and 0.179) and the average of all (0.191) confirmed the validity of the model for the defined dataset.

7.3.2.2. Design 2: Low sepiolite dose. This part of the study was conducted with a different region of the parameter space and a simpler design protocol. The concentration ranges of sepiolite and pH were 0.01-0.1 g L^{-1} and 4.5-7.0, respectively. The effect of these factors on the response variable was assessed by monitoring the concentration of MP during 10-min sonolysis at 856 kHz and 91% of the generator power (the optimized power output), followed by estimation of the apparent reaction rate constants. The data were then converted into a matrix (Table 7.4) to evaluate the model factors.

Table 7.4. Experimental design matrix and levels of independent process variables.

X_1	X_2	Catalyst (mg L^{-1})	pH
-1.00	1.00	50.00	7.00
-1.00	-1.00	50.00	4.50
1.00	-1.00	100.00	4.50
1.00	1.00	100.00	7.00
-1.41	0.00	39.60	5.75
1.41	0.00	110.00	5.75
0.00	-1.41	75.00	3.98
0.00	1.41	75.00	7.52
0.00	0.00	75.00	5.75
0.00	0.00	75.00	5.75
0.00	0.00	75.00	5.75
0.00	0.00	75.00	5.75
0.00	0.00	75.00	5.75
0.00	0.00	75.00	5.75
0.00	0.00	75.00	5.75
0.00	0.00	75.00	5.75

Analysis of the matrix by "backward stepwise regression" provided the following quadratic expression (adj. R^2 = 0.71905) to describe the relation between the response variable and the experimental parameters of interest:

$$k = 0.178 - 0.0016\ \mathbf{(S)} - 0.011\ \mathbf{(pH)} + 0.00024\ \mathbf{(S \times pH)} \qquad (7.2)$$

where: **k** (min^{-1}), **S** (g L^{-1}), and **pH** are the apparent reaction rate constant, concentration of sepiolite and pH, respectively. Residuals plots and regression diagnostic checks showed that residuals of the model were randomly distributed around zero and normally distributed. Hence, the model was found valid for the defined data range.

A 3-D surface response plot (Figure 7.6) to clarify individual and interactive relations between factors of the model showed that the response variable k approached a maximum when both pH and sepiolite were at their minimum levels. Another maximum was approached at the other extremes, i.e. when pH and sepiolite are at their maximum levels. The former maximum can be explained by improved dispersion and enhanced adsorption at acidic pH via cation exchange reactions. The other

maximum corresponding to high concentrations of the mineral and high alkalinity is the result of van der Waals attraction forces, as also depicted in Design 1. Note also that at acidic pH, **k** decreases sharply if the concentration of sepiolite is too high (despite the positive charges), most likely via the formation of particle clouds and attenuation of the acoustic field.

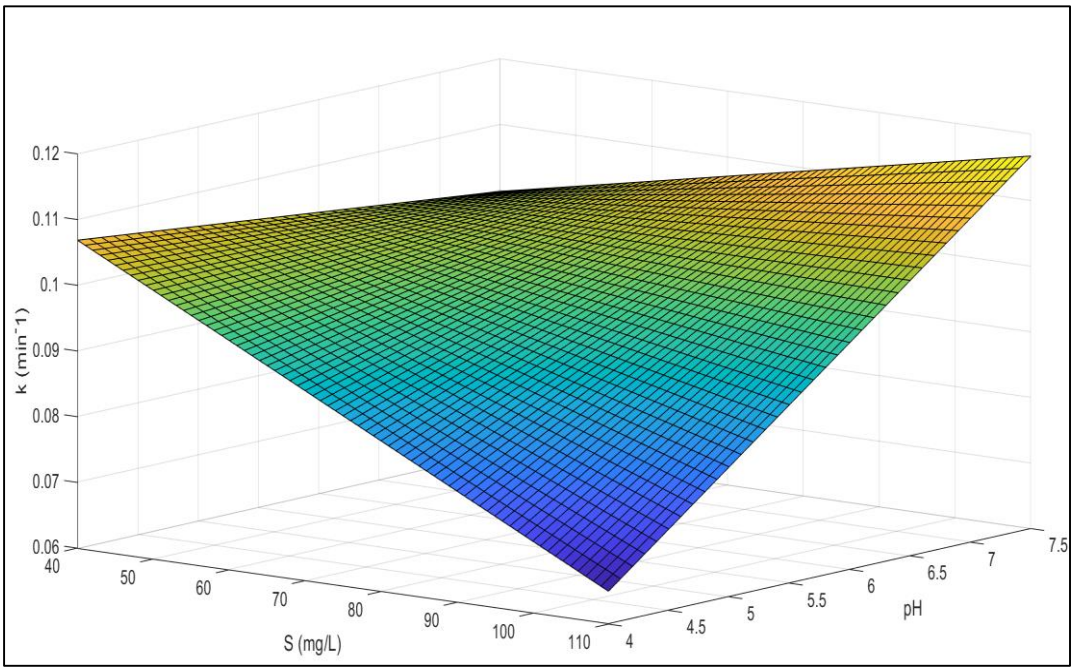

Figure 7.6. Interactive effects of **S** and **pH** on the response variable **k**.

7.3.2.3. Comparison of Design 1 and Design 2. Although the data range was different, the two models are comparable based on the prediction of MP decay rate constant in relation to the model factors and their optimized values. The results are summarized in Table 7.5.

Table 7.5. Prediction of the response variable **k** by Design 1 and Design 2 under the optimum conditions of each.

Design	Optimal Conditions				k_{max} (min^{-1})
1	**pH**=9	**S**=4 g L^{-1}	**t**=10 min	**P**=100%	1.68 x10^{-1}
	pH=3	**S**=0 g L^{-1}	**t**=10 min	**P**=100%	1.48 x10^{-1}
2	**pH**=7.5			**S**=0.11 g L^{-1}	1.18 x 10^{-1}
	pH=4			**S**=0.04 g L^{-1}	1.09 x 10^{-1}

7.4. Conclusions

The emerging water contaminant-methylparaben is rapidly decomposed by sonocatalysis using high frequency irradiation and a low-cost clay mineral-sepiolite. Nevertheless, the experimental system consists of too many factors that influence the reaction yield individually and interactively. Hence, an experimental design technique was used to simplify the system and to optimize the conditions that provided maximum reactions. The method was based on developing simple equations and 3-D response charts for predicting the reaction rate constant and for visualizing individual and interactive effects of the control variables, respectively. Two design protocols with four and two-factor composites were used to discriminate between high (0.1-4 g L^{-1}) and low sepiolite (0.01-0.1 g L^{-1}) doses.

The results showed that the rate of MP decay was highly sensitive to the catalyst concentration, pH, the applied power and time. Moreover, interactions of pH, catalyst dose and time were found significant. It was found that at the highest catalyst test concentration (4 g L^{-1}), the reaction rate constant reached a maximum when pH was also at its highest level (9.0) despite the negative charge on the surface of the mineral and the anionicity of the compound. The result was interpreted by increased affinity of MP to the catalyst surface through Van der Waals forces and enhanced hydrogen bonding. Another output of the design for high sepiolite concentration range was the convex variation pattern of the reaction rate constant with time, as explained by the competition between the oxidation byproducts and the parent compound. Finally, the results showed the reaction yield, or the rate constant could also be maximized by lowering the catalyst test concentration and pH to their minimum levels, which facilitated adsorption by cation exchange reactions.

8. HYDROXYL RADICAL-MEDIATED DEGRADATION OF SALICYLIC ACID AND METHYLPARABEN: AN EXPERIMENTAL AND COMPUTATIONAL APPROACH

The present chapter is a brief summary of the manuscript submitted to *Environmental Science and Pollution Research*, and reflects a collaborative work with the Chemistry Department of Boğaziçi University. The first part of the study consists of investigation of the sonochemical degradation of salicylic acid (SA) and methylparaben (MP) by high frequency ultrasound followed by identification of the oxidation byproducts. The secıond part contains a computational method to model the reaction mechanisms using the experimentally identified byproducts. The second part also encompasses prediction of the aquatic toxicity and potential risk of the byproducts to aquatic organisms using the ECOSAR (Ecological Structure Activity Relationships) protocol. In the following is a detailed explanation of the methods and results of the first part, which was conducted here, and a brief summary of the results of the second part conducted in the Chemistry Department.

8.1. Experimental

The ultrasonic device used in this study was Reactor 2. The effective volume and power density in the reactor were 250 mL and 0.21 W mL^{-1}, the latter estimated by calorimetric measurements. Initial solute concentrations and reaction time were and 30-min, respectively. Test samples of 10 mg L^{-1} adjusted to pH 3.0 were exposed to 572 kHz ultrasound for 30-min, during which samples were collected periodically for the analysis of target compound concentrations and total organic carbon (TOC). Samples were also withdrawn at t=10-min for use in the detection and identification of the oxidation byproducts.

8.2. Analytical

Concentrations of SA and MP were determined by HPLC. The mobile phase for SA and MP analysis were as given in Section 3.2.3.2. The degree of carbon mineralization was assessed by TOC analysis using a Shimadzu TOC-V CSH analyzer. The oxidation byproducts present in solution after 10-min sonolysis were identified by AB SCIEX QTRAP® 4500 LC-MS/MS system with a Turbo V™ ion source and Electron Spray Ionization (ESI), operated at the negative and “multiple reaction

monitoring" mode to enable identification of the chemical structures. More detailed information on analytical procedures was given in the section 3.2.3.

8.3. Results and Discussion

8.3.1. Experimental

Normalized concentrations of SA and MP during 30-min sonolysis at 572 kHz are plotted in Figure 8.1. The fitted curves (R^2=0.98) show that the rate of reaction in both cases was pseudo-first order, with rate constants of 0.067 and 0.091 min^{-1} for SA and MP, respectively. The inset at the top of the figure shows the degree of C-mineralization after 30-min sonolysis, and that after 24-h silent maintenance in the dark. It was interesting to find that the mineralization process continued for a long time after the ultrasonic generator was shut down, as the indication of "latent cavitation", i.e. the effect of stable reactive oxygen species (ROS) that form upon the violent collapse of acoustic cavitation bubbles.

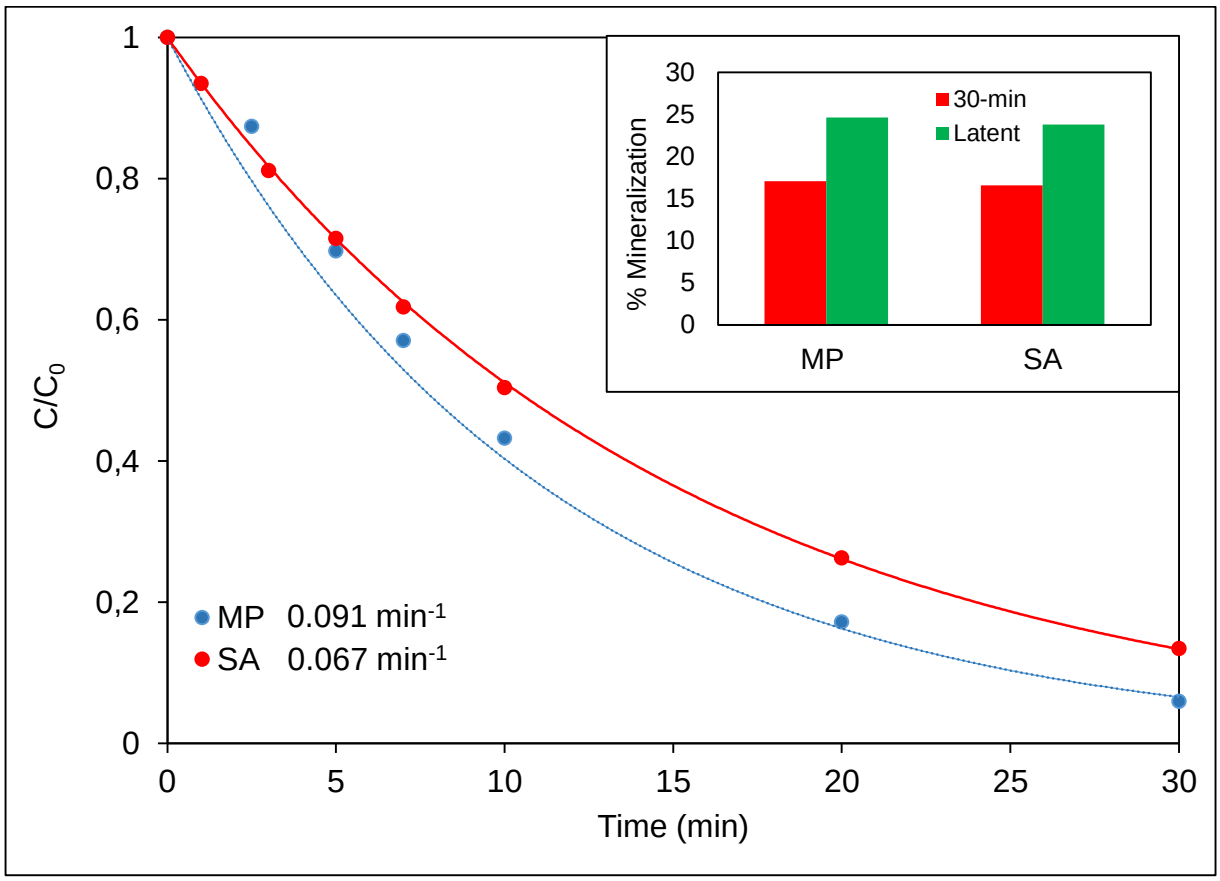

Figure 8.1. Normalized plots of concentration vs time to show sonochemical (at 577 kHz) degradation of SA and MP (C_0=10 mg L^{-1}) at pH 3.0.

LC/MS/MS spectra of 10-min sonicated samples are presented in Figure 8.2a and 8.2b, for SA and MP. The degradation of SA was verified by four major peaks at molecular weights of 62, 108, 110 and 154 g $mole^{-l}$ with intensities of 2.44, 1.53, 1.36 and 1.83, respectively. The degradation of MP was confirmed with six major peaks at molecular weights of 85, 108, 110, 134, 138 and 150 g $mole^{-l}$ and intensities of 1.42, 0.30, 0.15, 0.50, 0.42 and 0.15, respectively. The results for SA are consistent with those of Scheck and Frimmel, who identified benzoquinone (MW=108) and dihydroxybenzoic acid (MW =154) as the byproducts of UV/peroxide/O_2 process (Scheck and Frimmel 1995). The latter was also reported by Chang et al., together with catechol (MW=110) as the byproducts of SA oxidation in a Fenton process (Chang et al. 2008). In another study by Guinea et al., using electrochemical oxidation techniques dihydroxy benzoic acid, maleic acid (MW=116), fumaric acid (MW=116) and malic acid (MW=134) were identified as the byproducts of SA degradation (Guinea et al. 2008).

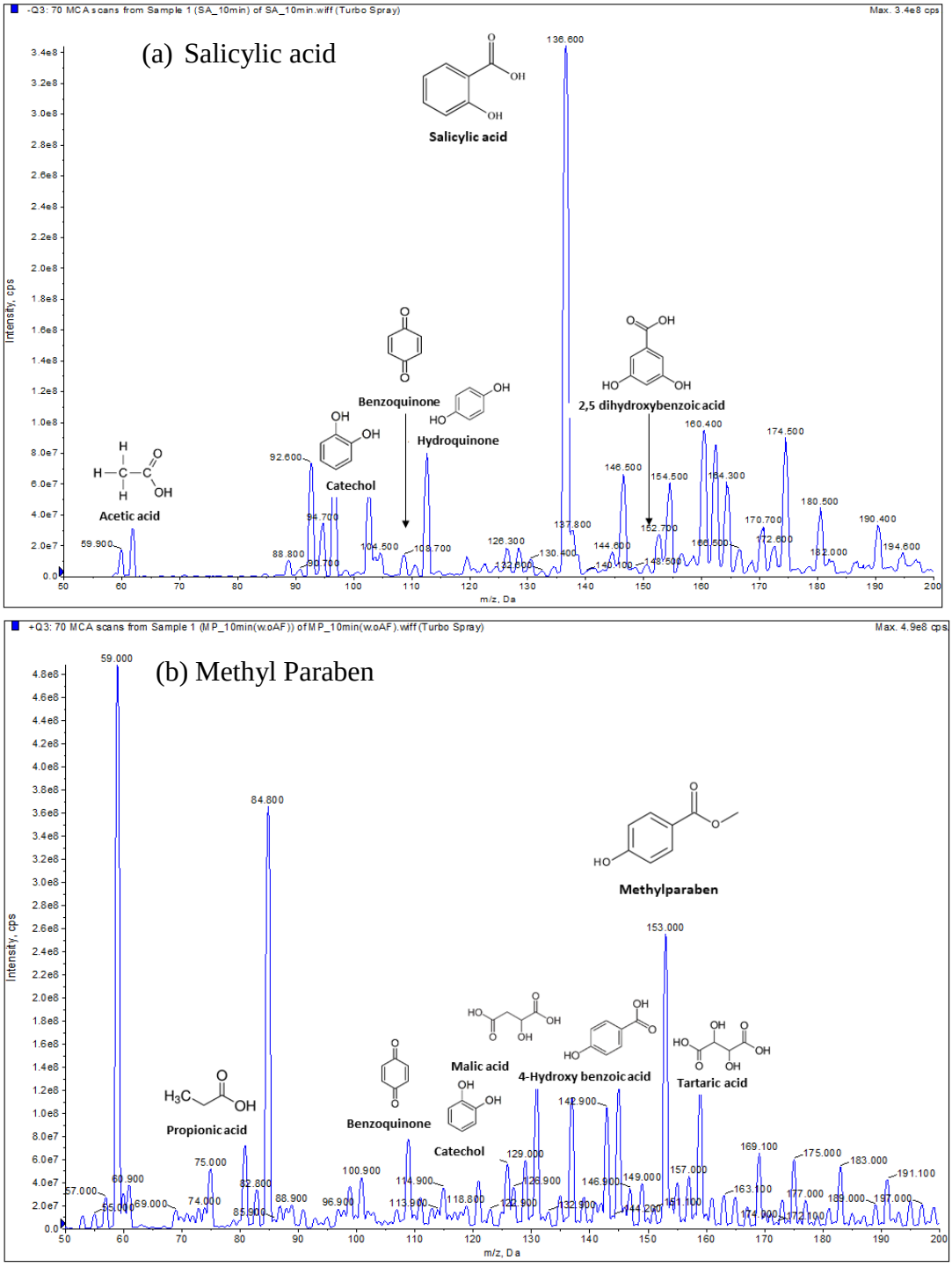

Figure 8.2. LC/MS/MS spectra of 10-min sonicated samples and the structure of the identified byproducts for (a) SA (b) MP.

8.3.2. Computational Results

For SA, the reaction was initiated by its conversion to hydroxyquinone (MW) and catechol (MW) (rate determining step), followed by the degradation of hydroxyquinone to acetic acid (MW) via sequential reactions: •OH addition and water eliminations followed by a highly energetic ring rupture. The latter undergoes C-C bond rupture and water addition, which finally overcomes an energetically demanding barrier (83.6 kcal mol^{-1}) to yield acetic acid.

The degradation pathway of MP resembled that of SA. The reaction was initiated by hydrolysis of the ester bond to produce 4-hydroxybenzoic acid (MW=138). The second stage was decarboxylation to produce phenol, which readily reacted with a •OH to produce catechol, and another •OH to yield hydroxyquinone.

The acute toxicity of the target compounds and their oxidation byproducts was predicted at three trophic levels (green algae, daphnia, and fish). The results showed that SA is harmful to green algae and daphnia and safe to fish, while MP is harmful to all three organisms. The results are consistent with the experimental findings reported in the literature (Cleuvers, M. 2004). It was also found that toxicity fluctuated between “harmful” and “toxic” levels during sonolysis, and the byproduct of both reactions-hydroquinone was more toxic than SA and MP. The finding is also consistent with the literature reporting the higher toxicity of quinones than their phenolic parents (Degraeve et al. 1980).

Finally, the results showed that the early oxidation byproducts of both SA and MP were harmful, while the products formed later were not, and the solution was non-toxic after the ring opening phase. The result is consistent with the literature reporting reduced estrogenic activity of parabens after oxidation by AOP’s or the hydroxyl radical (Fang et al. 2013).

8.4. Conclusions

This study has shown that the two common PPCP’s salicylic acid and methyl paraben are readily oxidized by ultrasonic irradiation at 572-kHz to produce a variety of oxidation byproducts, which are partially mineralized within the allowed reaction time. Computational analysis of the reactions based on •OH-mediated oxidation confirmed the formation of hydroquinone (110 g mol^{-1}), benzoquinone (108 g mol^{-1}), catechol (110 g mol^{-1}), acetic acid (62 g mol^{-1}), 2,5dihydroxybenzoic acid (154 g mol^{-1}), 4hydroxybenzoic acid (138 g mol^{-1}), maleic acid (134 g mol^{-1}), tartaric acid (150 g mol^{-1}), thus

providing for the first time a detailed mechanistic account for the degradation of SA and MP. ECOSAR toxicity analysis showed that SA is toxic to green algae and daphnid, but non-toxic to fish, while MP is “harmful” to all three levels of aquatic organisms. It was also found that toxicity fluctuated between “toxic”-“harmful”-“non-toxic” levels during the degradation process. The most toxic byproduct was benzoquinone, which was detected during the degradation of both compounds, and which is recognized as the most toxic derivative of benzene-bearing compounds. Finally, the study has shown that the oxidation byproducts formed later were non-toxic, confirming the environmental friendliness of the applied AOP method, implying that sonochemistry is a green technology.

9. PHOTOCATALYTIC DEGRADATION OF CAFFEINE ON SEPIOLITE-SUPPORTED TiO_2 AND THE ROLE OF ULTRASONIC POST-TREATMENT

The study presented in this section covers the manuscript entitled "Photocatalytic degradation of caffeine on sepiolite-supported TiO_2", which will be submitted to *Catalysis Today* in June, 2019.

The most effective methods of eliminating caffeine from water are adsorption (Sotelo et al., 2014), advanced biological treatment (Kim et al., 2014) and AOP's using homogeneous and heterogeneous catalysts (Miralles-Cuevas et al., 2018; Ganzenko et al., 2017; Shu et al., 2016). Among all, TiO_2 is the most commonly used heterogeneous catalyst owing to its photoactivity, low cost, chemical stability and non-toxicity. However, it is ineffective due to disadvantages such as a high band gap energy, rapid combination of e^-h^+ pairs and easily corroded surface (Ashokkumar 1998). Hence, much research has lately focused on increasing the efficiency of TiO_2 by immobilizing it with transition and/or noble metals, as well as rare earth minerals, which all inhibit combination of e^-h^+ pairs and corrosion of the surface by light, thus enhancing significantly the catalytic activity of the semiconductor in the UV-visible band (Kamat et al., 2002; Seo et al., 2006).

The present study aims to investigate and compare the degradation of caffeine by photocatalysis in the presence of commercial and sepiolite-immobilized nanoparticles of TiO_2. The use of sepiolite for supporting the semiconductor was based on its low-cost, high porosity and large specific surface area (Lemić et al. 2005).

9.1. Experimental Procedures

9.1.1. Immobilization of TiO_2 on Sepiolite

The immobilization process was performed by dispersion of powdered sepiolite in water, followed by addition of TiO_2 in a 1:1 weight ratio and sonication of the mixture for 30-min in a 200-kHz ultrasonic bath (Quava-Mini, Japan). The particles were then separated from solution through a 0.2 μm membrane (Milipore, OmniPore), thoroughly washed and dried at constant temperature (60°C) for 12 hours (Todorova et al., 2014).

9.1.2. Control Experiments

Dark adsorption experiments were performed with sepiolite, commercial TiO_2 and lab-made nanocomposites to test the adsorptive capacity of each for caffeine. In addition, caffeine was exposed to UV-irradiation and ultrasound in the absence of any catalysts to test the photo-and sono-degradability of the compound. The concentration of caffeine during the experiments was analyzed by a Shimadzu LC-20AT HPLC with a 20A UV-vis photo diode array detector.

9.1.3. Photocatalytic and Post-Sonolytic Experiments

Photocatalytic experiments were carried out at three pH levels (3.0, 6.0, 9.0) and various concentrations of commercial TiO_2 and its lab-made nanocomposites (Sep/TiO_2) added to 10 mg L^{-1} test solutions of caffeine, followed by 30-min irradiation by a xenon lamp (MAX-301, 300 W; Asahi Spectra, Japan). Sonolytic experiments were performed using reactor 2 to select the optimum frequency. In addition, samples irradiated for 15-min in the photo reactor were exposed to pulse-mode sonication for 30 and 60 minutes in a 1-s on and 1-s off operational mode to monitor the TOC of the solutions.

9.1.4. Testing of the Stability of the Catalysts

Upon 15-min photocatalysis of caffeine with Sep/TiO_2, the sample was adjusted to pH 12 and kept inert for 1-h to allow desorption of organic matter from the surface of the catalyst. The solution was centrifuged (15-min, 4000 rpm) and exposed to vacuum filtration to separate the catalyst. The filtrate was thoroughly washed with distilled water and dried at 60°C for 24-h for reuse in another photocatalytic run. The procedure was repeated three times to allow four consecutive uses of the catalyst.

9.2. Results and Discussion

9.2.1. Control Experiments

9.2.1.1. Dark adsorption. A set of dark experiments were carried out to investigate the adsorption of caffeine on the catalysts we used. Therefore, batch adsorption test with 10 mg L^{-1} caffeine and various concentrations (0.25, 0.5 and 1 g L^{-1}) of TiO_2, sepiolite and sepiolite-TiO_2 nanocomposite were done during 2 hours mixing at pH 3 and the data are presented in Table 9.1 and Figure 9.1.

Table 9.1. Adsorption of caffeine on the catalysts at various concentrations and pH 3.

	Sepiolite (g L^{-1})			**Sepiolite- TiO_2 (g L^{-1})**			**TiO_2 (g L^{-1})**		
	1.00	**0.5**	**0.25**	**1.00**	**0.5**	**0.25**	**1.00**	**0.5**	**0.25**
Time (min)	**% Adsorbed**								
0	0.00	0.00	0.00	0.00	0.00	0.00	0.00	0.00	0.00
5	73.25	55.04	52.27	74.84	56.98	58.89	7.09	7.71	8.22
15	88.35	76.28	62.99	75.48	60.40	66.77	7.11	7.99	8.38
30	90.13	76.98	65.96	78.41	69.99	65.14	8.02	8.06	8.50
60	90.53	78.79	68.34	79.39	78.08	73.29	9.83	9.36	9.13
120	90.66	79.52	73.62	81.65	80.15	73.90	11.79	11.08	9.96

It was found that caffeine adsorbed appreciably on sepiolite-TiO_2, while almost no adsorption was observed on commercial TiO_2 even at the highest test concentration. Furthermore, adsorption equilibrium was reached within 30-min when sepiolite-TiO_2 was 1 g L^{-1}, but took one hour at lower concentrations of the nanocomposite. It is clearly evident that at a very low catalyst amount of the available active sites are insufficient and with increasing amount of catalyst the adsorption also increases. Therefore, the optimum amount for caffeine degradation has been found to be equal to 1 g L^{-1}. According to the literature, with further increases of the catalyst concentration (above 1 g L^{-1}), the particles tend to agglomerate with a loss active sights and scattering of the incident light (Ghosh, 2019). Accordingly, the dose of all catalysts was 1 g L^{-1} in the rest of the experiments.

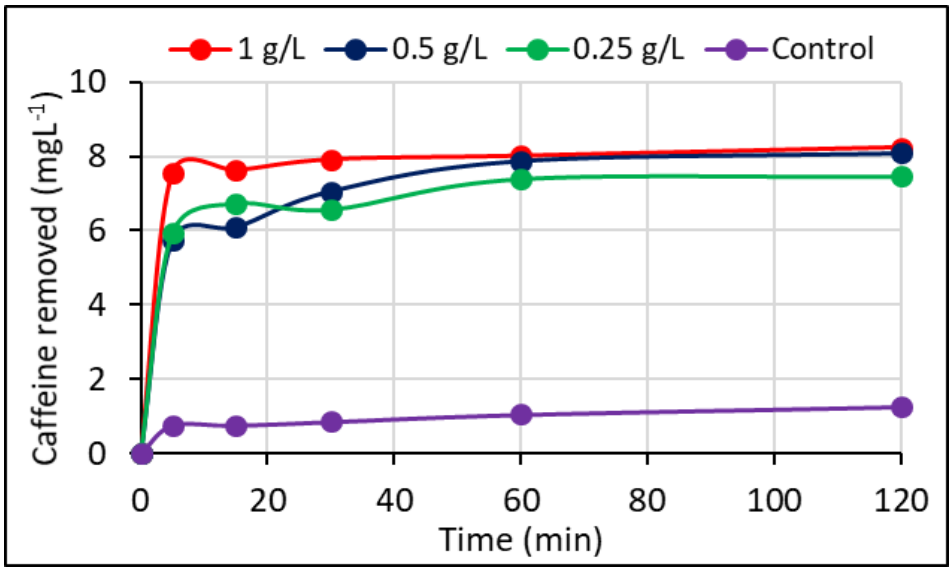

Figure 9.1. Adsorption equilibrium of caffeine on Sepiolite-TiO_2 at pH 3.0 and various concentrations of the nanocomposite. "Control" refers to Degussa-25 at 1.0 g L^{-1}.

9.2.1.2. Photodegradation without catalysts. The second set of control experiments were carried out in the absence of catalysts to determine the removal of caffeine with UV alone and it was found that photolysis alone was not a degradation pathway for caffeine. Similar findings are reported in the literature (Chuang et al., 2011). In the study of Sacco et al. 2017, 240 min photolysis showed only a slight decrease in caffeine concentration (7%) with no removal of TOC indicating that only photolysis cannot remove the organic substance in the water solution. These results suggest that photocatalytic degradation is primarily responsible for removing caffeine.

9.2.1.3. Sonodegradation without catalysts. The third set of control experiments were carried out in the presence of caffeine and ultrasound only (no catalysts) to select the optimum frequency at natural pH. We found that first order degradation rates were very close in both frequencies but slightly higher in 856 kHz. Therefore, 856 kHz was selected as operating frequency for the rest of the experiments. A higher reaction rate at 861 kHz is due to reduced resonant bubble size, leading to increased number of active bubbles and oscillations, and a larger efficiency of •OH ejection, as explained in a previous study (Gültekin et al., 2009; Ince et al., 2009).

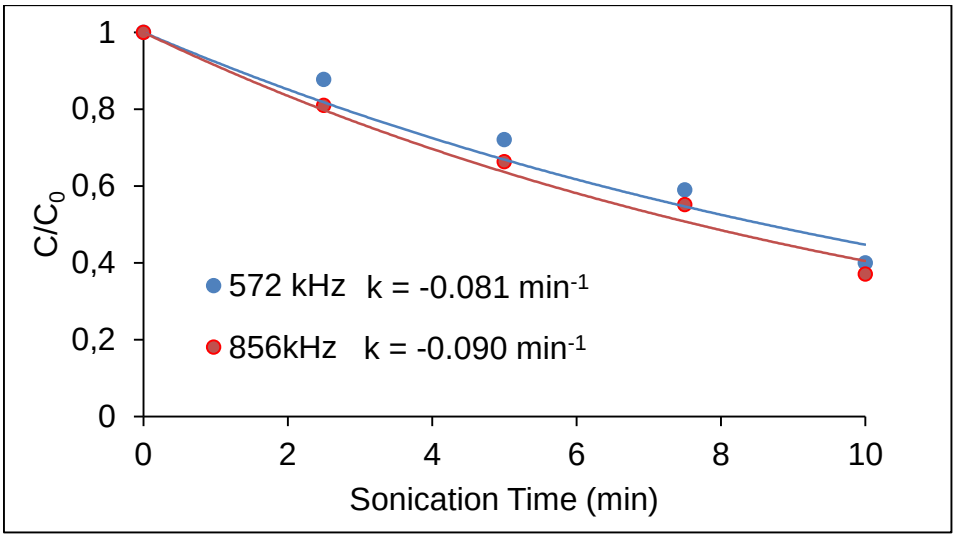

Figure 9.2. The effect of frequency on the rate of caffeine decomposition (C_0=10mg L^{-1}, pH= 6).

9.2.2. Characterization of TiO_2 and Sep-TiO_2

SEM images of commercial TiO_2 and Sepiolite- TiO_2 nanocomposites are presented in Figure 9.3, which show that TiO_2 nanoparticles were successfully immobilized on highly fibrous, loosely-packed sepiolite aggregates.

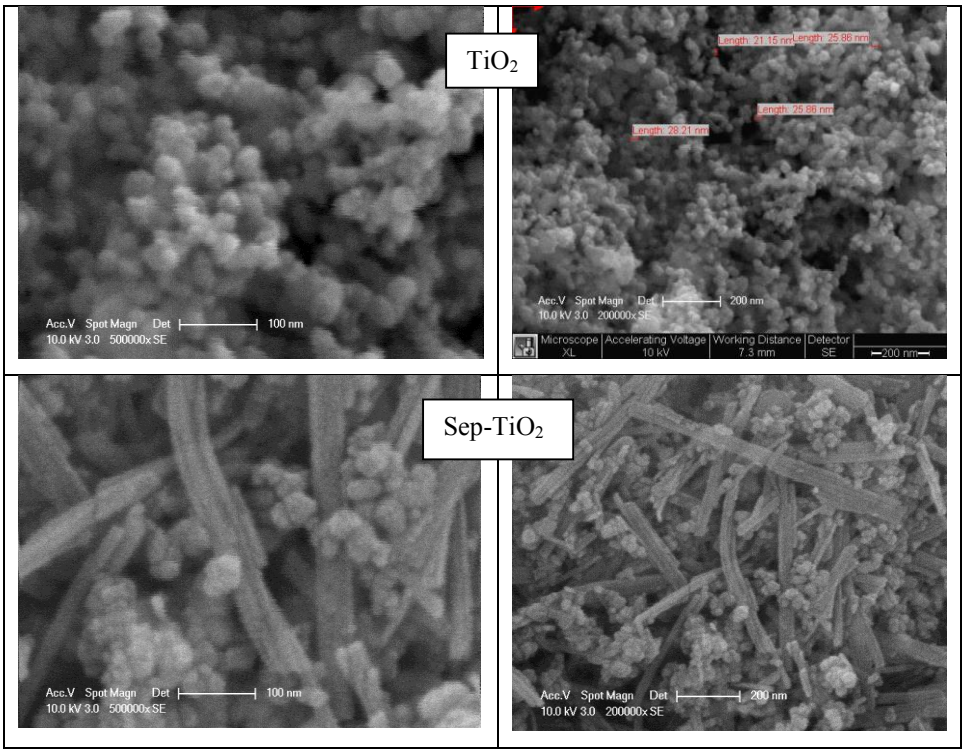

Figure 9.3. SEM images of commercial TiO_2 and Sepiolite-TiO_2 nanocomposite.

9.2.3. Photocatalytic Experiments

Photocatalytic experiments were initiated by adding 1 g L^{-1} pristine TiO_2 and sepiolite-immobilized particles to the open reactor containing 10 mg L^{-1} caffeine and mixing for 30 minutes under UV-Vis light. Three pH levels (3.0, 6.0 and 9.0) were tested to select the optimum pH level. The data are presented in Figure 9.4.

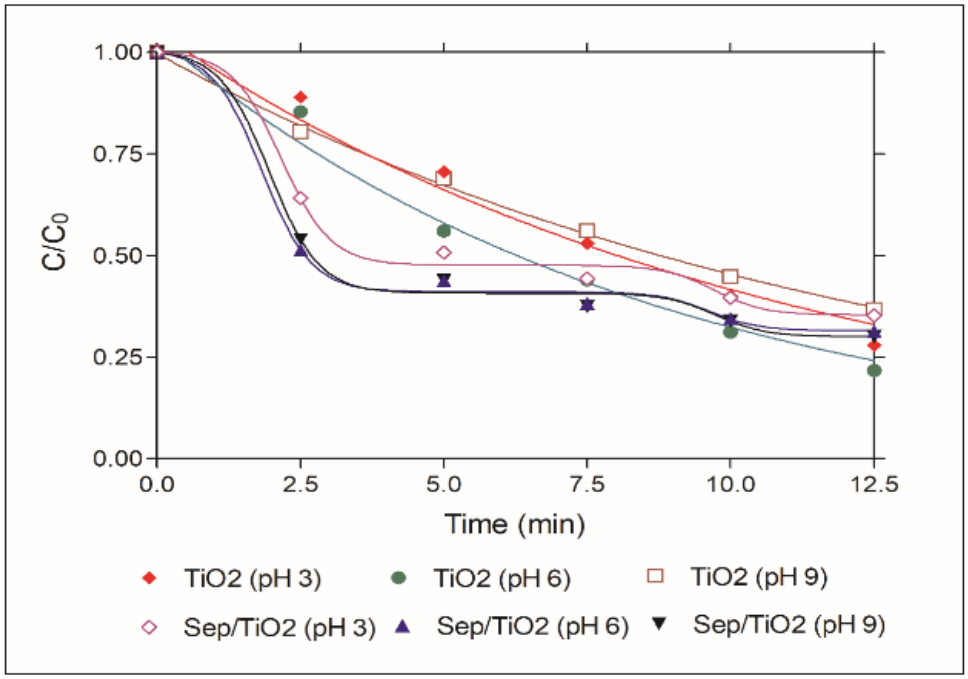

Figure 9.4. Influence of pH and catalyst properties on the rate of caffeine decay by photocatalysis. TiO_2 and Sep/TiO_2 refer to pristine, and sepiolite-immobilized particles, respectively.

As depicted in Figure 9.4 photocatalysis was an effective means of removing caffeine from water, especially at pH 6.0, which was the natural pH of the test solutions. The result is consistent with the literature, reporting 6-6.8 as the optimum pH for the photocatalysis of caffeine (Ghosh et al., 2019; Uğurlu et al., 2011). Lower reaction rates at acidic pH must be due to excessive number of positively charged sites on the catalyst surface that reduce the adsorption efficiency of the compound. Hence, at pH 3.0, the surface Sep/TiO_2 is positive and thus the attraction forces between caffeine and the catalyst surface is almost zero. On the other hand, at alkaline pH the surface of the catalyst is negative, but caffeine in in cationic form (pKa=14.0), so that it easily approaches the surface for adsorption. Considering the estimated reaction rate constants, the optimum pH is 6.0, at which the affinity between the catalyst surface and the molecules of caffeine was a maximum, resulting to maximum photocatalytic activity

The data also show that the rate of reaction followed pseudo-first order kinetics when catalyzed by commercial TiO_2, and competitive-binding kinetics when catalyzed by the nanocomposite. The data are presented in Table 9.2. Exploring the kinetic patterns in more detail, we found that the degradation of caffeine in the presence of sepiolite-TiO_2 was perfectly described by the Langmuir-Hinshelwood law (Eq. 9.1), which is commonly used for modeling heterogeneous reaction kinetics based on the assumption that adsorption and desorption are in equilibrium (Xiao et al., 2015):

$$\frac{1}{r_0} = \frac{1}{kKC_0} + \frac{1}{k} \tag{9.1}$$

where: r_0 is the initial reaction rate (mM min^{-1}), k and K are the second-order reaction rate and the equilibrium constants, respectively (mM min^{-1} and mM) and C_0 is the initial concentration of caffeine (mM). The data are presented in Figure 9.5.

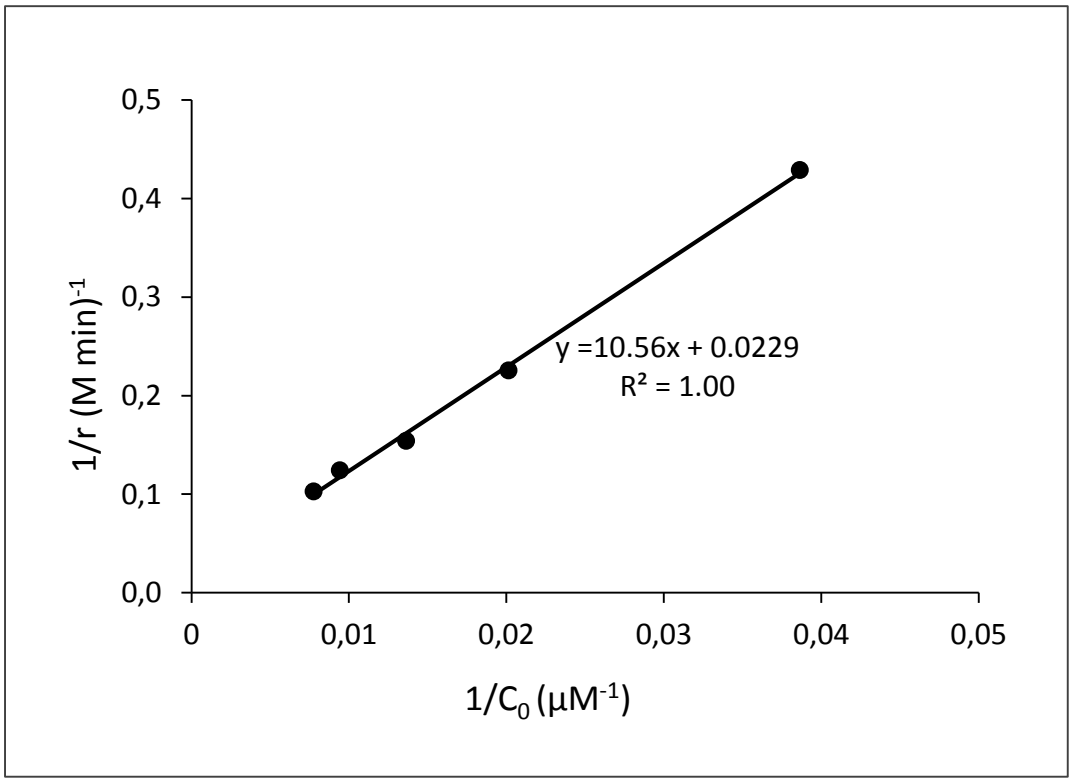

Figure 9.5. Heterogeneous kinetic modeling showing the rate of caffeine degradation as a function of time. Initial conditions were: pH=6, sep-TiO_2=1.0 g L^{-1}, t=12.5 min.

Table 9.2. Photocatalytic degradation of caffeine in the presence of 1.0 g L^{-1} TiO_2 and Sep- TiO_2 (pH=6).

Time	**TiO_2**					**Sepiolite-TiO_2**				
	Initial Concentration (mg L^{-1})									
	5	10	15	20	25	5	10	15	20	25
0	5.36	9.78	15.55	19.99	24.33	5.01	9.63	14.22	20.59	25.02
2.5	4.13	7.55	12.94	16.71	20.69	0.84	1.97	3.79	6.89	9.25
5	2.94	5.98	12.13	15.45	19.17	0.67	1.56	2.77	6.49	8.25
7.5	1.99	4.50	11.15	13.86	17.21	0.61	1.36	2.29	6.12	8.01
10	1.03	3.39	9.78	12.50	15.45	0.55	1.21	2.03	5.56	7.01

The rate of mineralization was also investigated as shown in Figure 9.6. Maximum TOC removal was achieved using sepiolite-TiO_2 particles in the presence of 15 mg L^{-1} initial caffeine concentration. Under the specified experimental conditions, Sep/TiO_2 was more efficient than TiO_2 when the initial concentration was greater than or equal to 15 mg L^{-1}.

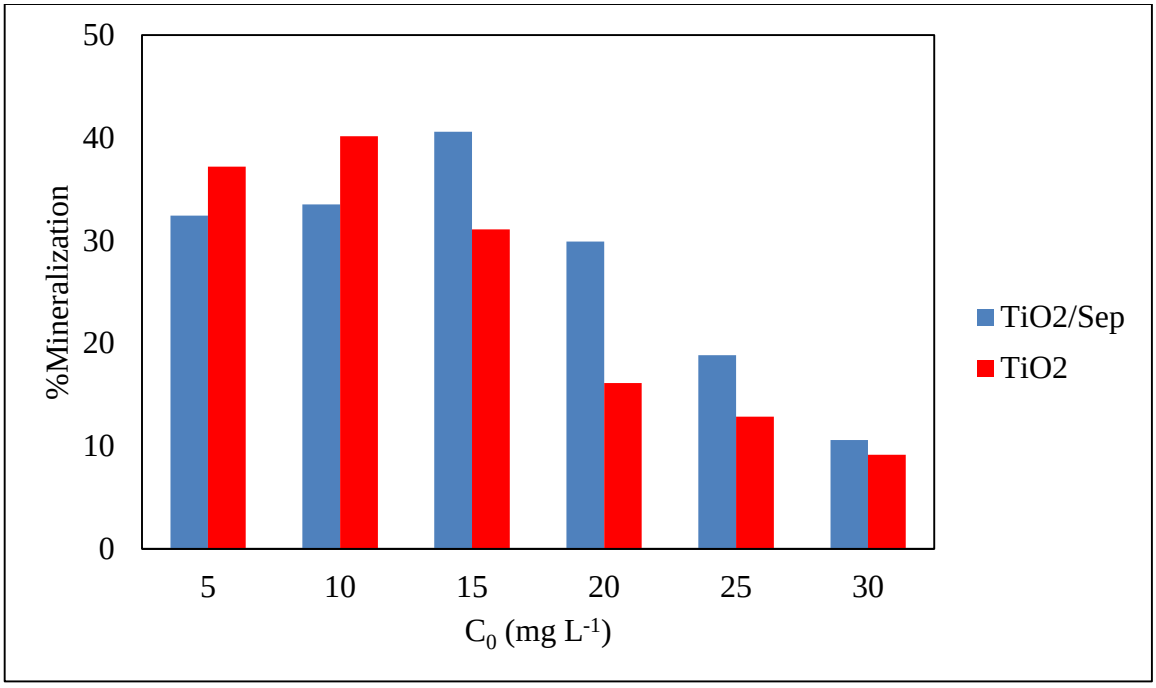

Figure 9.6. Mineralization of caffeine during 30-min photocatalysis in the presence of TiO_2 and TiO_2/Sepiolite nanoparticles.

We found that even though the both catalysts were efficient for the degradation of caffeine, complete mineralization was not achieved. Indeed, LC/MS analysis of the solution after 5 and 15-min photocatalysis showed that caffeine was converted to byproducts such as N-formylformamide, N-formyl-N-methyl-formamide and N-(5-formyl-1H-imidazol-4-yl) formamide (Figure 9.7). In order to achieve higher mineralization rates post-sonication experiments were conducted and described in the following section.

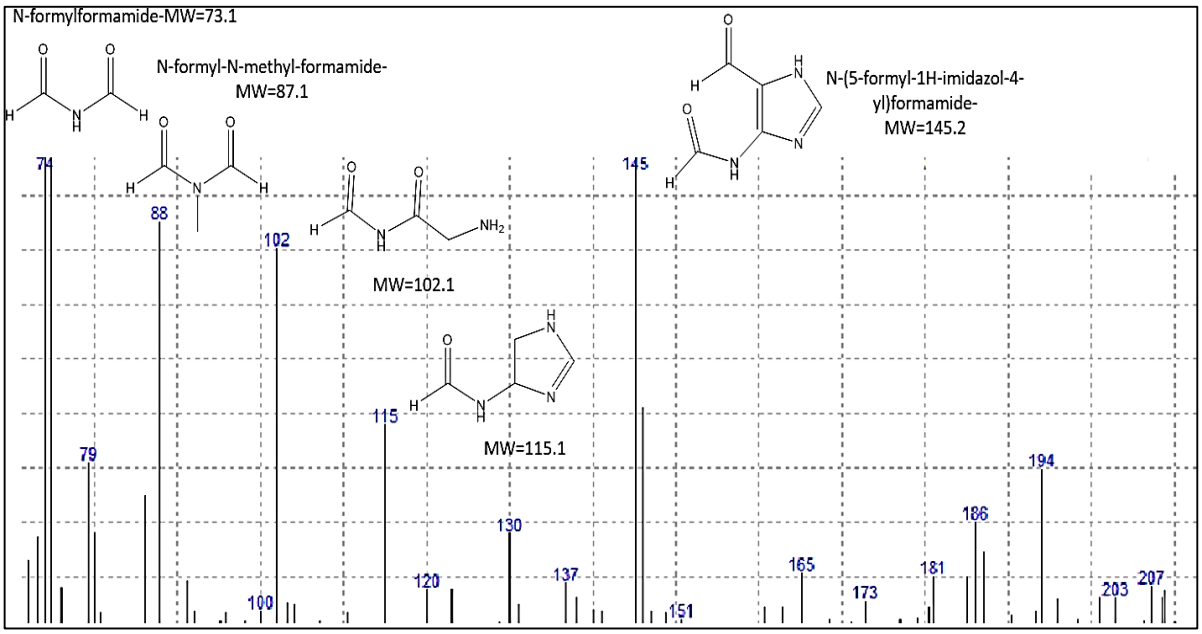

Figure 9.7. LC/MS spectra of 15-min irradiated samples and the structure of the identified byproducts.

9.2.4. Post-sonication

Post-sonication experiments were carried out using ultrasound in pulsed and continuous mode. In pulsed ultrasound, the ultrasonic equipment was run in repetitive cycles and the On:Off ratio was 1. We found that application of pulsed ultrasound was more efficient. This is in agreement with the literature, as pulsed ultrasound was reported to be more chemically reactive than the continuous ultrasound for the same level of ultrasonic energy (Al-Juboori et al., 2015). This is attributed to reduction of the energy demand of ultrasound by reducing waste of energy by wave scattering caused by cloud of bubbles (Wang et al., 1996).

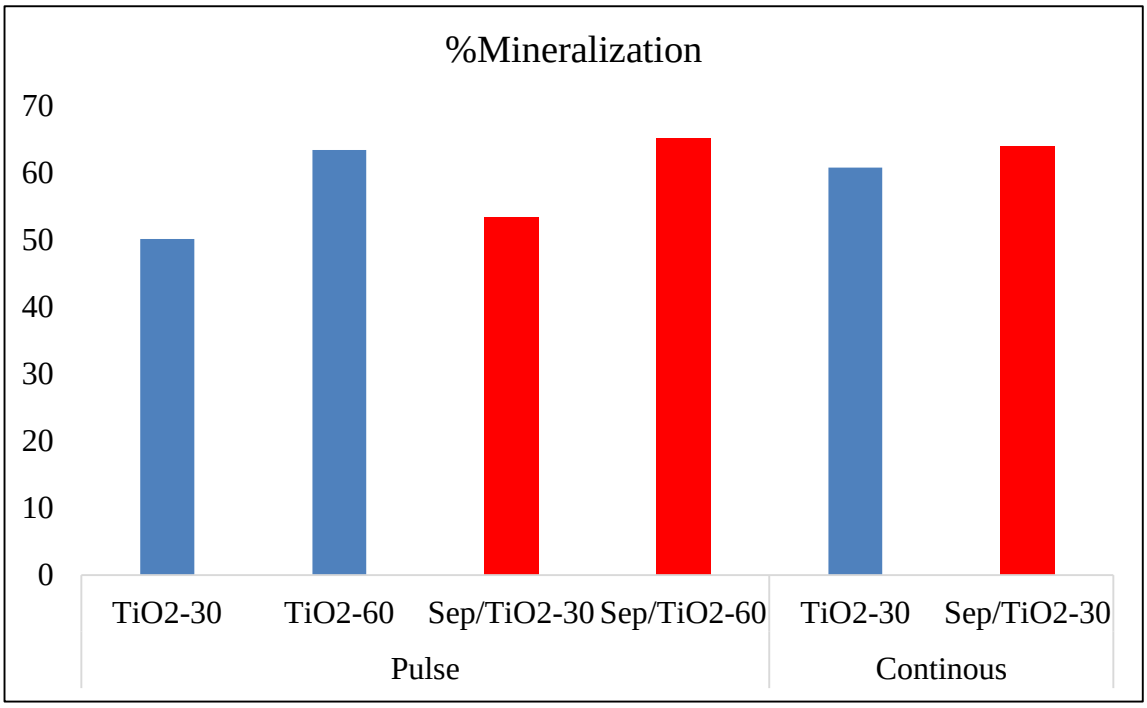

Figure 9.8. Mineralization of caffeine by Post-sonication. Initial conditions were C_0=10 mg L^{-1}, f= 856 kHz, Ps = 0.21 W mL^{-1}, pH= 6, Catalyst conc. 1 g L^{-1}.

Sonolysis of the samples right after UV irradiation without separating the nanocomposite was found effective for the mineralization of the oxidation byproducts. The mechanism of action may be comprised of a combination of the following:

i) Caffeine and some of its oxidation byproducts adsorbed on the surface of the nanocomposite were exposed to the extreme conditions of cavitation collapse that ocurred also on the active sites of the particles.

ii) The mechanical properties of ultrasound (e.g. sheer forces, jets of liquids, etc.) facilitated mass transfer from the bulk medium to the solid-liquid and gas-iquid interfaces, which are much richer in the quantity of •OH than the aqueous solution. Additionally, the mechanical effects enabled contiınous cleaning and polishing of the catalyst surface.

iii) The unique structure of the nanocomposite allowed surface reactions with OH- groups present on the sepiolite surface.

iv) The surface of TiO_2 (photo response range <380 nm) was excited by the sonoluminescence of collapsing cavities (ƛ =200-500 nm) to produce excess oxidizing species (as described in section 2.2.).

One of the most important features of solid catalysts is their stability, i.e. the ease of recovery and the loss of efficiency upon multiple-use. In general, the higher the recovery of a spent catalyst and the lower is the loss of efficiency in the next use, the more stable and economical it is. Our nanocomposite was found to be a stable catalyst providing 65%, 60%, 56% and 53% mineralization respectively at the end of 1st, 2nd, 3rd and 4rth consecutive uses in photocatalytic followed by sonolytic degradation of caffeine (Figure 9.9).

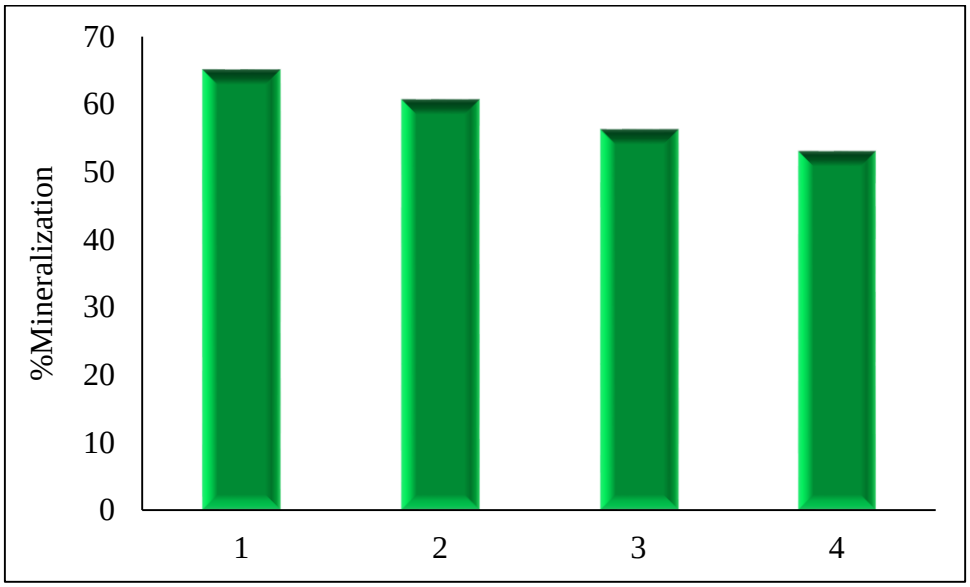

Figure 9.9. The loss in the mineralization efficiency of Sep-TiO_2 upon recovery and reuse.

9.3. Conclusions

Caffeine adsorbed poorly on raw TiO_2 (Degusa 25), but considerably well on sepiolite and Sep/TiO_2 nanocomposite. Moreover, the rate of degradation of the compound under UV-visible irradiation was a maximum at pH 6.0 and in the presence of the nanocomposite. Hence, immobilization of commercial TiO_2 on nanoparticles of a low cost clay mineral-sepiolite is a very effective method of enhancing the photocatalytic activity of the semiconductor. The effectiveness arises on one hand from the massive surface area promoting excess adsorption and surface reactions and on the other hand from reduced e-h+ pair combination and reduced surface corrosion. Finally, the stability of the nanocomposite was considerably high, allowing multiple use without significant loss of activity.

The nanocomposite was also effective in sonochemical mineralization of the photocatalytic oxidation byproducts, as the degree of TOC decay was increased from 33.5% (after 30-min photocatalysis) to 65.1% after post-sonolysis of the irradiated sample in the presence of the catalyst.

10. CONCLUSIONS AND RECOMMENDATIONS

The study has covered methods of PPCP removal in water by advanced oxidation processes (AOP's), using ultrasound (US), UV-vis irradiation and catalysts, as zero-valent iron (ZVI), sepiolite (Sep), TiO_2 and their various nanocomposites that were synthesized in the laboratory by ultrasound. A summary of the major findings are as follows:

1) Sonication of water at high frequency is effective for converting PPCPs, as salicylic acid (SA), methylparaben (MP), and caffeine to simpler and less toxic byproducts; but ineffective for their mineralization.
2) The response surface methodology (RSM) promises valid regression models that provide reliable predictions of the performance of sonocatalytic reaction systems, given sufficient experimental data are generated under well-specified reactor, reagent and ambient conditions. As such, it was found that sonocatalytic degradation of SA is strongly dependent on the ultrasonic power input and the regression model developed by RSM predicted 50% mineralization of the compound at the cost of pH=2.0, ZVI=24 mg L^{-1}, H_2O_2=0 mg L^{-1} and P_{app}=120 W. Considering that the condition is energy and chemical intensive, a compromise as 40% mineralization is possible at only 72 W energy and a higher pH ($2.75 \leq pH \leq 3.0$).
3) The pseudo-first order rate of sonochemical and sonocatalytic MP degradation follows Langmuir-Hinshelwood model, as typical of heterogeneous reaction systems. The addition of raw sepiolite into the reactor enhances the reaction rate, but not the degree of C-mineralization. The latter can considerably be improved by modification of the mineral surface via ultrasonication and sonolytic intercalation with SDS, particularly if the intercalation is terminated after 20-min sonolysis.
4) An experimental design technique to simplify the complexity of the sonocatalytic system described above and to optimize the reaction conditions provided the following: i) the rate of MP decay is highly sensitive to the concentration of sepiolite, pH, the applied power, time and the interactions of pH, catalyst dose and time; ii) the rate is a maximum when sepiolite and pH are at their highest test levels (4 g L^{-1} and 9, respectively), iii) the rate is still a maximum when sepiolite and pH are both at their minimum test levels, due to enhanced adsorption of MP on the catalyst surface by cation exchange reactions.
5) LC/MS analysis of the oxidation byproducts of SA and MP showed the formation of hydroquinone (110 g mol^{-1}), benzoquinone (108 g mol^{-1}), catechol (110 g mol^{-1}), acetic

acid (62 g mol^{-1}), 2,5dihydroxybenzoic acid (154 g mol^{-1}), 4hydroxybenzoic acid (138 g mol^{-1}), maleic acid (134 g mol^{-1}), and tartaric acid (150 g mol^{-1}). The Microtox assay showed that the reactor was no longer toxic after 30-min sonication of 10 mg L^{-1} MP at 572 kHz and pH 6.5.

6) Caffeine adsorbs poorly on TiO_2, but considerably well on sepiolite and a sonolytically synthesized Sep/TiO_2 nanocomposite. The rate of photocatalytic degradation under simulated solar radiation is a maximum at pH 6.5 and in the presence of the nanocomposite. The degree of mineralization under these conditions and after 30-min photocatalysis is 33.5%, which may be successfully improved to 65.1% by 30-min sonication at 856 kHz in the pulse mode.
7) Last but not least, the study has shown that the low cost clay mineral-sepiolite, which is very abundant in Turkey and rarely used for technical purposes, is not only an excellent adsorbent, but also a unique catalyst of sonochemical reactions and a wonderful support material for TiO_2. Hence, in addition to the scientific contribution to the elimination of PPCP's from water, the study promises a considerably important contribution to the economy of Turkey.

REFERENCES

Abbas, S., Hayat, K., Karangwa, E., Bashari, M., Zhang, X., 2013. An overview of ultrasound-assisted food-grade nanoemulsions. Food Engineering Reviews, 5, 139-157.

Adams, W.C., 2002. Comparison of chamber and face-mask 6.6-hour exposures to ozone on pulmonary function and symptoms responses. Inhalation Toxicology, 14, 745-764.

Adán, C., Coronado, J.M., Bellod, R., Soria, J., Yamaoka, H., 2006. Photochemical and photocatalytic degradation of salicylic acid with hydrogen peroxide over TiO2/SiO2 fibres. Applied Catalysis A: General, 303, 199-206.

Adewuyi, Y.G., 2001. Sonochemistry: environmental science and engineering applications. Industrial & Engineering Chemistry Research, 40, 4681-4715.

Ahlrichs, J.L., Serna, J.C., Serratosa, J.M., 1975. Sepiolite anhydride and crystal folding. Clays and Clay Minerals, 23, 119-124.

Akkari, M., Aranda, P., Amara, A., Ruiz-Hitzky, E., 2018. Clay-nanoarchitectures as photocatalysts by in situ assembly of ZnO nanoparticles and clay minerals. Journal of Nanoscience and Nanotechnology, 18, 223-233.

Akkari, M., Aranda, P., Belver, C., Bedia, J., Amara, A.B.H., Ruiz-Hitzky, E., 2018. ZnO/sepiolite heterostructured materials for solar photocatalytic degradation of pharmaceuticals in wastewater. Applied Clay Science, 156, 104-109.

Albero, B., Pérez, R. A., Sánchez-Brunete, C., Tadeo, J. L., 2012. Occurrence and analysis of parabens in municipal sewage sludge from wastewater treatment plants in Madrid. Journal of Hazardous Materials, 239, 48-55.

Alegria, A. E., Lion, Y., Kondo, T., Riesz, P., 1989. Sonolysis of aqueous surfactant solutions: probing the interfacial region of cavitation bubbles by spin trapping. The Journal of Physical Chemistry, 93, 4908-4913.

Al-Juboori, R. A., Yusaf, T., Aravinthan, V., Bowtell, L., 2016. Investigating natural organic carbon removal and structural alteration induced by pulsed ultrasound. Science of the Total Environment, 541, 1019-1030.

Alkan, M., Demirbaş, Ö., Doğan, M., 2007. Adsorption kinetics and thermodynamics of an anionic dye onto sepiolite. Microporous and Mesoporous Materials, 101, 388-396.

Alkan, M., Dog, M., 2005. Removal of reactive blue 221 and acid blue 62 anionic dyes from aqueous solutions by sepiolite. Dyes and Pigments, 65, 251-259.

Alkan, M., Tekin, G., Namli, H., 2005. FTIR and zeta potential measurements of sepiolite treated with some organosilanes. Microporous and Mesoporous Materials, 84, 75-83.

Almeida, B., Oehmen, A., Marques, R., Brito, D., Carvalho, G., Crespo, M.B., 2013. Modelling the biodegradation of non-steroidal anti-inflammatory drugs (NSAIDs) by activated sludge and a pure culture. Bioresource technology, 133, 31-37.

Alvarez, A., 1984. Sepiolite: properties and uses. Developments in sedimentology, 37, 253-287.

Álvarez, S., Ribeiro, R.S., Gomes, H.T., Sotelo, J.L., García, J., 2015. Synthesis of carbon xerogels and their application in adsorption studies of caffeine and diclofenac as emerging contaminants. Chemical Engineering Research and Design, 95, 229-238.

Ameta, S. C., Ameta, R., Ameta, G., 2018. Sonochemistry: An Emerging Green Technology. CRC Press, U.S.A.

Amin, L.P., Gogate, P.R., Burgess, A.E., Bremner, D.H., 2010. Optimization of a hydrodynamic cavitation reactor using salicylic acid dosimetry. Chemical engineering journal, 156, 165-169.

Arana, J., Dona-Rodrıguez, J.M., González-Dıaz, O., Rendón, E.T., Melián, J.H., Colon, G., Peña, J.P., 2004. Gas-phase ethanol photocatalytic degradation study with TiO2 doped with Fe, Pd and Cu. Journal of Molecular Catalysis A: Chemical, 215, 153-160.

Aranda, P., Kun, R., Martín-Luengo, M. A., Letaïef, S., Dékány, I., Ruiz-Hitzky, E., 2007. Titania−sepiolite nanocomposites prepared by a surfactant templating colloidal route. Chemistry of Materials, 20, 84-91.

Arrojo, S., Nerin, C., Benito, Y., 2007. Application of salicylic acid dosimetry to evaluate hydrodynamic cavitation as an advanced oxidation process. Ultrasonics Sonochemistry, 14, 343-349.

Arslan-Alaton, I., Tureli, G., Olmez-Hanci, T., 2009. Treatment of azo dye production wastewaters using Photo-Fenton-like advanced oxidation processes: Optimization by response surface methodology. Journal of Photochemistry and Photobiology A: Chemistry, 202, 142-153.

Asahi, R.Y., Morikawa, T.A., Ohwaki, T., Aoki, K., Taga, Y., 2001. Visible-light photocatalysis in nitrogen-doped titanium oxides. Science, 293, 269-271.

Ashokkumar, M., 1998. An overview on semiconductor particulate systems for photoproduction of hydrogen. International Journal of Hydrogen Energy, 23, 427-438.

Ashton, D., Hilton, M., Thomas, K.V., 2004. Investigating the environmental transport of human pharmaceuticals to streams in the United Kingdom. Science of the Total Environment, 333, 167-184.

Ay, F., Catalkaya, E.C., Kargi, F., 2009. A statistical experiment design approach for advanced oxidation of Direct Red azo-dye by photo-Fenton treatment. Journal of Hazardous Materials, 162, 230-236.

Ayare, S. D., Gogate, P. R., 2019. Sonocatalytic treatment of phosphonate containing industrial wastewater intensified using combined oxidation approaches. Ultrasonics Sonochemistry, 51, 69-76.

Bandara, J., Hadapangoda, C.C., Jayasekera, W.G., 2004. TiO2/MgO composite photocatalyst : the role of MgO in photoinduced charge carrier separation. Applied Catalysis B: Environmental, 50, 83-88.

Bang, J.H., Suslick, K.S., 2010. Applications of ultrasound to the synthesis of nanostructured materials. Advanced Materials, 22, 1039-1059.

Barbier, P. F., Petrier, C., 1996. Study at 20 kHz and 500 kHz of the ultrasound-ozone advanced oxidation system: 4-nitrophenol degradation. Journal of Advanced Oxidation Technologies, 1, 154-159.

Beale, R., Liss, P. S., Nightingale, P. D., 2010. First oceanic measurements of ethanol and propanol. Geophysical Research Letters, 37, 1-5.

Behnajady, M., Modirshahla, N., Fathi, H., 2006. Kinetics of decolorization of an azo dye in UV alone and UV/H2O2 processes. Journal of Hazardous Materials, 136, 816–821.

Belova, V., Mo, H. Shchukin, D.G., 2009. Ultrasonic intercalation of gold nanoparticles into a clay matrix in the presence of surface-active materials. Part II:Negative sodium dodecylsulfate and positive cetyltrimethylammonium bromide. The Journal of Physical Chemistry C, 113, 6751–6760.

Belova, V., Mo, H., Shchukin, D.G., 2008. Sonochemical intercalation of preformed gold nanoparticles into multilayered clays. Langmuir, 24, 9747-9753.

Bendz, D., Paxéus, N.A., Ginn, T.R., Loge, F.J., 2005. Occurrence and fate of pharmaceutically active compounds in the environment, a case study: Höje River in Sweden. Journal of Hazardous Materials, 122, 195-204.

Bhasarkar, J.B., Chakma, S., Moholkar, V.S., 2013. Mechanistic features of oxidative desulfurization using sono-Fenton–peracetic acid (ultrasound/Fe2+–CH3COOH–H2O2) system. Industrial & Engineering Chemistry Research, 52, 9038-9047.

Bielski, B.H., Cabelli, D.E., Arudi, R.L., Ross, A.B., 1985. Reactivity of HO2/O-2 radicals in aqueous solution. Journal of Physical and Chemical Reference Data, 14, 1041-1100.

Bogdan, J., Pławińska-Czarnak, J., Zarzyńska, J., 2017. Nanoparticles of titanium and zinc oxides as novel agents in tumor treatment: a review. Nanoscale Research Letters, 12, 225.

Bokhale, N.B., Bomble, S.D., Dalbhanjan, R.R., Mahale, D.D., Hinge, S.P., Banerjee, B.S., Gogate, P.R., 2014. Sonocatalytic and sonophotocatalytic degradation of rhodamine 6G containing wastewaters. Ultrasonics Sonochemistry, 21, 1797-1804.

Bratkovics, S., Sapozhnikova, Y., 2011. Determination of seven commonly used organic UV filters in fresh and saline waters by liquid chromatography-tandem mass spectrometry. Analytical Methods, 3, 2943-2950.

Brenner, M.P., Hilgenfeldt, S., Lohse, D., 2002. Single-bubble sonoluminescence. Reviews of Modern Physics, 74, 425.

Brotchie, A., Grieser, F., Ashokkumar, M., 2008. Sonochemistry and sonoluminescence under dual-frequency ultrasound irradiation in the presence of water-soluble solutes. The Journal of Physical Chemistry C, 112, 10247-10250.

Brown, J. L., Chen, T., Embree, H.D., Payne, G.F., 2002. Enhanced hydrogen bonding for the adsorptive recovery and separations of oxygenated aromatic compounds from renewable resources. Industrial & Engineering Chemistry Research, 41, 5058-5064.

Bruton, T., Alboloushi, A., De La Garza, B., Kim, B. O., Halden, R. U.,2010. Fate of caffeine in the environment and ecotoxicological considerations. American Chemical Society Symposium Series, 257-273.

Buxton, G.V., Greenstock, C.L., Helman, W.P., Ross, A.B., 1988. Critical review of rate constants for reactions of hydrated electrons, hydrogen atoms and hydroxyl radicals (·OH/·O− in aqueous solution. Journal of Physical and Chemical Reference Data, 17, 513-886.

Cabrera-Lafaurie, W.A., Román, F.R., Hernández-Maldonado, A.J., 2015. Single and multi-component adsorption of salicylic acid, clofibric acid, carbamazepine and caffeine from water onto transition metal modified and partially calcined inorganic–organic pillared clay fixed beds. Journal of Hazardous Materials, 282, 174-182.

Calamari, D., Zuccato, E., Castiglioni, S., Bagnati, R., Fanelli, R., 2003. Strategic survey of therapeutic drugs in the rivers Po and Lambro in northern Italy. Environmental Science & Technology, 37, 1241-1248.

Carballa, M., Omil, F., Lema, J. M., Llompart, M., Garcaares, C., Rodriguez, I., Ternes, T., 2004. Behavior of pharmaceuticals, cosmetics and hormones in a sewage treatment plant. Water Research, 38, 2918-2926.

Carmona, E., Andreu, V., Picó, Y., 2014. Occurrence of acidic pharmaceuticals and personal care products in Turia River Basin: from waste to drinking water. Science of the Total Environment, 484, 53-63.

Carp, O., Huisman, C. L., Reller, A., 2004. Photoinduced reactivity of titanium dioxide. Progress in Solid State Chemistry, 32, 33-177.

Caruso, R.A., Ashokkumar, M., Grieser, F., 2002. Sonochemical formation of gold sols. Langmuir, 18, 7831-7836.

Cass, P., Knower, W., Pereeia, E., Holmes, N.P., Hughes, T., 2010. Preparation of hydrogels via ultrasonic polymerization. Ultrasonics Sonochemistry, 17, 326-332.

Caturla, F., Molina-Sabio, M., Rodriguez-Reinoso, F., 1999. Adsorption–desorption of water vapor by natural and heat-treated sepiolite in ambient air. Applied Clay Science, 15, 367-380.

Cecilia, J.A., Vilarrasa-García, E., Cavalcante C.L., Azevedo, D.C.S., Franco, F., Rodríguez-Castellón, E., 2018. Evaluation of two fibrous clay minerals (sepiolite and palygorskite) for CO2 Capture. Journal of Environmental Chemical Engineering, 6, 4573-4587.

Celdeira, P.A., Gonçalves, M., Figueiredo, F.C., Dal Bosco, S.M., Mandelli, D., Carvalho, W.A., 2014. Sulfonated niobia and pillared clay as catalysts in etherification reaction of glycerol. Applied Catalysis A: General, 478, 98-106.

Chakma, S., Moholkar, V.S., 2014. Investigations in synergism of hybrid advanced oxidation processes with combinations of sonolysis+ fenton process+ UV for degradation of bisphenol A. Industrial & Engineering Chemistry Research, 53, 6855-6865.

Chang, C.Y., Hsieh, Y.H., Cheng, K.Y., Hsieh, L.L., Cheng, T.C., Yao, K.S., 2008. Effect of pH on Fenton process using estimation of hydroxyl radical with salicylic acid as trapping reagent. Water Science and Technology, 58, 873-879.

Chang, S.C., Wang, Y.F., You, S.J., Kuo, Y.M., Tsai, C.H., Wang, L.C., Hsu, P.Y., 2013. Toxicity evaluation of fly ash by Microtox®. Aerosol Air Qual Res, 13, 1002-1008.

Chatel, G., Novikova, L., Petit, S., 2016. How efficiently combine sonochemistry and clay science?. Applied Clay Science, 119, 193-201.

Chen, D., Ray, A.K., 1998. Photodegradation kinetics of 4-nitrophenol in TiO2 suspension. Water Research, 32, 3223-3234.

Chen, H., Jing, L., Teng, Y., Wang, J., 2018. Characterization of antibiotics in a large-scale river system of China: occurrence pattern, spatiotemporal distribution and environmental risks. Science of The Total Environment, 618, 409-418.

Chen, Y., Dionysiou, D.D., 2008. Bimodal mesoporous TiO2 – P25 composite thick films with high photocatalytic activity and improved structural integrity. Applied Catalysis B: Environmental, 80, 147-155.

Chen, Z. F., Ying, G. G., Lai, H. J., Chen, F., Su, H. C., Liu, Y. S., Zhao, J. L., 2012. Determination of biocides in different environmental matrices by use of ultra-high-performance liquid chromatography–tandem mass spectrometry. Analytical and Bioanalytical Chemistry, 404, 3175-3188.

Cho, J. K., Najman, R., Dean, T. W., Ichihara, O., Muller, C., Bradley, M., 2006. Captured and cross-linked palladium nanoparticles. Journal of the American Chemical Society, 128, 6276-6277.

Chong, M. N., Vimonses, V., Lei, S., Jin, B., Chow, C., Saint, C., 2009. Synthesis and characterisation of novel titania impregnated kaolinite nano-photocatalyst. Microporous and Mesoporous Materials, 117, 233-242.

Chuang, L.C., Luo, C.H., Huang, S.W., Wu, Y.C., Huang, Y.C., 2011. Photocatalytic degradation mechanism and kinetics of caffeine in aqueous suspension of nano-TiO2. In Advanced Materials Research, 214, 97-102.

Cinar, S. A., Ziylan-Yavaş, A., Catak, S., Ince, N. H., Aviyente, V., 2017. Hydroxyl radical-mediated degradation of diclofenac revisited: a computational approach to assessment of reaction mechanisms and by-products. Environmental Science and Pollution Research, 24, 18458-18469.

Cleuvers, M., 2004. Mixture toxicity of the anti-inflammatory drugs diclofenac, ibuprofen, naproxen, and acetylsalicylic acid. Ecotoxicology and Environmental Safety, 59, 309-315.

Corma, A., García, H., Leyva, A., Primo, A., 2004. Alkali-exchanged sepiolites containing palladium as bifunctional (basic sites and noble metal) catalysts for the Heck and Suzuki reactions. Applied Catalysis A: General, 257, 77-83.

Daneshkhah, M., Hossaini, H., Malakootian, M., 2017. Removal of metoprolol from water by sepiolite-supported nanoscale zero-valent iron. Journal of Environmental Chemical Engineering, 5, 3490-3499.

Daneshvar, N., Aber, S., Dorraji, M.S., Khataee, A. R., Rasoulifard, M.H., 2007. Photocatalytic degradation of the insecticide diazinon in the presence of prepared nanocrystalline ZnO powders under irradiation of UV-C light. Separation and Purification Technology, 58, 91-98.

Daneshvar, N., Rabbani, M., Modirshahla, N., Behnajady, M.A., 2004. Critical effect of hydrogen peroxide concentration in photochemical oxidative degradation of CI Acid Red 27 (AR27). Chemosphere, 56, 895-900.

Danks, A. E., Hall, S. R., Schnepp, Z., 2016. The evolution of ‘sol–gel’chemistry as a technique for materials synthesis. Materials Horizons, 3, 91-112.

de Haro, M. J., Pérez-Rodríguez, J. L., Poyato, J., Pérez-Maqueda, L. A., Ramírez-Valle, V., Justo, A., Wagner, F. E., 2005. Effect of ultrasound on preparation of porous materials from vermiculite. Applied clay science, 30, 11-20.

DeGraeve, G.M., Geiger, D.L., Meyer, J.S., Bergman, H.L., 1980. Acute and embryo-larval toxicity of phenolic compounds to aquatic biota. Archives of Environmental Contamination and Toxicology, 9, 557-568.

Dekany, I., Turi, L., Fonseca, A., Nagy, J.B., 1999. The structure of acid treated sepiolites: small-angle X-ray scattering and multi MAS-NMR investigations. Applied Clay Science, 14, 141-160.

Deming, S.N., Morgan, S.L., 1993. Experimental design: a chemometric approach, Elsevier Science Publishers, Amsterdam, The Netherlands.

Deming, S.N., Palasota, J.A., 1992. Central composite experimental designs: Applied to chemical systems, Journal of Chemical Education, 69, 560.

Deng, Y., Englehardt, J.D., 2006. Treatment of landfill leachate by the Fenton process. Water Research, 40, 3683-3694.

Devi, L.G., Kumar, S.G., Reddy, K.M., Munikrishnappa, C., 2009. Photo degradation of methyl orange an azo dye by advanced Fenton process using zero valent metallic iron: Influence of various reaction parameters and its degradation mechanism. Journal of Hazardous Materials, 164, 459-467.

Dewil, R., Baeyens, J., Neyens, E., 2005. Fenton peroxidation improves the drying performance of waste activated sludge. Journal of Hazardous Materials, 117, 161-170.

Dey, S., Bano, F., Malik, A., 2019. Pharmaceuticals and personal care product (PPCP) contamination-a global discharge inventory. In Pharmaceuticals and Personal Care Products: Waste Management and Treatment Technology, 1-26, Butterworth-Heinemann, Cambridge, U.S.A.

Dindar, B., Içli, S., 2001. Unusual photoreactivity of zinc oxide irradiated by concentrated sunlight. Journal of Photochemistry and Photobiology A: Chemistry, 140, 263–268.

Ding, H., Bian, G., 2015. Adsorption of metronidazole in aqueous solution by Fe-modified sepiolite. Desalination and Water Treatment, 55, 1620-1628.

Drijvers, D., Van Langenhove, H., Beckers, M., 1999. Decomposition of phenol and trichloroethylene by the ultrasound/H2O2/CuO process. Water Research, *33*, 1187-1194.

Dvininov, E., Ignat, M., Barvinschi, P., Smithers, M. A., Popovici, E., 2010. New SnO2/MgAl-layered double hydroxide composites as photocatalysts for cationic dyes bleaching. Journal of Hazardous Materials, 177, 150-158.

Eren, Z., Ince, N.H., 2010. Sonolytic and sonocatalytic degradation of azo dyes by low and high frequency ultrasound. Journal of Hazardous Materials, 177, 1019-1024.

Eriksson, E., Andersen, H. R., Ledin, A., 2008. Substance flow analysis of parabens in Denmark complemented with a survey of presence and frequency in various commodities. Journal of Hazardous Materials, 156, 240-259.

Esplugas, S., Bila, D.M., Krause, L.G.T., Dezotti, M., 2007. Ozonation and advanced oxidation technologies to remove endocrine disrupting chemicals (EDCs) and pharmaceuticals and personal care products (PPCPs) in water effluents. Journal of Hazardous Materials, 149, 631-642.

Fang, H., Gao, Y., Li, G., An, J., Wong, P. K., Fu, H., An, T., 2013. Advanced oxidation kinetics and mechanism of preservative propylparaben degradation in aqueous suspension of TiO2 and risk assessment of its degradation products. Environmental Science & Technology, 47, 2704-2712.

Fent, K., Kunz, P. Y., Zenker, A., Rapp, M., 2010. A tentative environmental risk assessment of the UV-filters 3-(4-methylbenzylidene-camphor), 2-ethyl-hexyl-4-trimethoxycinnamate, benzophenone-3, benzophenone-4 and 3-benzylidene camphor. Marine Environmental Research, 69, 4-6.

Fick, J., Söderström, H., Lindberg, R.H., Phan, C., Tysklind, M., Larsson, D.J., 2009. Contamination of surface, ground, and drinking water from pharmaceutical production. Environmental Toxicology and Chemistry, 28, 2522-2527.

Fischer, C. H., Hart, E. J., Henglein, A., 1986. Hydrogen/deuterium isotope exchange in the hydrogen deuteride-water system under the influence of ultrasound. The Journal of Physical Chemistry, 90, 3059-3060.

Franco, F., Pérez-Maqueda, L.A., Pérez-Rodriguez, J.L., 2004. The effect of ultrasound on the particle size and structural disorder of a well-ordered kaolinite. Journal of Colloid and Interface Science, 274, 107–117.

Ganzenko, O., Trellu, C., Papirio, S., Oturan, N., Huguenot, D., Van Hullebusch, E.D., Oturan, M.A., 2018. Bioelectro-Fenton: evaluation of a combined biological-advanced oxidation treatment for pharmaceutical wastewater. Environmental Science and Pollution Research, 25, 20283-20292.

Gao, Y., Ji, Y., Li, G., An, T., 2016. Theoretical investigation on the kinetics and mechanisms of hydroxyl radical-induced transformation of parabens and its consequences for toxicity: Influence of alkyl-chain length. Water Research, 91, 77-85.

García-López, D., Fernández, J. F., Merino, J. C., Santarén, J., Pastor, J. M., 2010. Effect of organic modification of sepiolite for PA 6 polymer/organoclay nanocomposites. Composites Science and Technology, 70, 1429-1436.

Ghosh, M., Adams, C.M., Dodd, S.K., Poor, S.H., 2019. Topical aqueous ophthalmic compositions containing a 1H-indole-1-carboxamide derivative and use thereof for treatment of ophthalmic disease. U.S. Patent Application No. 10/174,006.

Giannelis, E.P., 1996. Polymer layered silicate nanocomposites. Advanced Materials, 8, 29-35.

Glassmeyer, S.T., Furlong, E.T., Kolpin, D.W., Cahill, J.D., Zaugg, S.D., Werner, S.L., Kryak, D.D., 2005. Transport of chemical and microbial compounds from known wastewater discharges: potential for use as indicators of human fecal contamination. Environmental Science & Technology, 39, 5157-5169.

Gogate, P. R., Shaha, S., Csoka, L., 2014. Intensification of cavitational activity in the sonochemical reactors using gaseous additives. Chemical Engineering Journal, 239, 364-372.

Gogate, P.R., Pandit, A.B., 2000. Engineering design method for cavitational reactors: I. Sonochemical reactors. AIChE Journal, 46, 372-379.

Goi, A., Veressinina, Y., Trapido, M., 2008. Degradation of salicylic acid by Fenton and modified Fenton treatment. Chemical Engineering Journal, 143, 1-9.

Gonze, E., Fourel, L., Gonthier, Y., Boldo, P., Bernis, A., 1999. Wastewater pretreatment with ultrasonic irradiation to reduce toxicity. Chemical Engineering Journal, 73, 93-100.

Gouvea, C. A., Wypych, F., Moraes, S.G., Duran, N., Nagata, N., Peralta-Zamora, P., 2000. Semiconductor-assisted photocatalytic degradation of reactive dyes in aqueous solution. Chemosphere, 40, 433-440.

Grillet, Y., Cases, J.M., Francois, M., Rouquerol, J., Poirier, J.E., 1988. Modification of the porous structure and surface area of sepiolite under vacuum thermal treatment. Clays and Clay Minerals, 36, 233-242.

Gros, M., Petrović, M., Barceló, D., 2006. Development of a multi-residue analytical methodology based on liquid chromatography–tandem mass spectrometry (LC–MS/MS) for screening and trace level determination of pharmaceuticals in surface and wastewaters. Talanta, 70, 678-690.

Guinea, E., Arias, C., Cabot, P. L., Garrido, J. A., Rodríguez, R. M., Centellas, F., Brillas, E., 2008. Mineralization of salicylic acid in acidic aqueous medium by electrochemical advanced oxidation processes using platinum and boron-doped diamond as anode and cathodically generated hydrogen peroxide. Water Research, 42, 499-511.

Guisasola, A., Sin, G., Baeza, J.A., Carrera, J., Vanrolleghem, P.A., 2005. Limitations of ASM1 and ASM3: a comparison based on batch oxygen uptake rate profiles from different full-scale wastewater treatment plants. Water Science and Technology, 52, 69-77.

Gültekin, I., Ince, N.H., 2008. Ultrasonic destruction of bisphenol-A: the operating parameters. Ultrasonics Sonochemistry, 15, 524-529.

Gültekin, I., Tezcanli-Güyer, G., Ince, N.H., 2009. Sonochemical decay of CI Acid Orange 8: effects of CCl4 and t-butyl alcohol. Ultrasonics Sonochemistry, 16, 577-581.

Güyer, G.T., Ince, N.H., 2011. Degradation of diclofenac in water by homogeneous and heterogeneous sonolysis. Ultrasonics Sonochemistry, 18, 114-119.

Han, D.H., Nur, A., Morgan, D., 1986. Effects of porosity and clay content on wave velocities in sandstones. Geophysics, 51, 2093-2107.

Hansch, C., Leo, A., 1995. The hydrophobic parameter: measurement and calculation. Exploring QSAR. Fundamentals and Applications in Chemistry and Biology, 97-124.

Hartley, H.O., 1959. Smallest composite design for quadratic response surfaces. Biometrics, 16, 611.

Hartmann, J., Bartels, P., Mau, U., Witter, M., Tümpling, W.V., Hofmann, J., Nietzschmann, E., 2008. Degradation of the drug diclofenac in water by sonolysis in presence of catalysts. Chemosphere, 70, 453-461.

Heberer, T., 2002. Occurrence, fate, and removal of pharmaceutical residues in the aquatic environment: a review of recent research data. Toxicology Letters, 131, 5-17.

Henglein, A., Kormann, C., 1985. Scavenging of OH radicals produced in the sonolysis of water. International Journal of Radiation Biology and Related Studies in Physics, Chemistry and Medicine, 48, 251-258.

Hilgenfeldt, S., Grossmann, S., Lohse, D., 1999. Sonoluminescence light emission. Physics of Fluids, 11, 1318-1330.

Hu, J., Zhang, L.L., Chen, J.M., Liu, Y., 2013. Degradation of paracetamol by Pseudomonas aeruginosa strain HJ1012. Journal of Environmental Science and Health, Part A, 48, 791-799.

Huet, S., Belmonte, T., Thiebaut, J.M., Bockel, S., Michel, H., 2005. Reduction of TiO2 assisted by a microwave plasma at atmospheric pressure. Thin Solid Films, 475, 63-67.

Hummel, D., Löffler, D., Fink, G., Ternes, T. A., 2006. Simultaneous determination of psychoactive drugs and their metabolites in aqueous matrices by liquid chromatography mass spectrometry. Environmental Science & Technology, 40, 7321-7328.

Hyndman, R.J., Koehler, A.B., 2006. Another look at measures of forecast accuracy. International Journal of Forecasting, 22, 679-688.

Ince, N. H., Apikyan, I. G., 2000. Combination of activated carbon adsorption with light-enhanced chemical oxidation via hydrogen peroxide. Water Research, 34, 4169-4176.

Ince, N. H., Tezcanli, G., Belen, R. K., Apikyan, I. G. 2001. Ultrasound as a catalyzer of aqueous reaction systems: the state of the art and environmental applications. Applied Catalysis B: Environmental, 29, 167-176.

Ince, N.H., 2018. Ultrasound-assisted advanced oxidation processes for water decontamination. Ultrasonics Sonochemistry, 40, 97-103.

Ince, N.H., Gültekin, I., Tezcanli-Güyer, G., 2009. Sonochemical destruction of nonylphenol: effects of pH and hydroxyl radical scavengers. Journal of Hazardous Materials, 172, 739-743.

Isariebel, Q.P., Carine, J.L., Ulises-Javier, J.H., Anne-Marie, W., Henri, D., 2009. Sonolysis of levodopa and paracetamol in aqueous solutions. Ultrasonics Sonochemistry, 16, 610-616.

Johnson, A. C., Bowes, M. J., Crossley, A., Jarvie, H. P., Jurkschat, K., Jürgens, M. D., Xu, N., 2011. An assessment of the fate, behaviour and environmental risk associated with sunscreen TiO2 nanoparticles in UK field scenarios. Science of the Total Environment, 409, 2503-2510.

Jokar, A., Azizi, M. H., Esfehani, Z. H., Abbasi, S., 2017. Effects of ultrasound time on the properties of methylcellulose-montmorillonite films. International Nano Letters, 7, 59-68.

Jordan, J., Jacob, K. I., Tannenbaum, R., Sharaf, M. A., Jasiuk, I., 2005. Experimental trends in polymer nanocomposites-a review. Materials Science and Engineering: A, 393, 1-11.

Jung, C., Son, A., Her, N., Zoh, K.D., Cho, J., Yoon, Y., 2015. Removal of endocrine disrupting compounds, pharmaceuticals, and personal care products in water using carbon nanotubes: A review. Journal of Industrial and Engineering Chemistry, 27, 1-11.

Kamat, P.V., 2002. Photophysical, photochemical and photocatalytic aspects of metal nanoparticles. The Journal of Physical Chemistry B, 106, 7729–7744.

Kamaya, Y., Fukaya, Y., Suzuki, K., 2005. Acute toxicity of benzoic acids to the crustacean Daphnia magna. Chemosphere, 59, 255-261.

Karamanis, D., Ökte, A. N., Vardoulakis, E., Vaimakis, T., 2011. Water vapor adsorption and photocatalytic pollutant degradation with TiO2–sepiolite nanocomposites. Applied Clay Science, 53, 181-187.

Karnjanapiboonwong, A., Suski, J.G., Shah, A.A., Cai, Q., Morse, A.N., Anderson, T.A., 2011. Occurrence of PPCPs at a wastewater treatment plant and in soil and groundwater at a land application site. Water, Air, & Soil Pollution, 216, 257-273.

Kasprzyk-Hordern, B., Dinsdale, R.M., Guwy, A.J., 2008. The occurrence of pharmaceuti- cals, personal care products, endocrine disruptors and illicit drugs in surface water in South Wales, UK, Water Research, 42, 3498-3518.

Katdare, S.P., Ramaswamy, V., Ramaswamy, A.V, 2000. Factors affecting the preparation of alumina pillared montmorillonite employing ultrasonics. Microporous and Mesoporous Materials, 37, 329-336.

Katsoyiannis, A., Zouboulis, A., Samara, C., 2006. Persistent organic pollutants (POPs) in the conventional activated sludge treatment process: model predictions against experimental values. Chemosphere, 65, 1634-1641.

Khalaf, H., Bouras, O., Perrichon, V., 1997. Synthesis and characterization of Al-pillared and cationic surfactant modified Al-pillared Algerian bentonite. Microporous Materials, 8, 141–150.

Khaled, S., Sui, R., Charpentier, P.A., Rizkalla, A.S., 2007. Synthesis of TiO2-PMMA nanocomposite: Using methacrylic acid as a coupling agent. Langmuir, 23, 3988-3995.

Khalfaoui-Boutoumi, N., Boutoumi, H., Khalaf, H., David, B., 2013. Synthesis and characterization of TiO2–Montmorillonite/Polythiophene-SDS nanocomposites: Application in the sonophotocatalytic degradation of rhodamine 6G. Applied Clay Science, 80, 56-62.

Khataee, A., Darvishi Cheshmeh Soltani, R., Hanifehpour, Y., Safarpour, M., Gholipour Ranjbar, H., Joo, S.W., 2014. Synthesis and characterization of dysprosium-doped ZnO nanoparticles for photocatalysis of a textile dye under visible light irradiation. Industrial & Engineering Chemistry Research, 53, 1924-1932.

Khataee, A., Mohamadi, F.T., Rad, T.S., Vahid, B., 2018. Heterogeneous sonocatalytic degradation of anazolene sodium by synthesized dysprosium doped CdSe nanostructures. Ultrasonics Sonochemistry, 40, 361-372.

Khodja, A. A., Sehili, T., Pilichowski, J. F., Boule, P., 2001. Photocatalytic degradation of 2-phenylphenol on TiO2 and ZnO in aqueous suspensions. Journal of Photochemistry and Photobiology A: Chemistry, 141, 231-239.

Khunjar, W.O., Mackintosh, S.A., Skotnicka-Pitak, J., Baik, S., Aga, D.S., Love, N.G., 2011. Elucidating the relative roles of ammonia oxidizing and heterotrophic bacteria during the

biotransformation of 17α-ethinylestradiol and trimethoprim. Environmental Science & Technology, 45, 3605-3612.

Kibanova, D., Sleiman, M., Cervini-Silva, J., Destaillats, H., 2012. Adsorption and photocatalytic oxidation of formaldehyde on a clay-TiO2 composite. Journal of Hazardous Materials, 211, 233-239.

Kidak, R., Ince, N.H., 2006. Effects of operating parameters on sonochemical decomposition of phenol. Journal of Hazardous Materials, 137, 1453-1457.

Kidak, R., Ince, N.H., 2007. Catalysis of advanced oxidation reactions by ultrasound: A case study with phenol. Journal of Hazardous Materials, 146, 630-635.

Kim, M., Guerra, P., Shah, A., Parsa, M., Alaee, M., Smyth, S.A., 2014. Removal of pharmaceuticals and personal care products in a membrane bioreactor wastewater treatment plant. Water Science and Technology, 69, 2221-2229.

Klassen, N. V., Marchington, D., McGowan, H.C., 1994. H2O2 determination by the I3-method and by KMnO4 titration. Analytical Chemistry, 66, 2921-2925.

Klavarioti, M., Mantzavinos, D., Kassinos, D., 2009. Removal of residual pharmaceuticals from aqueous systems by advanced oxidation processes. Environment International, 35, 402-417.

Kolodziej, E. P., Sedlak, D. L., 2007. Rangeland grazing as a source of steroid hormones to surface waters. Environmental Science & Technology, 41, 3514-3520.

Kotronarou, A., Mills, G., Hoffmann, M.R., 1991. Ultrasonic irradiation of p-nitrophenol in aqueous solution. The Journal of Physical Chemistry, 95, 3630-3638.

Kumar, R. V., Palchik, O., Koltypin, Y., Diamant, Y., Gedanken, A., 2002. Sonochemical synthesis and characterization of Ag2S/PVA and CuS/PVA nanocomposite. Ultrasonics Sonochemistry, 9, 65-70.

Kutty, T.R.N., Avudaithai, M., 1990. Sacrificial water photocleavage using Nb-doped TiO2 fine particles under band gap irradiation. International Journal of Hydrogen Energy, 15, 621–628.

Kyzas, G.Z., Fu, J., Lazaridis, N.K., Bikiaris, D.N., Matis, K.A., 2015. New approaches on the removal of pharmaceuticals from wastewaters with adsorbent materials. Journal of Molecular Liquids, 209, 87-93.

Legrini, O., Oliveros, E., Braun, A. M., 1993. Photochemical processes for water treatment. Chemical Reviews, 93, 671-698.

Lei, B., Huang, S., Zhou, Y., Wang, D., Wang, Z., 2009. Levels of six estrogens in water and sediment from three rivers in Tianjin area, China. Chemosphere, 76, 36-42.

Lemić, J., Tomašević-Čanović, M., Djuričić, M., Stanić, T., 2005. Surface modification of sepiolite with quaternary amines. Journal of Colloid and Interface Science, 292, 11-19.

Lepoint, T., Mullie, F., 1994. What exactly is cavitation chemistry?. Ultrasonics Sonochemistry, 1, 13-22.

Li, F.B., Li, X.Z., 2002. The enhancement of photodegradation efficiency using Pt–TiO2 catalyst. Chemosphere, 48, 1103-1111.

Li, Y.Z., He, Y.L., Liu, Y.H., Yang, S.C., Zhang, G.J., 2005. Comparison of the filtration characteristics between biological powdered activated carbon sludge and activated sludge in submerged membrane bioreactors. Desalination, 174, 305-314.

Liao, L.M., Wang, Z.Q., Liang, H., Feng, J., Zhang, D., 2016. Synthesis and photocatalytic activity of sepiolite supportednano-TiO2 composites prepared by a mild solid-state sintering process. IOP Conference Series: Earth and Environmental Science, 39, 1-6.

Lin, Y., Ferronato, C., Deng, N., Wu, F., Chovelon, J. M., 2009. Photocatalytic degradation of methylparaben by TiO2: Multivariable experimental design and mechanism. Applied Catalysis B: Environmental, 88, 32-41.

Lindsey, M.E., Tarr, M.A., 2000. Inhibition of hydroxyl radical reaction with aromatics by dissolved natural organic matter. Environmental Science & Technology, 34, 444-449.

Lizama, C., Freer, J., Baeza, J., Mansilla, H.D., 2002. Optimized photodegradation of reactive blue 19 on TiO2 and ZnO suspensions. Catalysis Today, 76, 235-246.

López-Serna, R., Jurado, A., Vázquez-Suñé, E., Carrera, J., Petrović, M., Barceló, D., 2013. Occurrence of 95 pharmaceuticals and transformation products in urban groundwaters underlying the metropolis of Barcelona, Spain. Environmental Pollution, 174, 305-315.

Lorimer, J.P., Mason, T.J., 1987. Sonochemistry. Part 1-the physical aspects. Chemical Society Reviews, 16, 239-274.

Lorimer, J.P., Mason, T.J., Fiddy, K., 1991. Enhancement of chemical reactivity by power ultrasound: an alternative interpretation of the hot spot. Ultrasonics, 29, 338-343.

Mabovu, B., 2011. Brine treatment using natural adsorbents, Ph.D. Dissertation, University of the Western Cape.

Mandal, S., 2018. Reaction rate constants of hydroxyl radicals with micropollutants and their significance in advanced oxidation processes. Journal of Advanced Oxidation Technologies, 21, 20170075.

Mahvi, A. H., 2009. Application of ultrasonic technology for water and wastewater treatment. Iranian Journal of Public Health, 38, 1-17.

Marques, R. R., Sampaio, M. J., Carrapiço, P. M., Silva, C. G., Morales-Torres, S., Dražić, G., Silva, A. M., 2013. Photocatalytic degradation of caffeine: Developing solutions for emerging pollutants. Catalysis Today, 209, 108-115.

Martínez-Tarifa, A., Arrojo, S., Ávila-Marín, A.L., Pérez-Jiménez, J.A., Sáez, V., Ruiz-Lorenzo, M.L., 2010. Salicylic acid dosimetry applied for the statistical determination of significant parameters in a sonochemical reactor. Chemical Engineering Journal, 157(2-3), 420-426.

Mason, T. J., 1999. Sonochemistry. Oxford University Press, New York, U.S.A.

Mason, T. J., Peters, D., 2002. Practical sonochemistry: Power ultrasound uses and applications. Woodhead Publishing, Philadelphia, U.S.A.

Mason, T.J., de Meulenaer, E.C., 1998. Practical considerations for process optimization. In Synthetic Organic Sonochemistry, 301-329, Chichester, U.K.

Mason, T.J., Lorimer, J.P., 1990. A general introduction to sonochemistry. Sonochemistry: The Uses of Ultrasound in Chemistry. The Royal Society of Chemistry, 1-8.

McKay, M.D., Beckman, R.J., Conover, W.J., 1979. Comparison of three methods for selecting values of input variables in the analysis of output from a computer code. Technometrics, 21, 239-245.

Méndez-Arriaga, F., Torres-Palma, R.A., Pétrier, C., Esplugas, S., Gimenez, J., Pulgarin, C., 2008. Ultrasonic treatment of water contaminated with ibuprofen. Water Research, 42, 4243-4248.

Mestre, A.S., Pires, J., Nogueira, J.M.F., Carvalho, A.P., 2007. Activated carbons for the adsorption of ibuprofen. Carbon, 45, 1979-1988.

Miralles-Cuevas, S., Oller, I., Ruíz-Delgado, A., Cabrera-Reina, A., Cornejo-Ponce, L., Malato, S., 2018. EDDS as complexing agent for enhancing solar advanced oxidation processes in natural water: Effect of iron species and different oxidants. Journal of Hazardous Materials, in Press.

Mizukoshi, Y., Oshima, R., Maeda, Y., Nagata, Y., 1999. Preparation of platinum nanoparticles by sonochemical reduction of the Pt (II) ion. Langmuir, 15, 2733-2737.

Mohajeri, S., Aziz, H.A., Isa, M.H., Zahed, M.A., Adlan, M.N., 2010. Statistical optimization of process parameters for landfill leachate treatment using electro-Fenton technique. Journal of Hazardous Materials, 176, 749-758.

Moldovan, Z., 2006. Occurrences of pharmaceutical and personal care products as micropollutants in rivers from Romania. Chemosphere, 64, 1808-1817.

Montes-Grajales, D., Fennix-Agudelo, M., Miranda-Castro, W., 2017. Occurrence of personal care products as emerging chemicals of concern in water resources: A review. Science of the Total Environment, 595, 601-614.

Montgomery, D.C., 2008. Design and analysis of experiments. John Wiley & Sons, New Jersey, U.S.A.

Morgan, A.B., Harris, J.D., 2004. Exfoliated polystyrene-clay nanocomposites synthesized by solvent blending with sonication. Polymer, 45, 8695–8703.

Mulroy, A., 2001. When the cure is the problem. Water Environment & Technology, 13, 32-37.

Muruganandham, M., Suri, R. P. S., Jafari, S., Sillanpää, M., Lee, G. J., Wu, J. J., Swaminathan, M., 2014. Recent developments in homogeneous advanced oxidation processes for water and wastewater treatment. International Journal of Photoenergy, 1-21.

Myers, R.H., Montgomery, D.C., Anderson-Cook, C.M., 2009. Response surface methodology: process and product optimization using designed experiments, John Wiley & Sons, New Jersey, U.S.A.

Naddeo, V., Belgiorno, V., Kassinos, D., Mantzavinos, D., Meric, S., 2010. Ultrasonic degradation, mineralization and detoxification of diclofenac in water: optimization of operating parameters. Ultrasonics Sonochemistry, 17, 179-185.

Nakada, N., Shinohara, H., Murata, A., Kiri, K., Managaki, S., Sato, N., Takada, H., 2007. Removal of selected pharmaceuticals and personal care products (PPCPs) and endocrine-disrupting chemicals (EDCs) during sand filtration and ozonation at a municipal sewage treatment plant. Water Research, 41, 4373-4382.

Nam, S. W., Choi, D. J., Kim, S. K., Her, N., Zoh, K. D., 2014. Adsorption characteristics of selected hydrophilic and hydrophobic micropollutants in water using activated carbon. Journal of Hazardous Materials, 270, 144-152.

Newman, C. M. H., Bettinger, T., 2007. Gene therapy progress and prospects: ultrasound for gene transfer. Gene Therapy, 14, 465.

Neyens, E., Baeyens, J., 2003. A review of classic Fenton's peroxidation as an advanced oxidation technique. Journal of Hazardous Materials, 98, 33-50.

Nghiem, L.D., Schäfer, A.I., Elimelech, M., 2004. Removal of natural hormones by nanofiltration membranes: measurement, modeling, and mechanisms. Environmental Science & Technology, 38, 1888-1896.

Okitsu, K., Ashokkumar, M., Grieser, F., 2005. Sonochemical synthesis of gold nanoparticles: effects of ultrasound frequency. The Journal of Physical Chemistry B, 109, 20673-20675.

Okitsu, K., Cavalieri, F., 2018. Chemical and Physical Effects of Acoustic Bubbles. In Sonochemical Production of Nanomaterials, 1-17.

Okitsu, K., Iwasaki, K., Yobiko, Y., Bandow, H., Nishimura, R., Maeda, Y., 2005. Sonochemical degradation of azo dyes in aqueous solution: a new heterogeneous kinetics model taking into account the local concentration of OH radicals and azo dyes. Ultrasonics Sonochemistry, 12, 255-262.

Oulton, R. L., Kohn, T., Cwiertny, D. M., 2010. Pharmaceuticals and personal care products in effluent matrices: a survey of transformation and removal during wastewater treatment and implications for wastewater management. Journal of Environmental Monitoring, 12, 1956-1978.

Palasota J.A., Demin J.N., 1992. Central composite experimental designs: Applied to chemical systems. Journal of Chemical Education, 69, 560.

Palominos, R., Freer, J., Mondaca, M.A., Mansilla, H.D., 2008. Evidence for hole participation during the photocatalytic oxidation of the antibiotic flumequine. Journal of Photochemistry and Photobiology A: Chemistry, 193, 139-145.

Perez-Pariente, J., Martens, J.A., Jacobs, P.A., 1988. Factors affecting the synthesis efficiency of zeolite BETA from aluminosilicate gels containing alkali and tetraethylammonium ions. Zeolites, 8, 46-53.

Pérez-Rodríguez, J.L., Carrera, F., Poyato, J., Pérez-Maqueda, L.A., 2002. Sonication as a tool for preparing nanometric vermiculite particles. Nanotechnology, 13, 382-387.

Petrier, C., Jeunet, A., Luche, J.L., Reverdy, G., 1992. Unexpected frequency effects on the rate of oxidative processes induced by ultrasound. Journal of the American Chemical Society, 114, 3148-3150.

Pietrogrande, M. C., Basaglia, G., 2007. GC-MS analytical methods for the determination of personal-care products in water matrices. Trends in Analytical Chemistry, 26, 1086-1094.

Popa, C., Favier, L., Dinica, R., Semrany, S., Djelal, H., Amrane, A., Bahrim, G., 2014. Potential of newly isolated wild Streptomyces strains as agents for the biodegradation of a recalcitrant pharmaceutical, carbamazepine. Environmental Technology, 35, 3082-3091.

Rao, A. N., Sivasankar, B., Sadasivam, V., 2009. Kinetic study on the photocatalytic degradation of salicylic acid using ZnO catalyst. Journal of Hazardous Materials, 166, 1357-1361.

Reif, A.G., Crawford, J.K., Loper, C.A., Proctor, A., Manning, R., Titler, R., 2012. Occurrence of pharmaceuticals, hormones, and organic wastewater compounds in Pennsylvania waters, 2006-09. US Geological Survey, Reston, Virginia, U.S.A.

Reis, P.J., Reis, A.C., Ricken, B., Kolvenbach, B.A., Manaia, C.M., Corvini, P.F., Nunes, O.C., 2014. Biodegradation of sulfamethoxazole and other sulfonamides by Achromobacter denitrificans PR1. Journal of Hazardous Materials, 280, 741-749.

Reisse, J., Caulier, T., Deckerkheer, C., Fabre, O., Vandercammen, J., Delplancke, J. L., Winand, R., 1996. Quantitative sonochemistry. Ultrasonics Sonochemistry, 3, 147-151.

Reisse, J., Caulier, T., Deckerkheer, C., Fabre, O., Vandercammen, J., Delplancke, J. L.,
Rigg, T., Taylor, W., Weiss, J., 1954. The rate constant of the reaction between hydrogen peroxide and ferrous ions. The Journal of Chemical Physics, 22, 575-577.

Rodriguez, E., Campinas, M., Acero, J.L., Rosa, M.J., 2016. Investigating PPCP removal from wastewater by powdered activated carbon/ultrafiltration. Water, Air, & Soil Pollution, 227, 177.

Rodriguez, M.A.V., Gonzalez, J. de D.L., Munoz, M.A.B., 1994. Acid activation of a Spanish sepiolite: physico-chemical characterization, free silica content and surface area of products obtained. Clay Minerals, 29, 361–368.

Rodriguez, M.A.V., González, J. de D.L., Munoz, M.A.B., 1995. Preparation of microporous solids by acid treatment of a saponite. Microporous Materials, 4, 251–264.

Rooze, J., Rebrov, E.V., Schouten, J.C., Keurentjes, J.T., 2013. Dissolved gas and ultrasonic cavitation–a review. Ultrasonics Sonochemistry, 20, 1-11.

Ruiz-Hitzky, E., 2001. Molecular access to intracrystalline tunnels of sepiolite. Journal of Materials Chemistry, 11, 86-91.

Rytwo, G., Nir, S., Margulies, L., Casal, B., Merino, J., Ruiz-Hitzky, E., Serratosa, J. M., 1998. Adsorption of monovalent organic cations on sepiolite: experimental results and model calculations. Clays and Clay Minerals, 46, 340-348.

Sabah, E., Cinar, M., Çelik, M.S., 2007. Decolorization of vegetable oils: adsorption mechanism of β-carotene on acid-activated sepiolite. Food Chemistry, 100, 1661-1668.

Sabah, E., Majdan, M., 2009. Removal of phosphorus from vegetable oil by acid-activated sepiolite. Journal of Food Engineering, 91, 423–427.

Sacco, O., Vaiano, V., Matarangolo, M., 2018. ZnO supported on zeolite pellets as efficient catalytic system for the removal of caffeine by adsorption and photocatalysis. Separation and Purification Technology, 193, 303-310.

Sacks, J., Welch, W.J., Mitchell, T.J., Wynn, H.P., 1989. Design and analysis of computer experiments. Statistical Science, 409-423.

Sakthivel, S., Neppolian, B., Shankar, M. V., Arabindoo, B., Palanichamy, M., Murugesan, V., 2003. Solar photocatalytic degradation of azo dye: comparison of photocatalytic efficiency of ZnO and TiO2. Solar Energy Materials and Solar Cells, 77, 65-82.

Sandhya, K. P., Haridas, S., Sugunan, S., 2013. Visible light induced photocatalytic activity of polyaniline modified TiO2 and Clay-TiO2 composites. Bulletin of Chemical Reaction Engineering & Catalysis, 8, 145-153.

Sasi, S., Rayaroth, M.P., Devadasan, D., Aravind, U.K., Aravindakumar, C.T., 2015. Influence of inorganic ions and selected emerging contaminants on the degradation of Methylparaben: a sonochemical approach. Journal of Hazardous Materials, 300, 202-209.

Savun-Hekimoğlu, B., Ince, N. H., 2017. Decomposition of PPCPs by ultrasound-assisted advanced Fenton reaction: A case study with salicylic acid. Ultrasonics Sonochemistry, 39, 243-249.

Scheck, C.K., Frimmel, F.H., 1995. Degradation of phenol and salicylic acid by ultraviolet radiation/hydrogen peroxide/oxygen. Water Research, 29, 2346-2352.

Schlittenbauer, L., Seiwert, B., Reemtsma, T., 2016. Ultrasound-assisted hydrolysis of conjugated parabens in human urine and their determination by UPLC–MS/MS and UPLC–HRMS. Analytical and Bioanalytical Chemistry, 408, 1573-1583.

Schlumpf, M., Kypke, K., Wittassek, M., Angerer, J., Mascher, H., Mascher, D., Lichtensteiger, W., 2010. Exposure patterns of UV filters, fragrances, parabens, phthalates, organochlor pesticides, PBDEs, and PCBs in human milk: correlation of UV filters with use of cosmetics. Chemosphere, 81, 1171-1183.

Semmens, M.J., Martin, W.P., 1988. The influence of pretreatment on the capacity and selectivity of clinoptilolite for metal ions. Water Research, 22, 537–542.

Serpone, N., Terzian, R., Hidaka, H., Pelizzetti, E., 1994. Ultrasonic induced dehalogenation and oxidation of 2-, 3-, and 4-chlorophenol in air-equilibrated aqueous media. Similarities with irradiated semiconductor particulates. The Journal of Physical Chemistry, 98, 2634-2640.

Shi, L., Yang, J., 2009. Preparation of TiO2/sepiolite composite and its adsorption and photo-catalysis property to simulated dye water. International Conference on Energy and Environment Technology, ICEET 2009, 3, 465–468.

Shichi, T., Takagi, K., 2000. Clay minerals as photochemical reaction fields. Journal of Photochemistry and Photobiology C: Photochemistry Reviews, 1, 113-130.

Shirsath, S. R., Hage, A. P., Zhou, M., Sonawane, S. H., Ashokkumar, M., 2011. Ultrasound assisted preparation of nanoclay Bentonite-FeCo nanocomposite hybrid hydrogel: a potential responsive sorbent for removal of organic pollutant from water. Desalination, 281, 429-437.

Sivakumar, M., Gedanken, A., 2004. Insights into the sonochemical decomposition of Fe (CO) 5: theoretical and experimental understanding of the role of molar concentration and power density on the reaction yield. Ultrasonics Sonochemistry, 11, 373-378.

Sivalingam, G., Nagaveni, K., Hegde, M. S., Madras, G., 2003. Photocatalytic degradation of various dyes by combustion synthesized nano anatase TiO2. Applied Catalysis B: Environmental, 45, 23-38.

Soares, O.S.G., Orfao, J. J., Portela, D., Vieira, A., Pereira, M.F.R., 2006. Ozonation of textile effluents and dye solutions under continuous operation: Influence of operating parameters. Journal of Hazardous Materials, 137, 1664-1673.

Sonawane, S., Chaudhari, P., Ghodke, S., Ambade, S., Gulig, S., Mirikar, A., Bane, A., 2008. Combined effect of ultrasound and nanoclay on adsorption of phenol. Ultrasonics Sonochemistry, 15, 1033-1037.

Soni, M. G., Taylor, S. L., Greenberg, N. A., Burdock, G. A., 2002. Evaluation of the health aspects of methyl paraben: a review of the published literature. Food and Chemical Toxicology, 40, 1335-1373.

Sotelo, J. L., Ovejero, G., Rodríguez, A., Álvarez, S., Galán, J., García, J., 2014. Competitive adsorption studies of caffeine and diclofenac aqueous solutions by activated carbon. Chemical Engineering Journal, 240, 443-453.

Sotelo, J. L., Ovejero, G., Rodríguez, A., Álvarez, S., García, J., 2013. Study of natural clay adsorbent sepiolite for the removal of caffeine from aqueous solutions: batch and fixed-bed column operation. Water, Air, & Soil Pollution, 224, 1466.

Steter, J. R., Dionisio, D., Lanza, M.R.D.V., Motheo, A.D.J., 2014. Electrochemical and sonoelectrochemical processes applied to the degradation of the endocrine disruptor methyl paraben. Journal of Applied Electrochemistry, 44, 1317-1325.

Stuart, M., Lapworth, D., Crane, E., Hart, A., 2012. Review of risk from potential emerging contaminants in UK groundwater. Science of the Total Environment, 416, 1-21.

Suárez, S., Coronado, J. M., Portela, R., Martín, J. C., Yates, M., Avila, P., Sánchez, B., 2008. On the preparation of TiO2- sepiolite hybrid materials for the photocatalytic degradation of TCE: influence of TiO2 distribution in the mineralization. Environmental Science & Technology, 42, 5892-5896.

Suarez, S., Lema, J.M., Omil, F., 2010. Removal of pharmaceutical and personal care products (PPCPs) under nitrifying and denitrifying conditions. Water Research, 44, 3214-3224.

Suárez, S., Yates, M., Petre, A. L., Martin, J. A., Avila, P., Blanco, J., 2006. Development of a new Rh/TiO2–sepiolite monolithic catalyst for N2O decomposition. Applied Catalysis B: Environmental, 64, 302-311.

Sui, Q., Huang, J., Deng, S., Chen, W., Yu, G., 2011. Seasonal variation in the occurrence and removal of pharmaceuticals and personal care products in different biological wastewater treatment processes. Environmental Science & Technology, 45, 3341-3348.

Sun, J. H., Dong, S. Y., Wang, Y. K., Sun, S. P., 2009. Preparation and photocatalytic property of a novel dumbbell-shaped ZnO microcrystal photocatalyst. Journal of Hazardous Materials, 172, 1520-1526.

Suslick, K. S., 1994. The chemistry of ultrasound. Encyclopaedia Britannica, 138-155.

Suslick, K.S., 1990. Sonochemistry. Science, 247, 1439-1445.

Suslick, K.S., McNamara, W.B., Didenko, Y., 1999. Hot spot conditions during multi-bubble cavitation. Sonochemistry and Sonoluminescence, 191-204.

Tai, Y., Watanabe, M., Kaneko, K., Tanemura, S., Miki, T., Murakami, J. and Tajiri, K., 2001. Preparation of gold cluster/silica nanocomposite aerogel via spontaneous wet- gel formation. Advanced Materials, 13, 1611-1614.

Tay, K. S., Rahman, N.A., Abas, M.R.B., 2010. Ozonation of parabens in aqueous solution: Kinetics and mechanism of degradation. Chemosphere, 81, 1446-1453.

Teo, B. M., Suh, S. K., Hatton, T. A., Ashokkumar, M., Grieser, F., 2010. Sonochemical synthesis of magnetic Janus nanoparticles. Langmuir, 27, 30-33.

Ternes, T. A., 1998. Occurrence of drugs in German sewage treatment plants and rivers. Water Research, 32, 3245-3260.

Todorova, N., Giannakopoulou, T., Karapati, S., Petridis, D., Vaimakis, T., Trapalis, C., 2014. Composite TiO2/clays materials for photocatalytic NOx oxidation. Applied Surface Science, 319, 113-120.

Tunç, S., Duman, O., Uysal, R., 2008. Electrokinetic and rheological behaviors of sepiolite suspensions in the presence of poly (acrylic acid sodium salt) s, polyacrylamides, and poly (ethylene glycol) s of different molecular weights. Journal of Applied Polymer Science, 109, 1850-1860.

Uğurlu, M., Karaoğlu, M.H., 2011. TiO2 supported on sepiolite: preparation, structural and thermal characterization and catalytic behaviour in photocatalytic treatment of phenol and lignin from olive mill wastewater. Chemical Engineering Journal, 166, 859-867.

Ullerstam, M., Langer, S., Ljungström, E., 2000. Gas phase rate coefficients and activation energies for the reaction of butanal and 2- methyl- propanal with nitrate radicals. International Journal of Chemical Kinetics, 32, 294-303.

Vaizoğullar, A.İ., 2017. TiO2/ZnO supported on sepiolite: preparation, structural characterization, and photocatalytic degradation of flumequine antibiotic in aqueous solution. Chemical Engineering Communications, 204, 689-697.

Valkova, N., Lépine, F., Valeanu, L., Dupont, M., Labrie, L., Bisaillon, J. G., Villemur, R., 2001. Hydrolysis of 4-hydroxybenzoic acid esters (parabens) and their aerobic transformation into phenol by the resistant Enterobacter cloacae strain EM. Applied Environmental Microbiology, 67, 2404-2409.

Van der Bruggen, B., Vandecasteele, C., 2003. Removal of pollutants from surface water and groundwater by nanofiltration: overview of possible applications in the drinking water industry. Environmental pollution, 122, 435-445.

Vasiliadou, I.A., Molina, R., Martínez, F., Melero, J.A., 2013. Biological removal of pharmaceutical and personal care products by a mixed microbial culture: sorption, desorption and biodegradation. Biochemical Engineering Journal, 81, 108-119.

Walling, C., Goosen, A., 1973. Mechanism of the ferric ion catalyzed decomposition of hydrogen peroxide. Effect of organic substrates. Journal of the American Chemical Society, 95, 2987-2991.

Walpole, R.E., Myers, R.H., Myers, S.L., 1998. Some Discrete Probability Distributions. Probability and Statistics for Engineers and Scientists, 132-134, Prentice Hall International, New Jersey, U.S.A.

Wang, J., Wang, S., 2016. Removal of pharmaceuticals and personal care products (PPCPs) from wastewater: a review. Journal of Environmental Management, 182, 620-640.

Wang, X., Ji, Z., Zhang, L., Wang, J., 2006. Study of rutile TiO2 in situ supported on crude sepiolite by liquid phase method. Journal -Chinese Ceramic Society, 34, 932.

Watanabe, Y., Banno, K., Sugiura, M., 2000. Calcined sepiolite-supported Pt/Fe catalyst. Applied clay science, 16, 59–71.

Weavers, L.K., Ling, F.H., Hoffmann, M.R., 1998. Aromatic compound degradation in water using a combination of sonolysis and ozonolysis. Environmental Science & Technology, 32, 2727-2733.

Westerhoff, P., Yoon, Y., Snyder, S., Wert, E., 2005. Fate of endocrine-disruptor, pharmaceutical, and personal care product chemicals during simulated drinking water treatment processes. Environmental Science & Technology, 39, 6649-6663.

Wetzel, B., Haupert, F., Zhang, M.Q., 2003. Epoxy nanocomposites with high mechanical and tribological performance. Composites Science and Technology, 63, 2055–2067.

Wiewióra, A., Pérez-Rodrıguez, J.L., Perez-Maqueda, L.A., Drapała, J., 2003. Particle size distribution in sonicated high-and low-charge vermiculites. Applied Clay Science, 24, 51-58.

Winand, R., 1996. Quantitative sonochemistry. Ultrasonics Sonochemistry, 3, 147-151.

Xiao, J., Nie, X., Sun, S., Song, X., Li, P., Yu, J., 2015. Lithium ion adsorption–desorption properties on spinel Li4Mn5O12 and pH-dependent ion-exchange model. Advanced Powder Technology, 26, 589-594.

Xiao, J., Song, C., Ma, X., Li, Z., 2012. Effects of aromatics, diesel additives, nitrogen compounds, and moisture on adsorptive desulfurization of diesel fuel over activated carbon. Industrial & Engineering Chemistry Research, 51, 3436-3443.

Xiao, M., Wei, D., Li, L., Liu, Q., Zhao, H., Du, Y., 2014. Formation pathways of brominated products from benzophenone-4 chlorination in the presence of bromide ions. Journal of Environmental Sciences, 26, 2387-2396.

Xiao, X., Hu, R., Tu, S., Zheng, C., Zhong, H., Zuo, X., Nan, J., 2015. One-pot synthesis of micro/nano structured β-Bi 2 O 3 with tunable morphology for highly efficient photocatalytic degradation of methylparaben under visible-light irradiation. RSC Advances, 5, 38373-38381.

Yalkowsky, S.H., 1992. Aquasol database of aqueous solubility. Ph.D. Dissertation, University of Arizona.

Yang, G.C., Tang, P.L., 2016. Removal of phthalates and pharmaceuticals from municipal wastewater by graphene adsorption process. Water Science and Technology, 73, 2268-2274.

Yang, Y., Ok, Y.S., Kim, K.H., Kwon, E.E., Tsang, Y.F., 2017. Occurrences and removal of pharmaceuticals and personal care products (PPCPs) in drinking water and water/sewage treatment plants: A review. Science of the Total Environment, 596, 303-320.

Yang, Y., Xu, C., Cao, X., Lin, H., Wang, J., 2017. Antibiotic resistance genes in surface water of eutrophic urban lakes are related to heavy metals, antibiotics, lake morphology and anthropic impact. Ecotoxicology, 26, 831-840.

Ying, G. G., Kookana, R. S., Kumar, A., Mortimer, M., 2009. Occurrence and implications of estrogens and xenoestrogens in sewage effluents and receiving waters from South East Queensland. Science of the Total Environment, 407, 5147-5155.

Yu, J., Yu, X., 2008. Hydrothermal synthesis and photocatalytic activity of zinc oxide hollow spheres. Environmental Science & Technology, 42, 4902–4907.

Yu, K., Li, B., Zhang, T., 2012. Direct rapid analysis of multiple PPCPs in municipal wastewater using ultrahigh performance liquid chromatography–tandem mass spectrometry without SPE pre-concentration. Analytica Chimica Acta, 738, 59-68.

Zhang, D., 2019. The role of microorganisms in the removal of pharmaceutical and personal care products. In Pharmaceuticals and Personal Care Products: Waste Management and Treatment Technology, 341-382, Butterworth-Heinemann, Cambridge, U.S.A.

Zhang, G., Xiong, Q., Xu, W., Guo, S., 2014. Synthesis of bicrystalline TiO2 supported sepiolite fibers and their photocatalytic activity for degradation of gaseous formaldehyde. Applied Clay Science, 102, 231-237.

Zhang, L.N., Hou, Z.T., Ye, X., Xu, Z.B., Bai, X.L., Shang, P., 2013. The effect of selected alloying element additions on properties of Mg-based alloy as bioimplants: A literature review. Frontiers of Materials Science, 7, 227-236.

Zhang, L.W., Fu, H.B., Zhu, Y.F., 2008. Efficient TiO2 photocatalysts from surface hybridization of TiO2 particles with graphite- like carbon. Advanced Functional Materials, 18, 2180-2189.

Zhang, Y., Wang, D. and Zhang, G., 2011. Photocatalytic degradation of organic contaminants by TiO2/sepiolite composites prepared at low temperature. Chemical Engineering Journal, 173, 1-10.

Zhang, Z.H., Li, J.J., Li, T.S., 2008. Ultrasound-assisted synthesis of pyrroles catalyzed by zirconium chloride under solvent-free conditions. Ultrasonics Sonochemistry, 15, 673-676.

Zhou, N.A., Lutovsky, A.C., Andaker, G.L., Ferguson, J.F., Gough, H.L., 2014. Kinetics modeling predicts bioaugmentation with Sphingomonad cultures as a viable technology for enhanced pharmaceutical and personal care products removal during wastewater treatment. Bioresource Technology, 166, 158-167.

Ziylan, A., Ince, N.H., 2015. Catalytic ozonation of ibuprofen with ultrasound and Fe-based catalysts. Catalysis Today, 240, 2-8.

Ziylan, A., Koltypin, Y., Gedanken, A., Ince, N.H., 2013. More on sonolytic and sonocatalytic decomposition of Diclofenac using zero-valent iron. Ultrasonics Sonochemistry, 20, 580-586.

Zuccato, E., Castiglioni, S., Bagnati, R., Chiabrando, C., Grassi, P., Fanelli, R., 2008. Illicit drugs, a novel group of environmental contaminants. Water Research, 42, 961-968.

Zúñiga-Benítez, H., Peñuela, G.A., 2017. Methylparaben removal using heterogeneous photocatalysis: effect of operational parameters and mineralization/biodegradability studies. Environmental Science and Pollution Research, 24, 6022-6030.